EUROPEAN COMMISSION
Community research

PAMINA
Performance Assessment Methodologies in Application to Guide the Development of the Safety Case

(Contract Number: FP6-036404)

Report on calculations in granite
DELIVERABLE (D-N°:4.2.2)

Author(s): **J. Jaime Gómez-Hernández, Javier Rodrigo-Ilarri, Liangping Li, Miguel Angel Cuñado, José Luis Cormenzana**

Date of issue of this report : **01/14/2010**

Start date of project : **01/10/2006**

Duration : 36 Months

Project co-funded by the European Commission under the Euratom Research and Training Programme on Nuclear Energy within the Sixth Framework Programme (2002-2006)		
Dissemination Level		
PU	Public	X
RE	Restricted to a group specified by the partners of the [PAMINA] project	
CO	Confidential, only for partners of the [PAMINA] project	

Foreword

The work presented in this report was developed within the Integrated Project PAMINA: **P**erformance **A**ssessment **M**ethodologies **IN** **A**pplication to Guide the Development of the Safety Case. This project is part of the Sixth Framework Programme of the European Commission. It brings together 25 organisations from ten European countries and one EC Joint Research Centre in order to improve and harmonise methodologies and tools for demonstrating the safety of deep geological disposal of long-lived radioactive waste for different waste types, repository designs and geological environments. The results will be of interest to national waste management organisations, regulators and lay stakeholders.

The work is organised in four Research and Technology Development Components (RTDCs) and one additional component dealing with knowledge management and dissemination of knowledge:

- In RTDC 1 the aim is to evaluate the state of the art of methodologies and approaches needed for assessing the safety of deep geological disposal, on the basis of comprehensive review of international practice. This work includes the identification of any deficiencies in methods and tools.

- In RTDC 2 the aim is to establish a framework and methodology for the treatment of uncertainty during PA and safety case development. Guidance on, and examples of, good practice will be provided on the communication and treatment of different types of uncertainty, spatial variability, the development of probabilistic safety assessment tools, and techniques for sensitivity and uncertainty analysis.

- In RTDC 3 the aim is to develop methodologies and tools for integrated PA for various geological disposal concepts. This work includes the development of PA scenarios, of the PA approach to gas migration processes, of the PA approach to radionuclide source term modelling, and of safety and performance indicators.

- In RTDC 4 the aim is to conduct several benchmark exercises on specific processes, in which quantitative comparisons are made between approaches that rely on simplifying assumptions and models, and those that rely on complex models that take into account a more complete process conceptualization in space and time.

The work presented in this report was performed in the scope of RTDC 4.

All PAMINA reports can be downloaded from http://www.ip-pamina.eu.

PAMINA Sixth Framework programme, 26.05.2010

INDEX

LIST OF FIGURES

Page

LIST OF TABLES

1.- Introduction

This deliverable describes the work performed by UPV and ENRESA within the PAMINA project WP 4.2 “PA approaches based on different geometric complexity of modeling”.

As stated in the Annex I of PAMINA contract [6] “the main objective of the work package is to investigate the usefulness of more complex codes for modelling the transport behaviour in the far field on the basis of well-defined benchmark cases”. ENRESA and UPV have defined and studied a benchmark case for a repository in granite based on the generic granite formation adopted for the Spanish PA exercise Enresa 2000 [1].

UPV has done many simulations using two finite elements models of different degrees of detail (“fine scale” and “coarse” models) in order to study how to define a coarse model that represents a significant simplification (a factor 100 of reduction in the number of finite elements) of the more detailed “fine scale model”, while providing similar results for the transport of radionuclides released from the repository. Enresa has investigated how to define an even more simplified 1D advective pathway (to be used in PA calculations) that reproduces with reasonable precision the detailed results of the “fine scale model”.

This deliverable contains the following information:

- description of the benchmark case in granite (section 2),
- effect of the heterogeneity in the transport parameters in the results of the “fine scale” model of UPV (section 3),
- flow and transport up-scaling when passing from the “fine scale model” to the “coarse model” (section 4),
- definition of a 1D pathway to be used in PA calculations that reproduces the results obtained with the “fine scale model” (section 5), and
- conclusions (section 6).

The work done by UPV on this WP 4.2 is related to the work done on WP 2.2.D, described on the Deliverable document D2.2.D.1 – Evaluation and testing of approaches to treat spatial variability in PA.

2.- Benchmark specification for the granite case

The documents M4.2.2 - Benchmark specification for the granite case and M4.2.5 - Second Version of the Benchmark Specification in Granite with Additional Data describe a test case for the comparison of far-field migration models with different degree of detail for a HLW repository located at a depth of 500m in a generic granite formation, whose properties are representative of Spanish crystalline rocks.

2.1.- General description of the test case

The test case is based on the granite site and repository geometry described in Enresa 2000 [1]. The reference host formation is a crystalline rock ovoid elongated in the N-S direction, 25km long and 12km wide with lateral shale intrusions. The repository is located in the northern area of the granite formation, where it is wider. Fig.1 shows the areas considered in the hydro-geological modelling (both at regional and local level) and the location of the repository underground disposal areas.

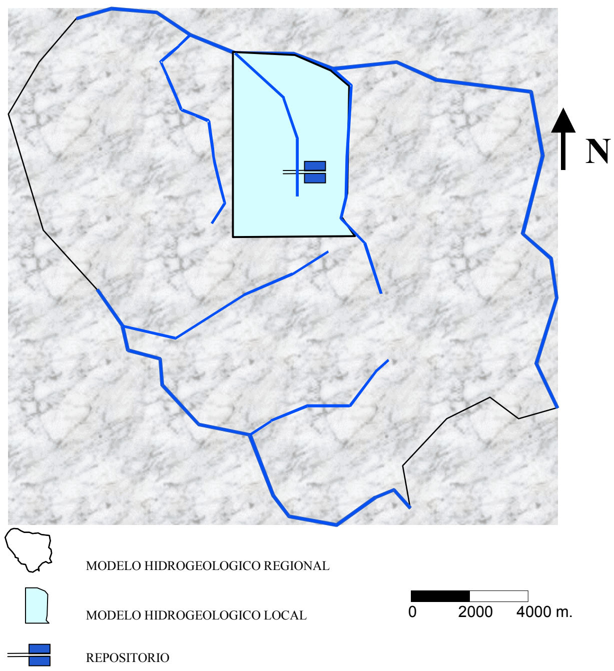

Figure 1: Domains of the regional hydro-geological model and the local hydro-geological model (blue area) [1]

Hydro-geological modelling at regional scale is performed to identify the dominant flow directions and discharge areas, and to establish boundary conditions for the local model. A continuum porous media model is used without explicit consideration of fractures, but anisotropic hydraulic conductivities allow taking into account the general fracture trends of the granite at regional scale.

The hydro-geological modelling at local scale is done to quantify the flows in the repository surroundings. The local model explicitly includes the most relevant fractures identified because they are potential fast transport pathways from the repository to the Biosphere (see Figure 2).

The regional and local hydro-geological calculations are performed for stationary conditions.

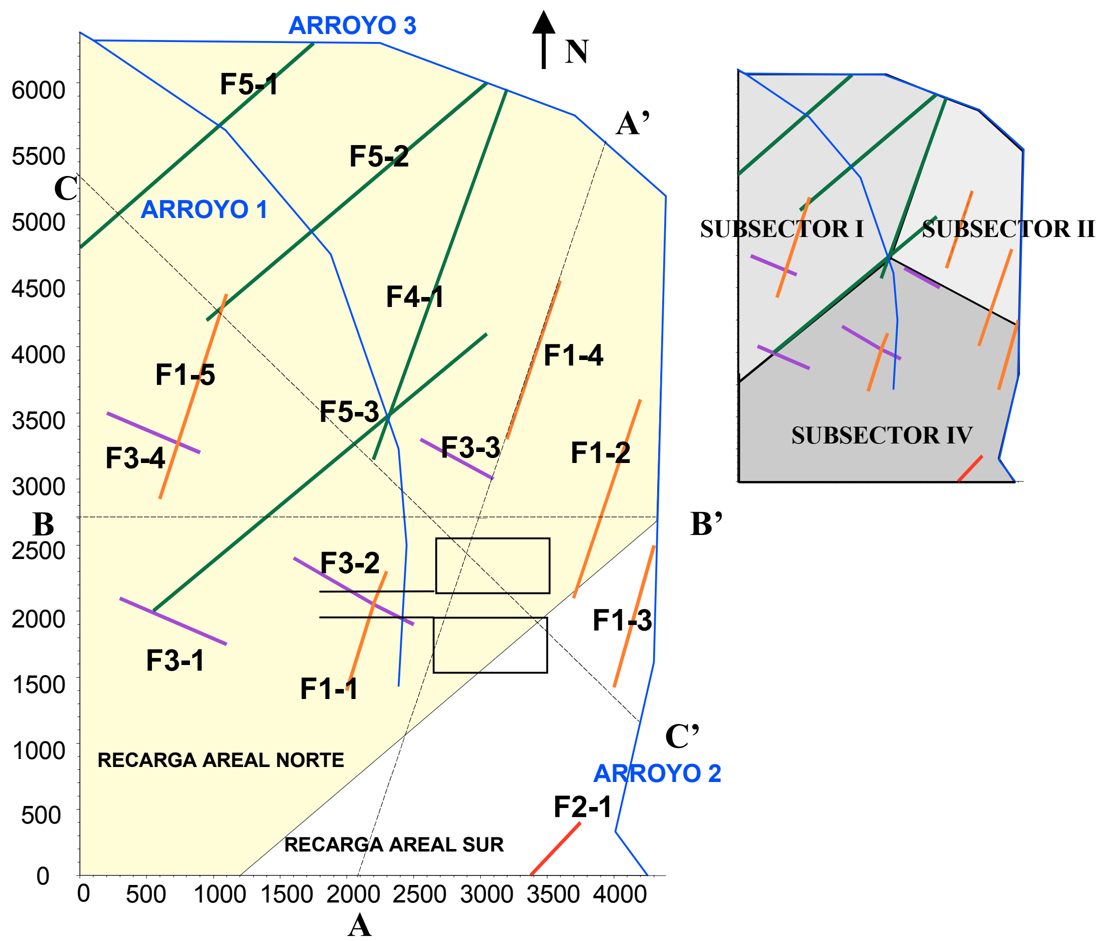

Figure 2: Fractures included in the local hydro-geological model [1].

The local hydro-geological model of Figure 2 has been used by UPV for the detailed transport calculations too. Radionuclides with different properties (sorbed and non-sorbed species, and decay chains) will be injected into the formation at repository level and the fluxes released to the Biosphere at different discharge points will be quantified.

After developing the hydro-geological model, a particle-tracking code is used. Several hundreds of particles are released at different points of the repository, their trajectories are followed in order to identify the discharge points and their travel times are calculated too.

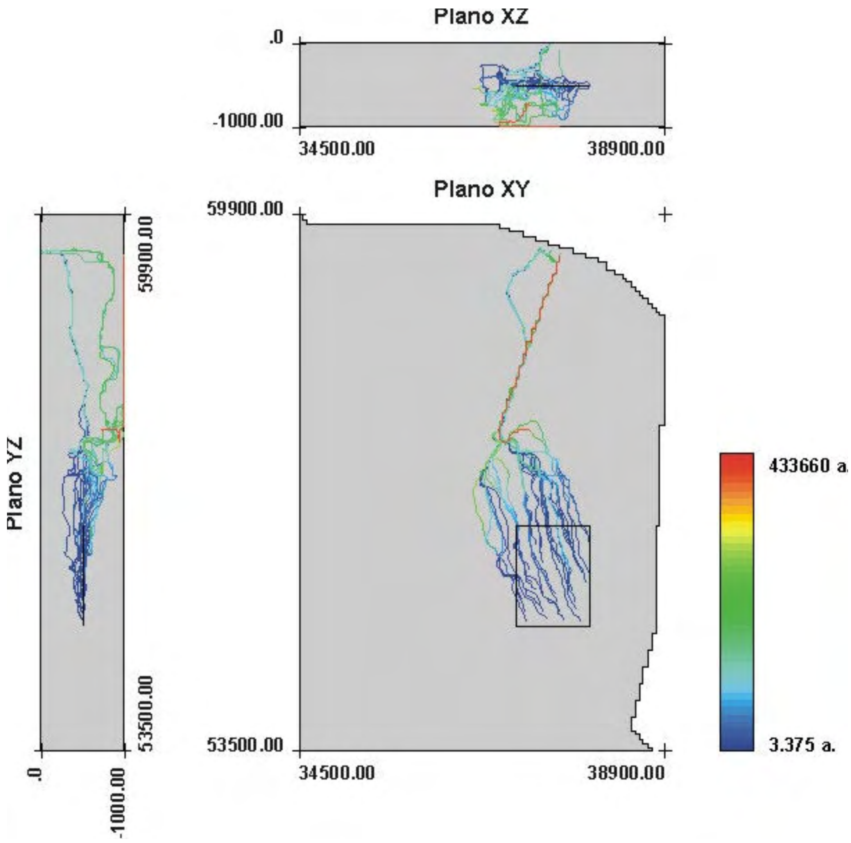

Figure 3: Graphical representation of the results of the “particle tracking” calculations [1]

The information obtained with the particle tracking code is used to generate the values of some of the parameters needed by the 1D flow tubes used in the PA code GoldSim for far field transport:

- fraction of the particles reaching each discharge point,
- length of the trajectories, and
- particle travel times

while the rest of the parameters used in the 1D flow tubes are based on bibliographical data.

A systematic comparison of the results obtained with the detailed and simplified (PA) methods will be done, in order to:

- find out if the traditional PA methods provide reasonably good results,
- identify potential improvements that should be implemented in PA far-field transport models and codes, and
- optimize the generation of input data for the PA models on the base of the results obtained with the detailed model.

The previous description of the detailed and simplified PA approaches for far field transport are based on the work performed in Enresa2000 [1] PA exercise. The work of UPV on "upscaling" within Task 2.2.D of PAMINA have been taken into account in order to identify and evaluate potential improvements for the detailed and the PA models to be used within WP4.2.

2.2.- Additional model data

Model geometry:

- 2D Equivalent heterogenous media
- Study Area is inscribed in a rectangle with dimensions 14650 m (direction E-W) by 10400 m (direction N-S)
- Discretization is 1465 x 8365 cells (10 x 10 m each)

Fracture geometry

- Fracture distribution and orientation data

    Family 1 - Direction N20E → 2.5 %

    Family 2 – Direction N50E → 2.5 %

    Family 3 - Direction N110E → 1.0 %

Hydraulic significance:

Type 1 → deterministic

Type 2 → stochastic

Type 3 → equivalent porous media

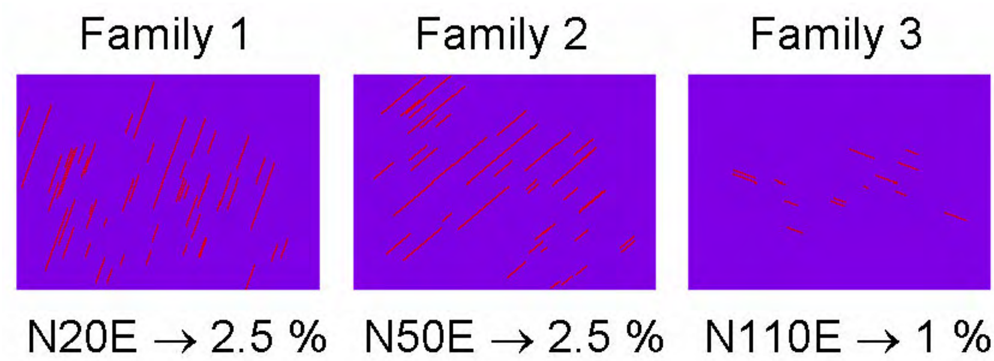

Figure 4.- Graphical representation of fractures

Variography

Exponential models with ranges defined by the following anysotropy ellipsoids:

Family 1: principal direction is N20E with length 2250 m. Second principal direction is orthogonal with range 225 m

Family 2: same as family 1 but oriented N50E

Family 3: same as family 1 but oriented N110E with ranges 1350 m and 180 m

Generation of K fields

- Sequential Gaussian Simulation is used to generate independently three fracture famillies.
- Afterwards deterministic fractures are assigned.
- Finally, the fractures are superposed to the equivalent porous media.
- K data are available from 3D borehole data provided by ENRESA 2000

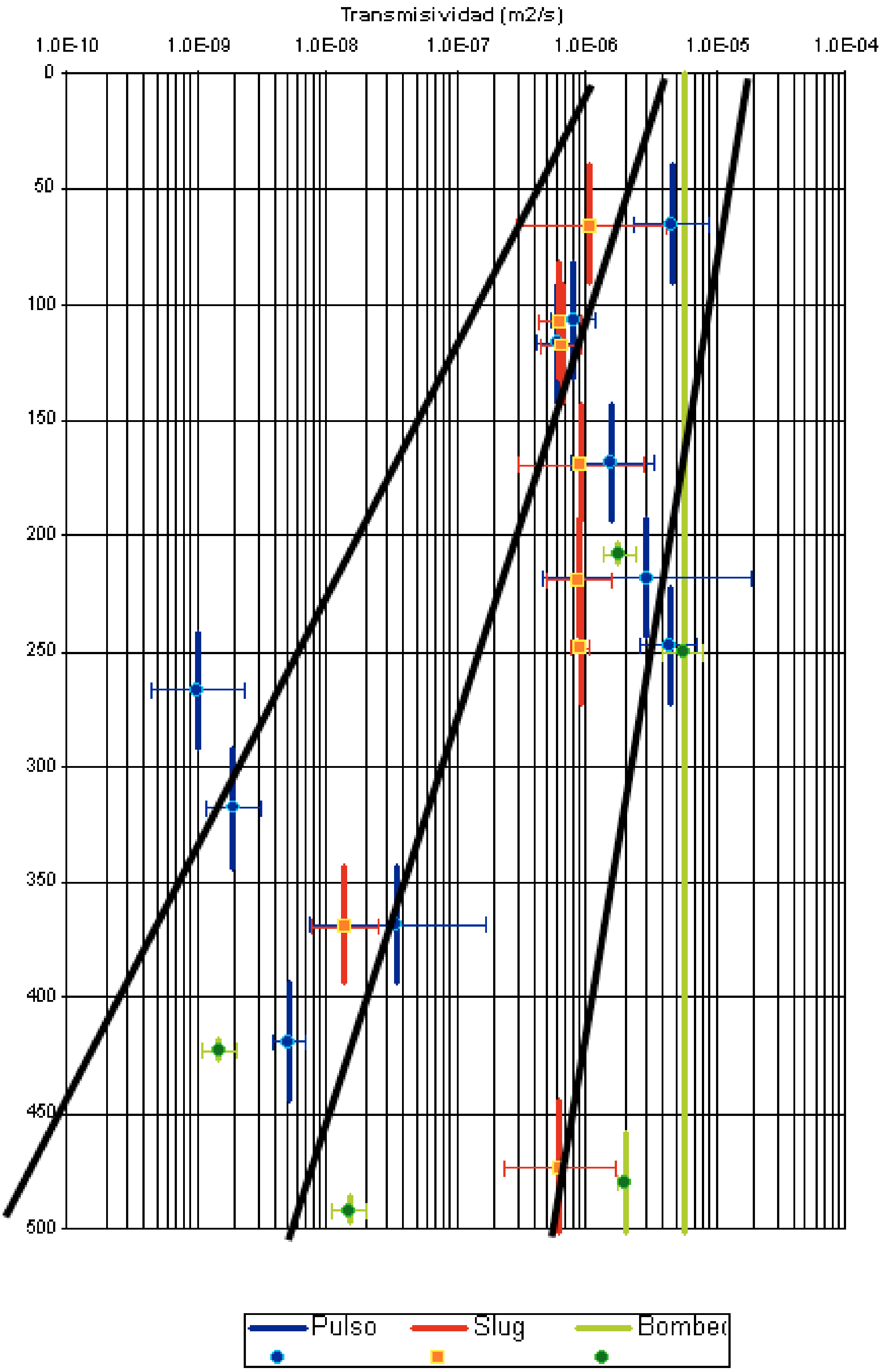

Figure 5.- Conductivity data available

2.3.- Geometric model

The hydro-geological model is based on a geometric model. This geometric model has a critical role in describing the behaviour of flow and transport. In this test case, the geometric model mainly consists of three families of stochastic fractures and four deterministic fractures. A sequential indicator simulation method was employed for the generation of the stochastic fractures.

Figures 6, 7 and 8 show the simulation results for each stochastic fracture. The parameters of each family stochastic fracture are listed in Table 1.

Figure 9 shows the geometric model including both the stochastic and the deterministic fractures.

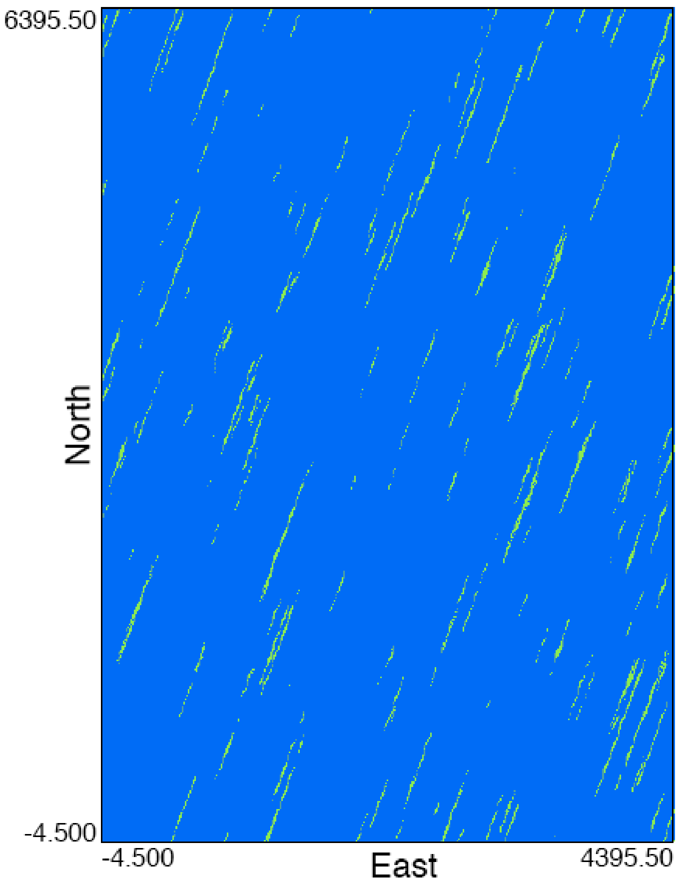

Figure 6.- Stochastic fracture family 1

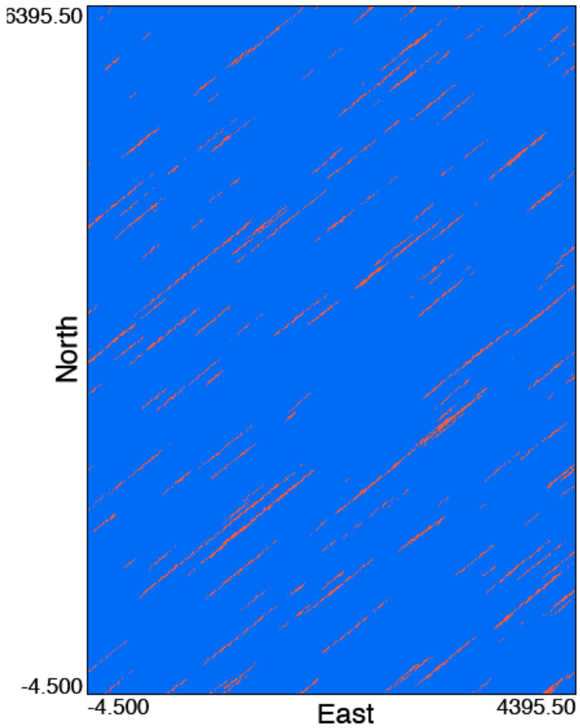

Figure 7.- Stochastic fracture family 2

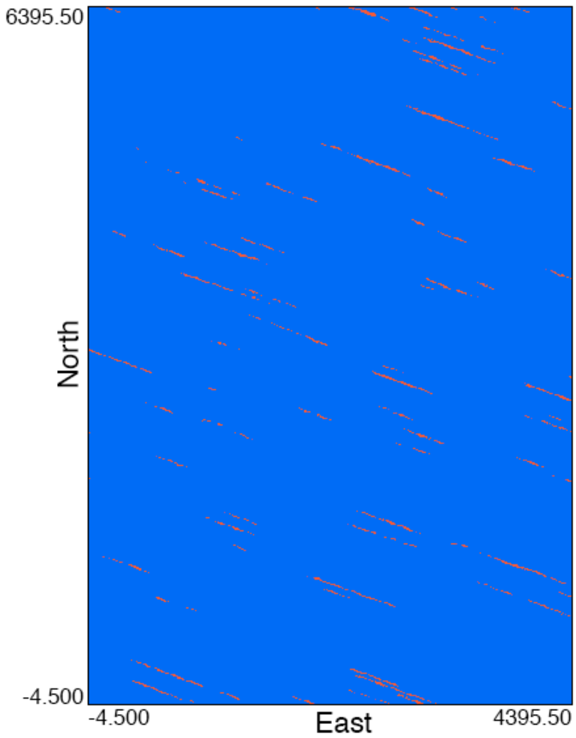

Figure 8.- Stochastic fracture family 3

	Direction	Range	Direction	Range
Family 1:	N20E	2250m	N110E	225m
Family 2:	N50E	2250m	N140E	225m
Family 3:	N110E	1350m	N20E	180m

Table 1.- Variogram parameters for each stochastic fracture

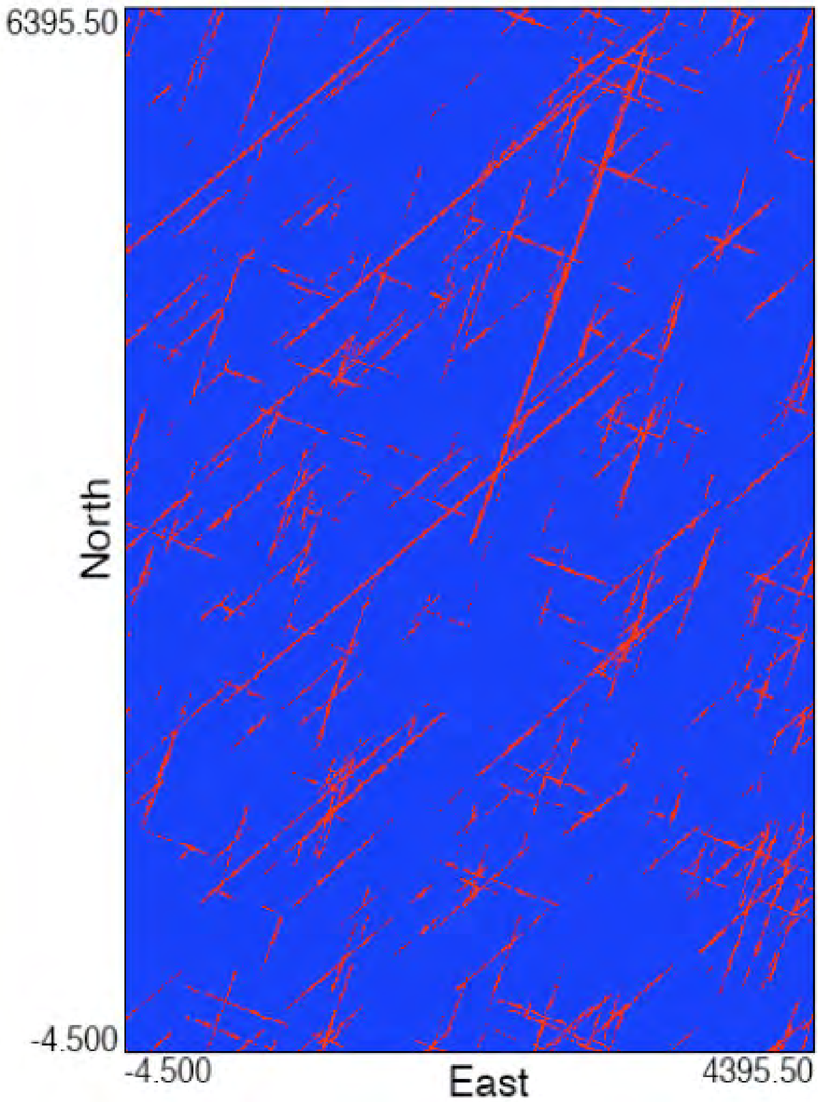

Figure 9.- Geometric model

2.4.- Simulation of the conductivity field

Sequential Gaussian simulation (SGS) was used to generate the log hydraulic conductivity field with a zero mean variance. Meanwhile, model is characterized by an isotropic spatial correlation with the range 150m and nugget 5%.

According to conductive capacity in fracture and matrix, the hydraulic field generated by the SGS was transferred based on the mean LogK values of -7.5 for deterministic fractures, -8.6 for stochastic fractures and -11 for matrix and variance value of 0.5 for all.

The final result of hydraulic conductivities field is shown in Figure 10.

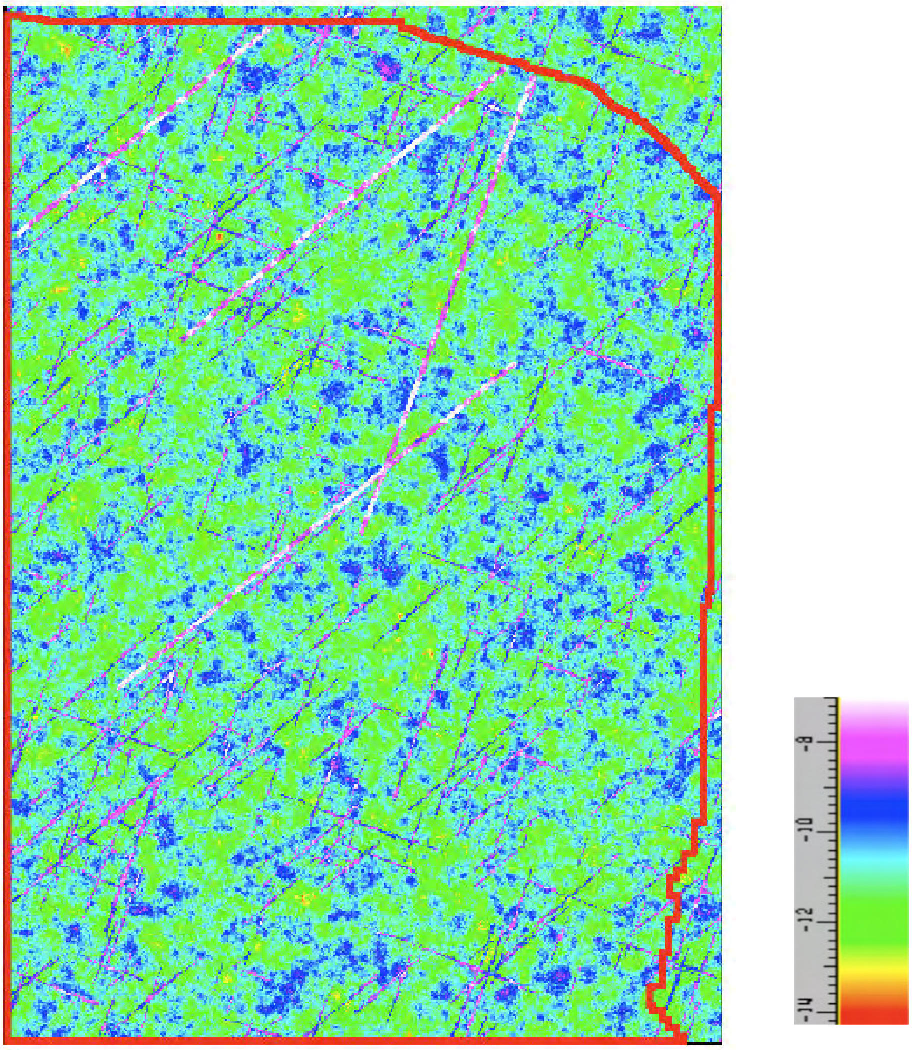

Figure 10.- LogK field

According to the hydraulic conductivity field, Figure 11 shows the histogram of LogK. This histogram reflects that LogK adopts a normal distribution with mean -10.83 and standard deviation 0.95, with a tail corresponding to the fracture conductivity.

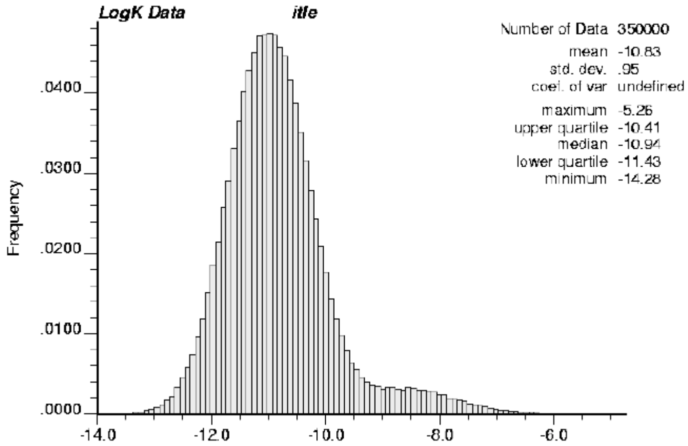

Figure 11.- LogK histogram

Directions of anisotropy are usually evident from a variogram map. Figure 12 shows a variogram map calculated with the 350000 data values in one realization. The variogram map reveals strong anisotropy due to three deterministic fractures.

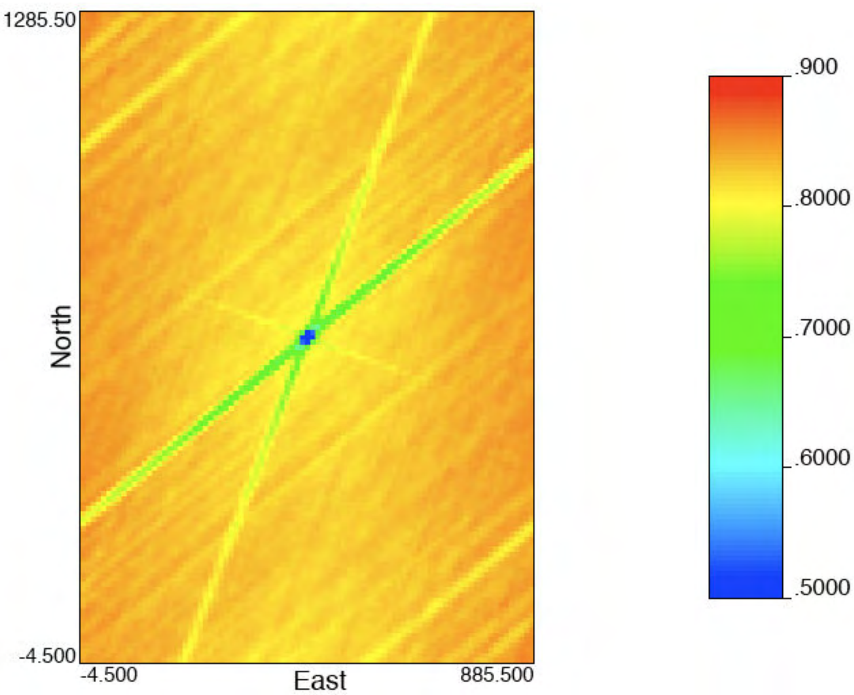

Figure 12.- LogK surface variogram

2.5.- Flow simulations

The aquifer is assumed to be confined and with prescribed-head boundaries as shown in Figure 13. The prescribed head values along the entire perimeter can be read from the piezometric head distribution in Figure 14. Steady-state flow simulation results are also shown in Figure 14.

Generally speaking, groundwater flows from the south-east corner to the north-west corner under the hydraulic gradient, that is, groundwater is discharged into the rivers located in the north boundary.

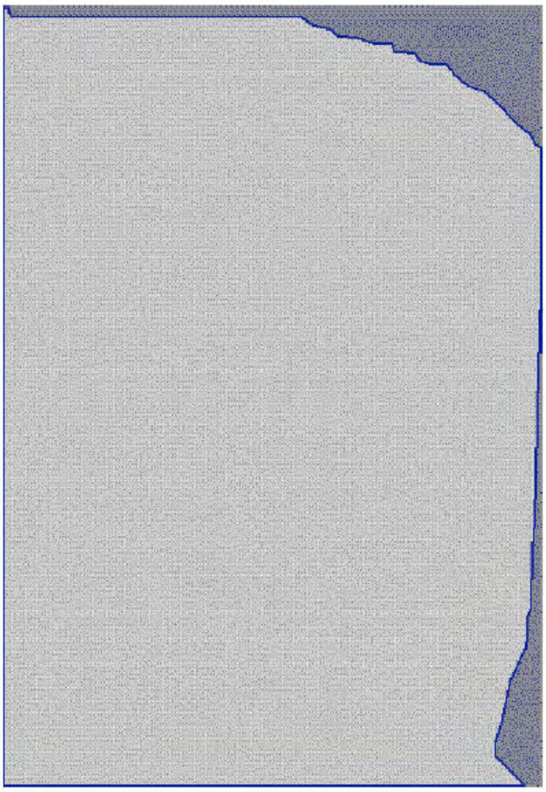

Figure 13.- Boundary conditions

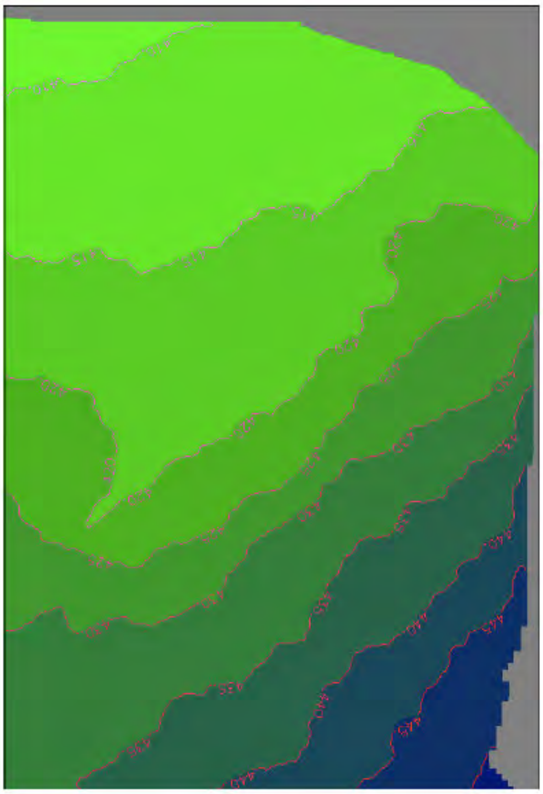

Figure 14.- Hydraulic field

3.- Effect of heterogeneity in the transport parameters

3.1.- Definition of scenarios

Some exercises considering heterogeneous distribution of transport parameters have also been performed.

Three scenarios have been defined for a non-sorbing solute depending of the parameter that is considered to have a heterogeneous distribution. The definition of scenarios is defined on Tables 2, 3 and 4.

SCENARIO 1	Mobile Porosity
Run 0	Reference Homogeneous
Run 1	Heterogenous

Table 2.- Scenario 1. Definition of parameters

SCENARIO 2	Mobile porosity	Immobile porosity
Run 0	Homog	Homog
Run 1	Heterog	Homog
Run 2	Homog	Heterog
Run 3	Heterog	Heterog

Table 3.- Scenario 2. Definition of parameters

SCENARIO 3	Enhanced Mobile porosity	Matrix porosity	Flow wetted area	Matrix thickness	Water diffusion
Run 0	Homog	Homog	Homog	Homog	Homog
Run 1	Heterog	Homog	Homog	Homog	Homog
Run 2	Homog	Heterog	Homog	Homog	Homog
Run 3	Homog	Homog	Heterog	Homog	Homog
Run 4	Homog	Homog	Homog	Heterog	Homog
Run 5	Homog	Homog	Homog	Homog	Heterog
Run 6	Heterog	Heterog	Heterog	Heterog	Heterog

Table 4.- Scenario 3. Definition of parameters

No results for the sorbing solute have been included due to fundamental problems with the implementation of the sorption processes in our numerical code. We have not been able to get consistent results with the expected average retardation so we have decided not to include in this report any simulation considering sorptive solute.

3.2.- Transport parameter distributions

Whenever heterogeneous distributions are considered, the values of the best estimates and distribution shapes used on the simulations are those shown on Table 5 [4].

Parameter	Best estimate	Distribution
Deterministic Fractures (LogK)	-7.5	Log-normal
Stochastic Fractures (LogK)	-8.6	Log-normal
Matrix (LogK)	-11	Log-normal
Matrix porosity	0.005	Triangular
Pore water diffusion coefficient	1.00E-11	Log-uniform
Matrix Thickness	0.05	Log-uniform
Density of granite solid	2630	Constant
Kinematic porosity	1.00E-04	Log-triangular
Flow wetted area	0.1	Log-triangular

Table 5.- Transport parameters best estimate values and distributions

When a homogeneous value is used, the best estimate is selected.

We assume that the spatial correlation is the same for all parameters and equal to the one already used to generate the hydraulic conductivities, i.e., the range is 150m.

The immobile porosity of the fracture is set equal to the mobile*0.25

Constant longitudinal and transversal dispersion coefficients are set to 0.2 and 0.02 m (only in the cells without fracture)

400 particles are analyzed, distributed in the centre rectangle out of the 9 equal rectangles in which the repository area can be divided after overlying a 3x3 grid.

Figures 15 to 19 show the histograms of the different heterogeneous parameters.

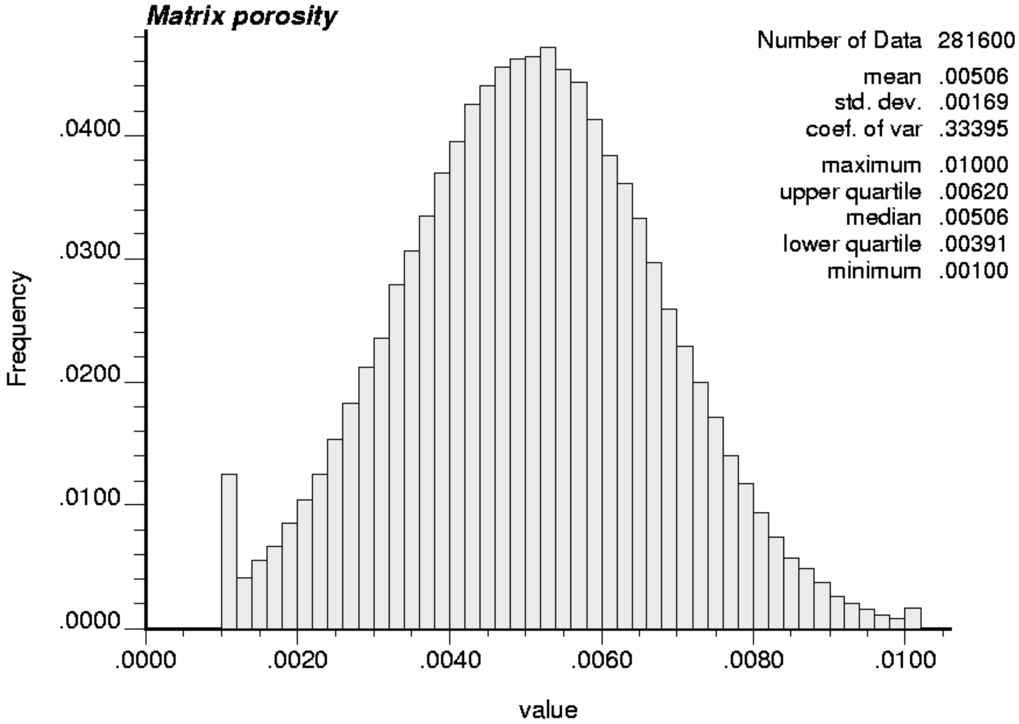

Figure 15.- Matrix porosity histogram

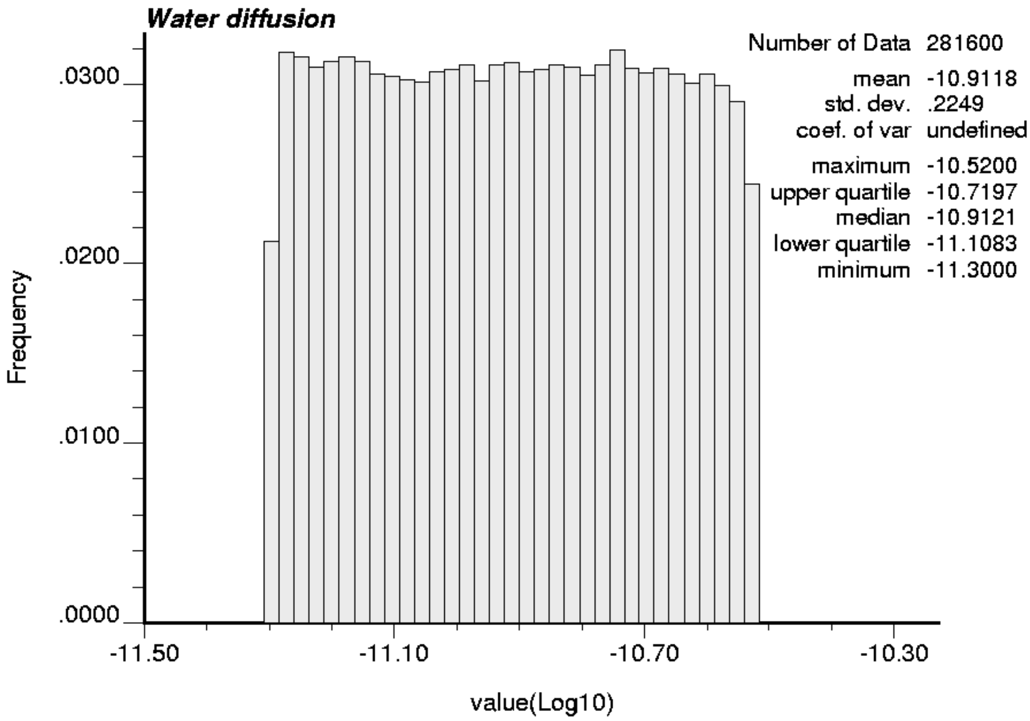

Figure 16.- Porewater diffusion coefficient histogram

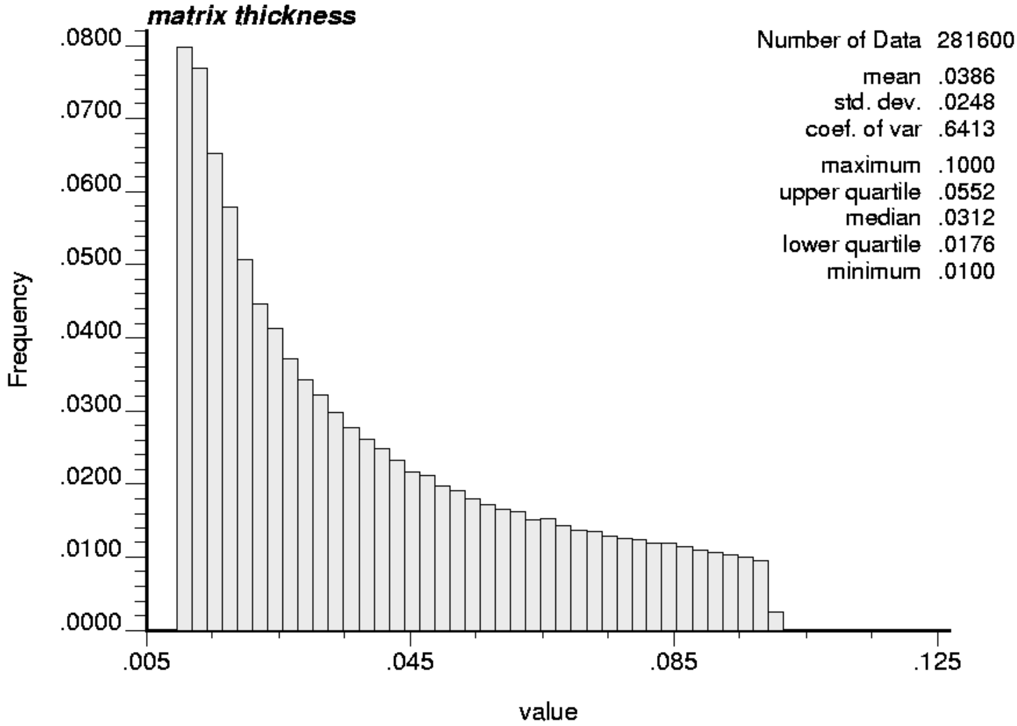

Figure 17.- Matrix thickness histogram

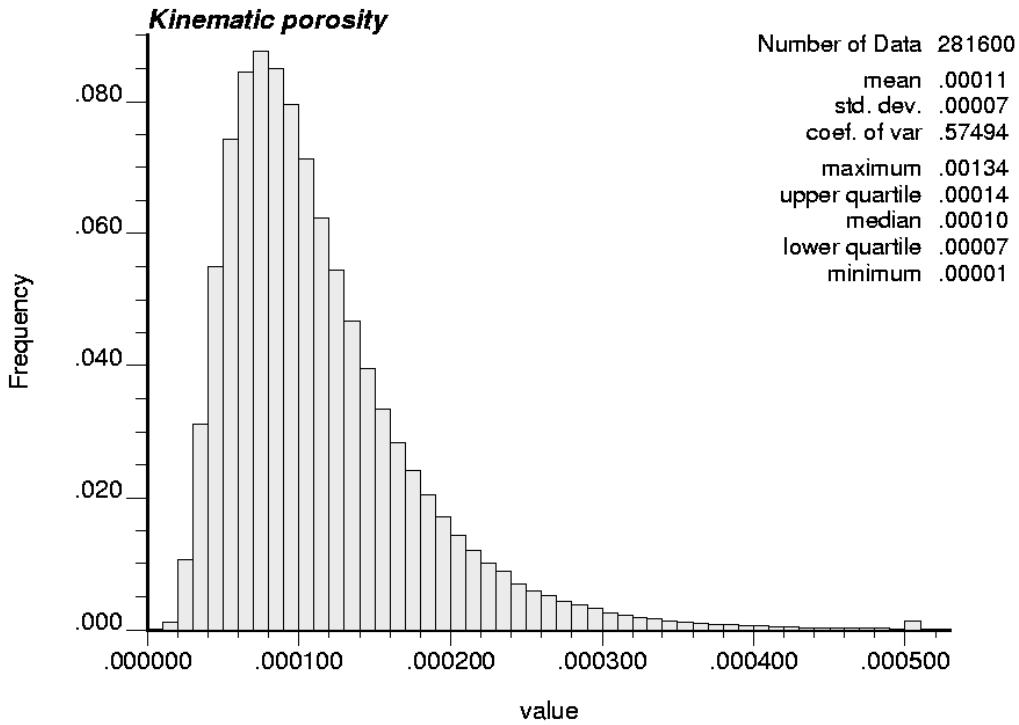

Figure 18.- Kinematic porosity histogram

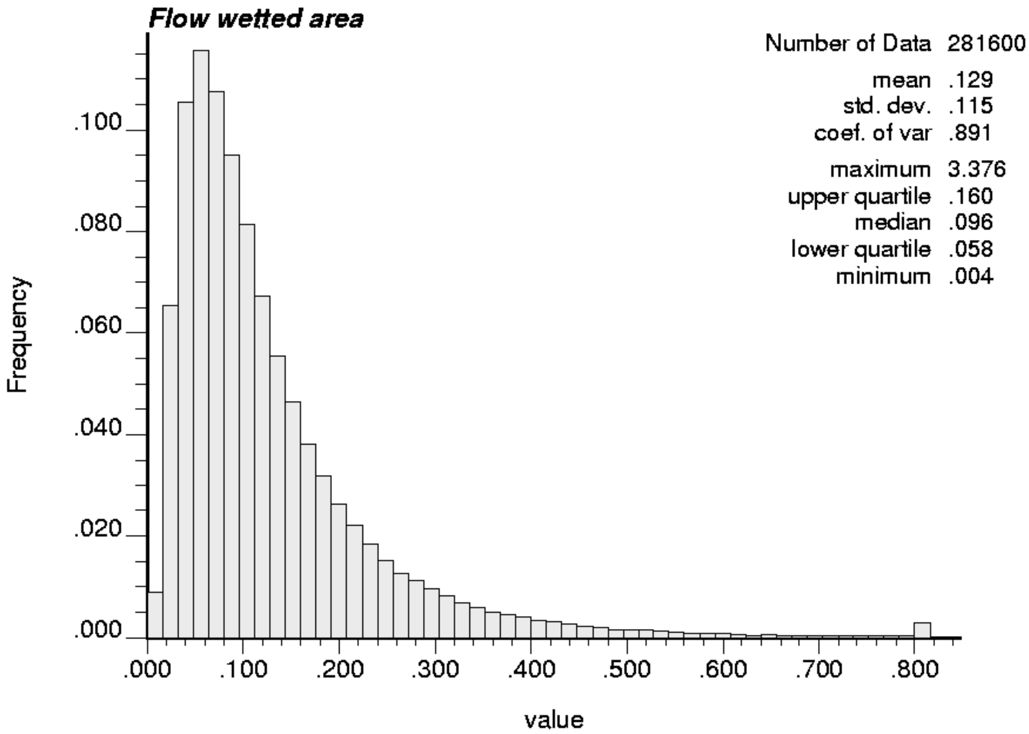

Figure 19.- Flow wetted area histogram

3.3.- Transport simulations on each scenario

3.3.1.- Scenario 1:

In this scenario the advection-dispersion equation is solved and only fracture flow is considered.

Parameters: only mobile porosity is used.

SCENARIO 1	**Mobile Porosity**
Run 0	Reference Homogeneous
Run 1	Heterogenous

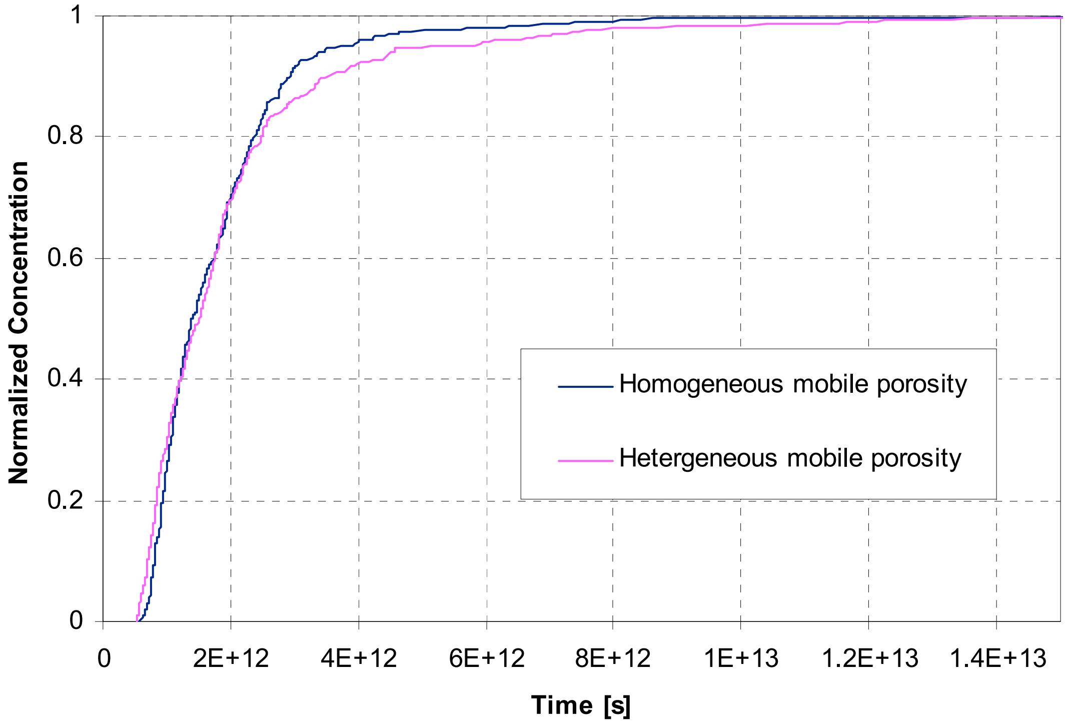

Figure 20.- Scenario 1. BTC up to the main fracture.

The impact of the heterogeneous mobile porosity is small and it only affects the tail of the BTC with longer residence times for the case of heterogeneous porosity. This effect is induced by the larger impact (with respect to the mean breakthrough curve) of the large porosity values (smaller velocities) than the small porosity values.

3.3.2.- Scenario 2

In this case, we only consider the fracture flow and with one immobile fracture zone.
Mobile porosity and immobile porosity are used.
The immobile porosity equals the mobile*0.25.

SCENARIO 2	Mobile porosity	Immobile porosity
Run 0	Homog	Homog
Run 1	Heterog	Homog
Run 2	Homog	Heterog
Run 3	Heterog	Heterog

The net effect of the immobile porosity is a retardation of 1+0,25=1,25

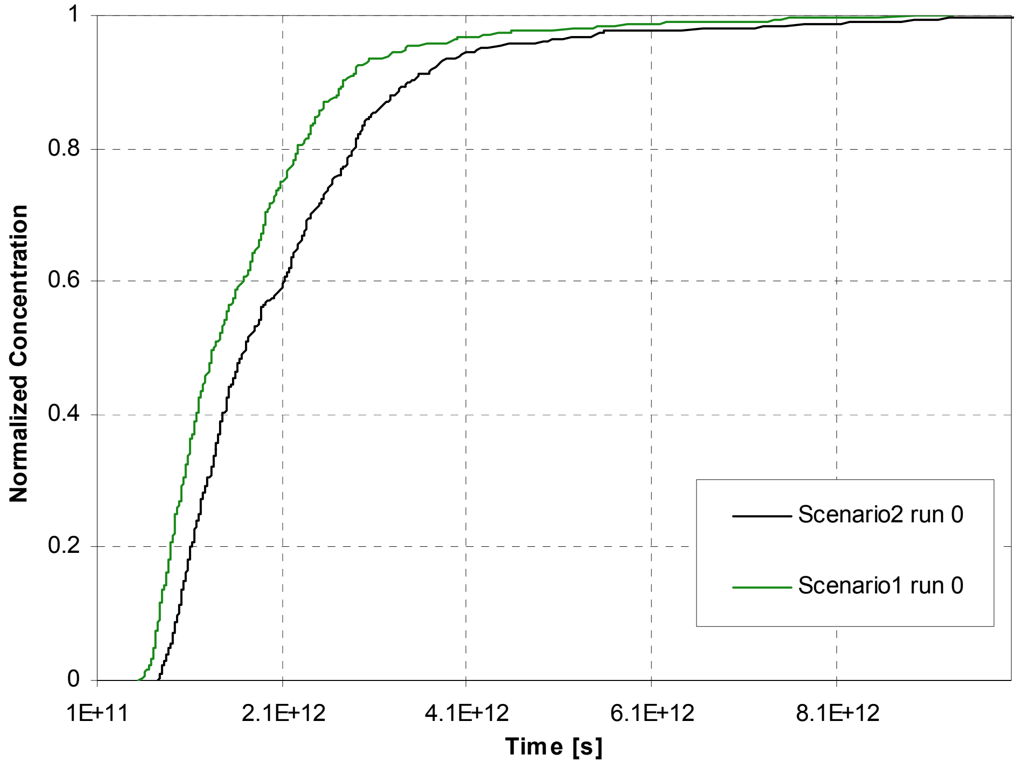

Figure 21.- Scenario 1 Run 0 and Scenario 2 Run 0

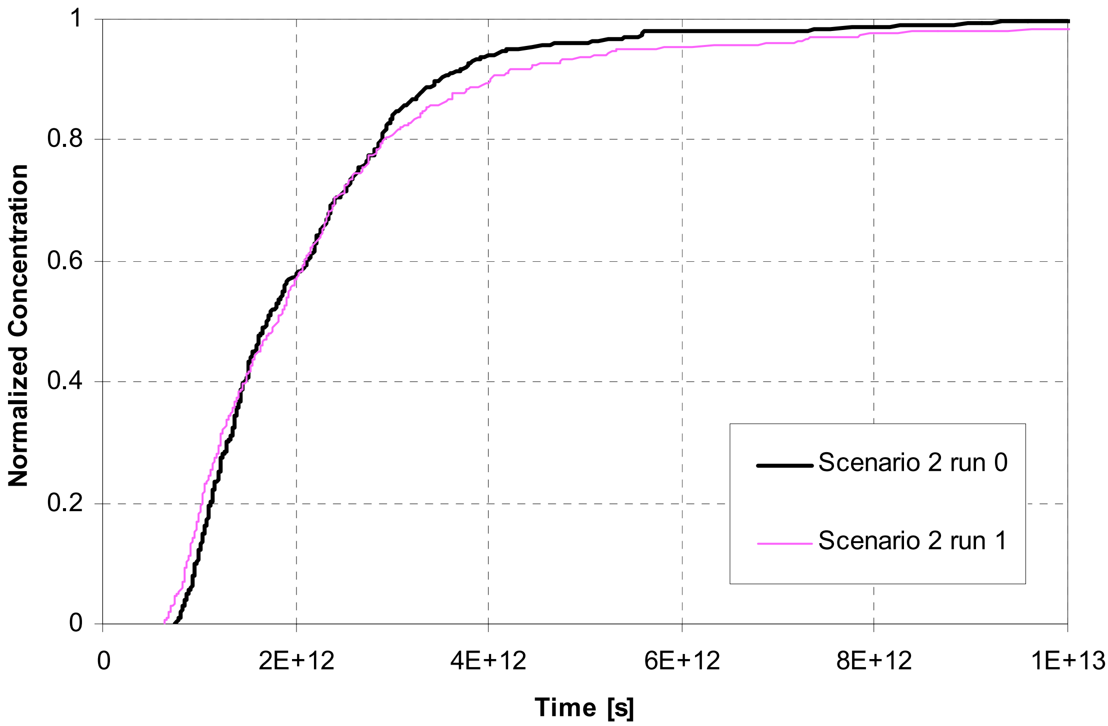

Figure 22.- Scenario 2 Run 1. BTC up to the main fracture (mobile porosity heterogeneous)

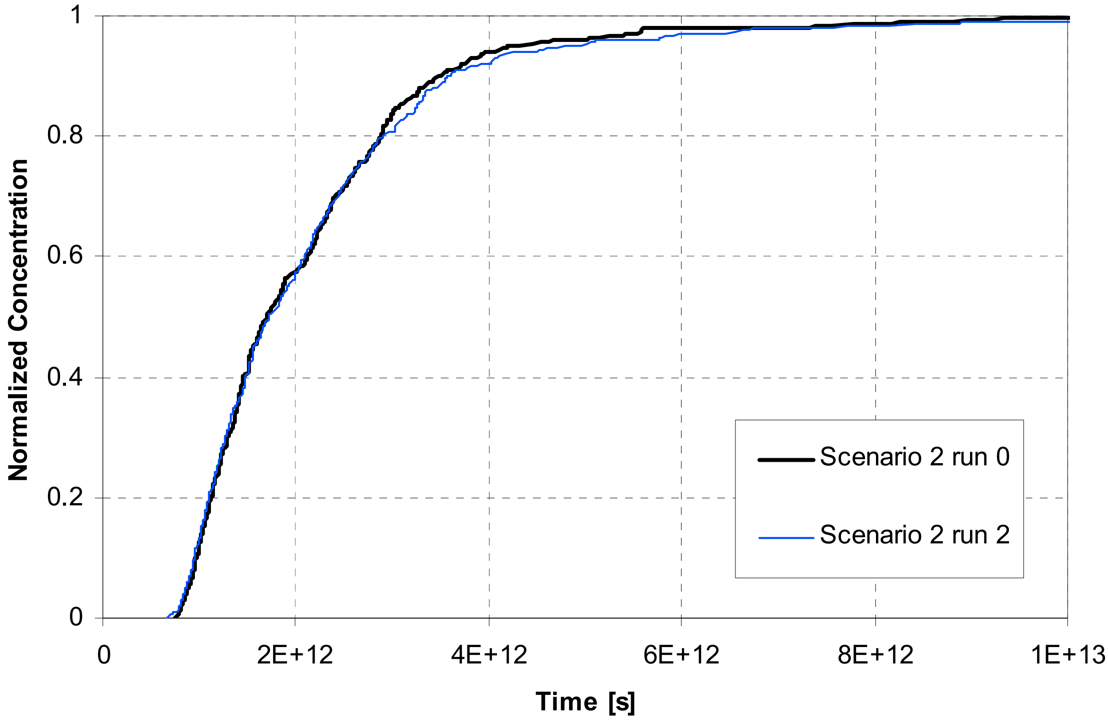

Figure 23.- Scenario 2 Run 2. BTC up to the main fracture (immobile porosity heterogeneous)

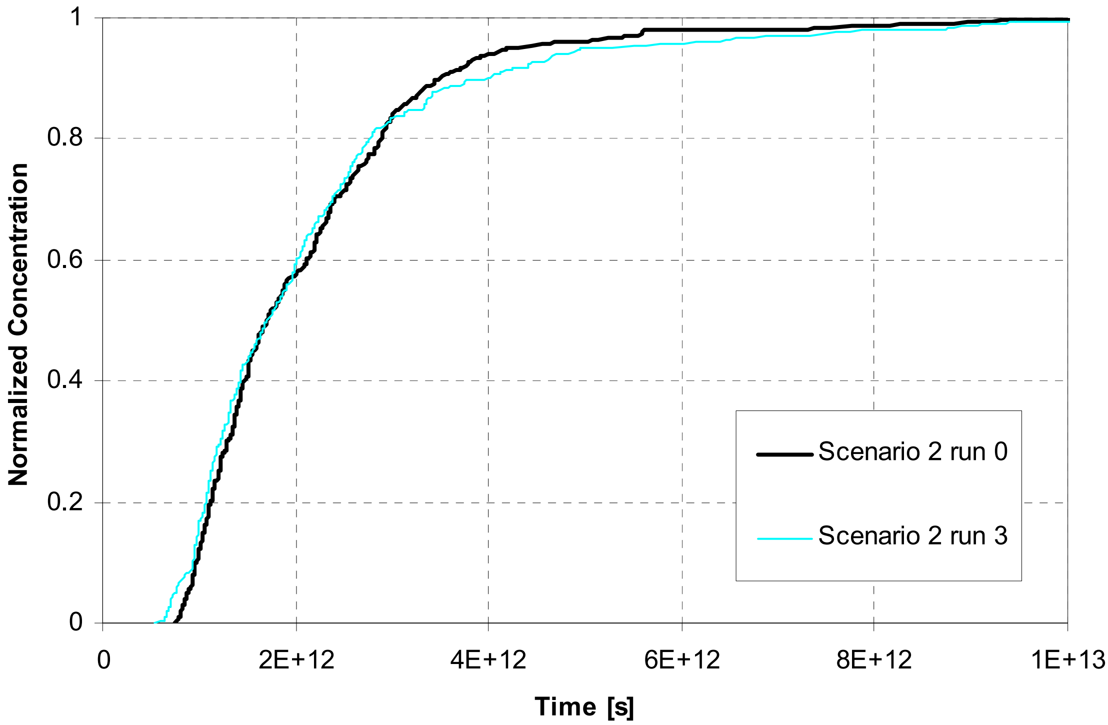

Figure 24.- Scenario 2 Run 3. BTC up to the main fracture (immobile and mobile porosity heterogeneous)

Similarly to the previous scenario, heterogeneous porosities induce a tailing in the BTCs. This tailing is more prominent for the heterogeneity in the mobile porosity than in the immobile one. The immobile zone in the fracture with a local equilibrium assumption simply implies an enhanced porosity by 1,25.

3.3.3.- Scenario 3

In this scenario, two immobile zones are considered, one in the fracture and one in the matrix. Since the immobile fracture porosity has been set equal to 0,25 times the mobile porosity, the modelling of the impact of heterogeneity in the fracture porosity has been lumped onto a single enhanced porosity.

For the diffusion into the matrix we have accounted for the heterogeneity in the flow wetted area, matrix thickness and water diffusion coefficient since they impact the heterogeneity in the active matrix porosities and in the mass transfer rate according to the relations:

Mass transfer rate= water diffusion coefficient / matrix thickness^2.

Active immobile matrix porosity= matrix porosity* flow wetted area* matrix thickness.

SCENARIO 3	**Enhanced Fracture porosity**	**Matrix porosity**	**Flow wetted area**	**Matrix thickness**	**Water diffusion**
Run 0	Homog	Homog	Homog	Homog	Homog
Run 1	Heterog	Homog	Homog	Homog	Homog
Run 2	Homog	Heterog	Homog	Homog	Homog
Run 3	Homog	Homog	Heterog	Homog	Homog
Run 4	Homog	Homog	Homog	Heterog	Homog
Run 5	Homog	Homog	Homog	Homog	Heterog
Run 6	Heterog	Heterog	Heterog	Heterog	Heterog

In this case, compared with scenario 2, a retardation factor about 1.5 is obtained due to the matrix diffusion effect.

Besides, mobile porosity, flow wetted area and matrix thickness show a certain impact on the BTCs. Results are shown on Figures 25 to 31. All of these breakthrough curves are represented up to the main fracture. The breakthrough curves up to the north boundary have the same shape as them.

It can be seen that the heterogeneity in matrix porosity has little impact with respect to the simulation with a homogeneous value. However, the heterogeneity in the flow wetted area has a larger impact. Both matrix porosity and flow wetted area are used to compute the active immobile matrix porosity, but the distribution shape and the degree of variability is larger in the flow wetted area thus its larger effect.

The impact of heterogeneity is a small retardation of the BTC. The explanation of this retardation has to be analysed by the relative position of the best value in the porosity distribution of the parameter. In this case this distribution is log-triangular with the best value very close to the median. This implies that the heterogeneous distribution has enough larger values in the upper two quartiles of the distribution that induce larger porosities which imply a retardation. The impact of heterogeneity in the matrix thickness is just the opposite to the one of the flow wetted area, the reason being that the log-uniform distribution adopted for the parameter. This implies that in the heterogeneous distribution there is a substantial fraction of lower values than the best estimate, inducing smaller retardation times.

The impact of heterogeneity in water diffusion is negligible for the probability distribution considered.

When all parameters are considered heterogeneous the net result is an enhanced dispersion with some tailing.

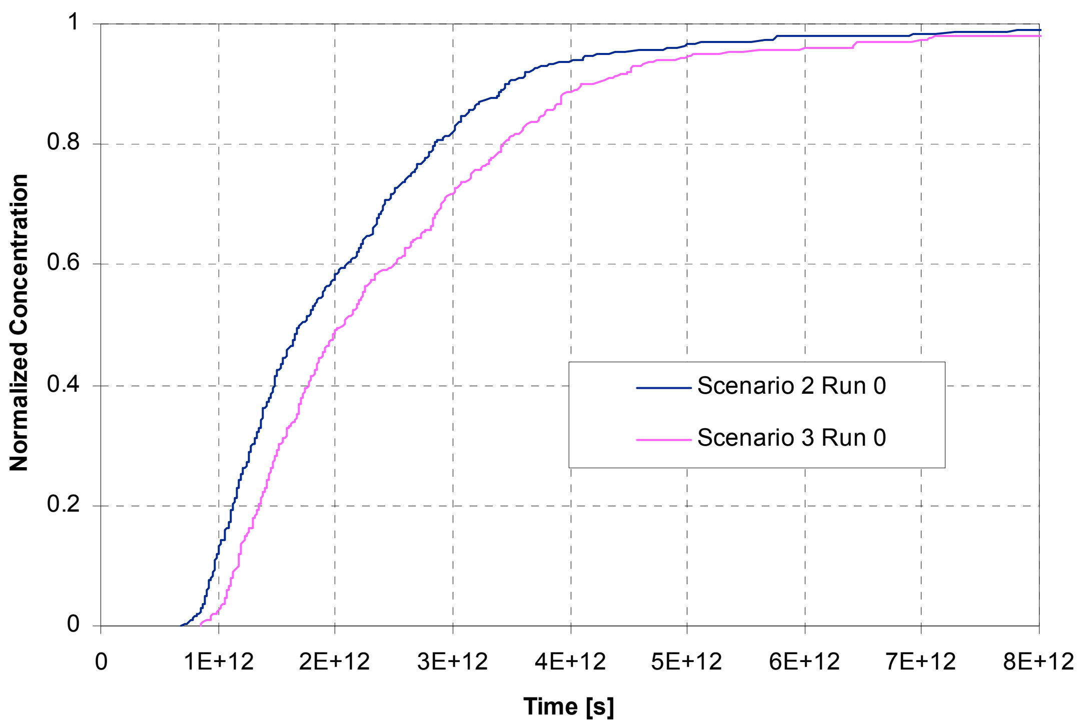

Figure 25.- Scenario 3 Run 0 and comparison with Scenario 2 Run 0. BTC up to the main fracture

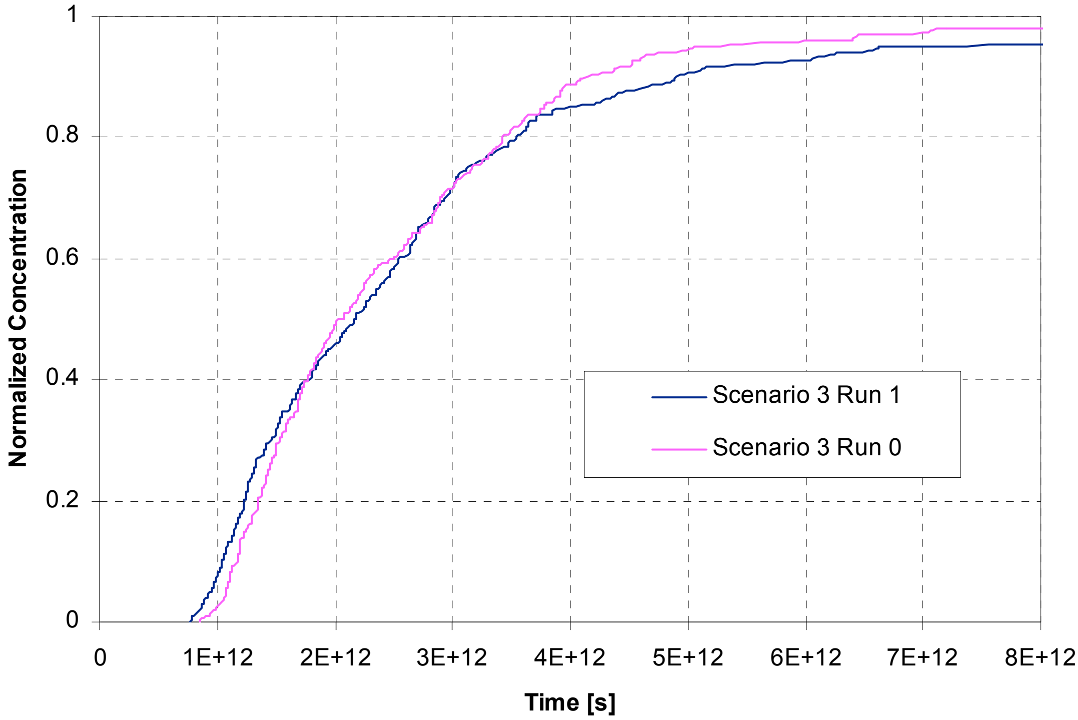

Figure 26.- Scenario 3 Run 1. BTC up to the main fracture (mobile porosity heterogeneous)

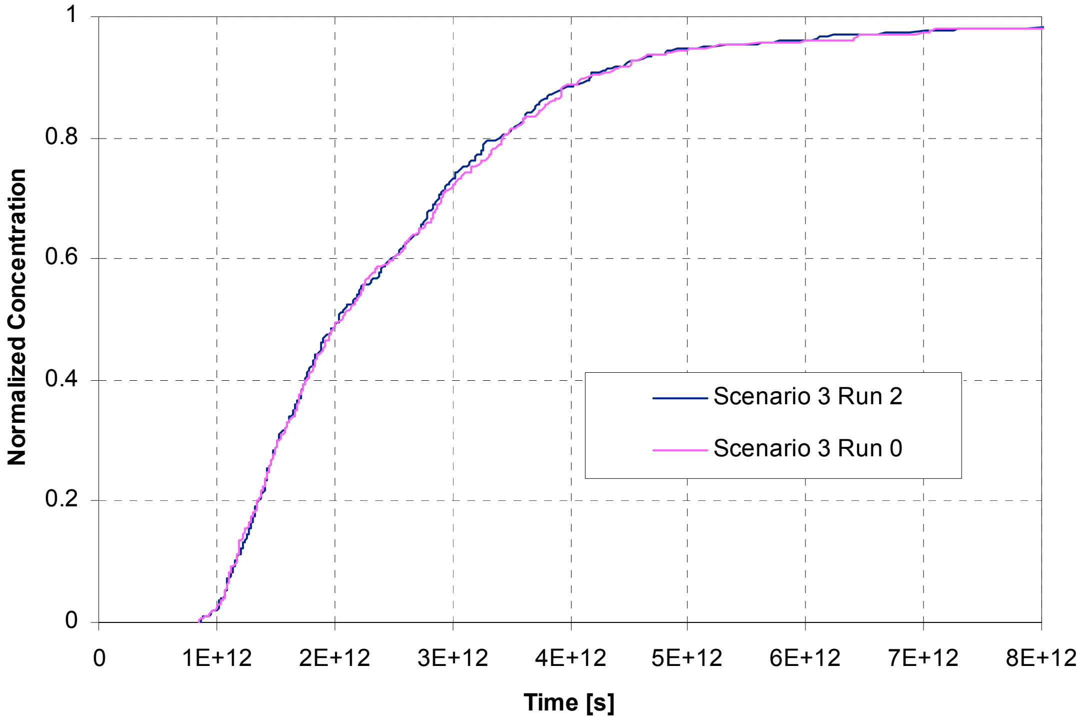

Figure 27.- Scenario 3 Run 2. BTC up to the main fracture (immobile porosity heterogeneous, i.e., matrix porosity heterogeneous)

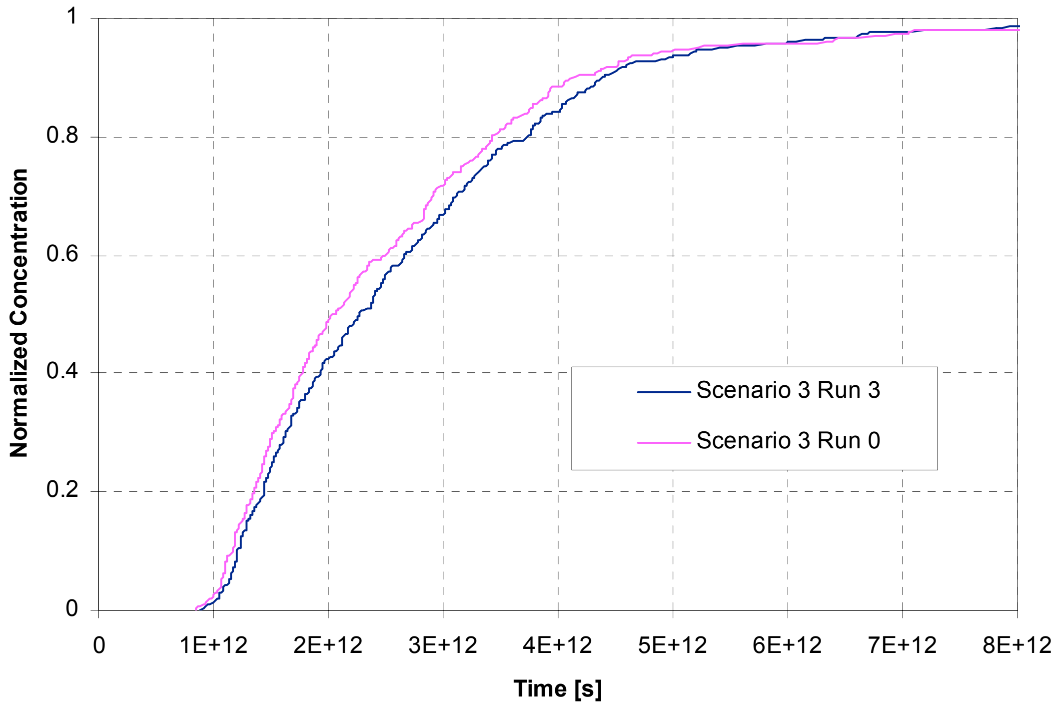

Figure 28.- Scenario 3 Run 3. BTC up to the main fracture (immobile porosity heterogeneous, i.e flow wetted area heterogeneous)

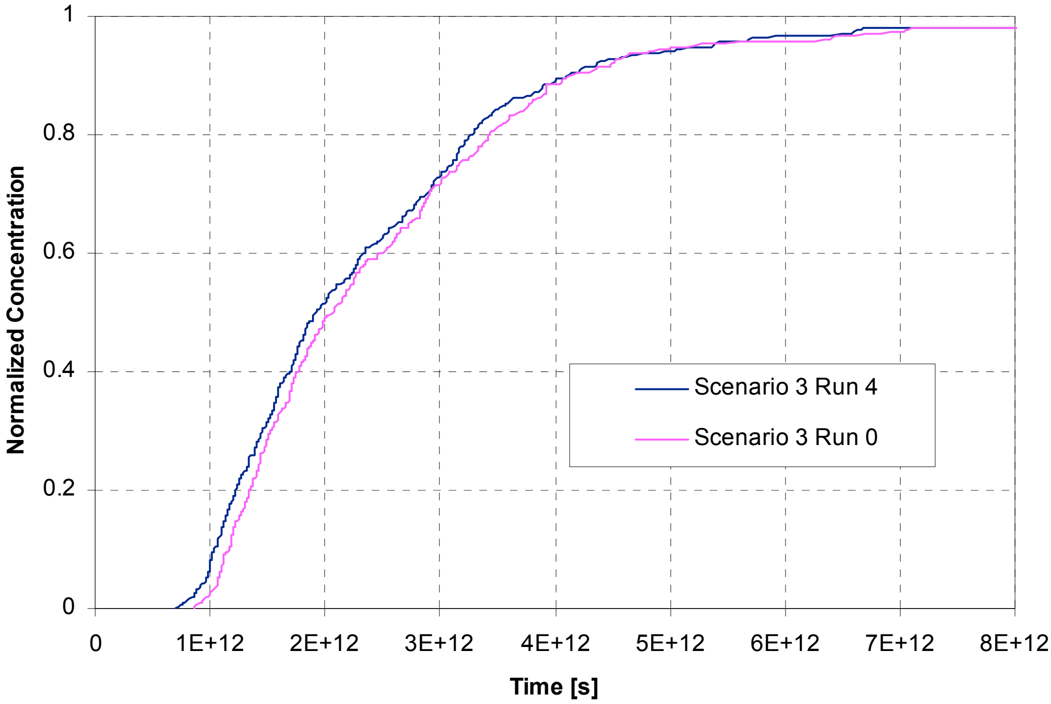

Figure 29.- Scenario 3 Run 4. BTC up to the main fracture (immobile porosity and mass transfer rate heterogeneous, i.e., matrix thickness heterogeneous)

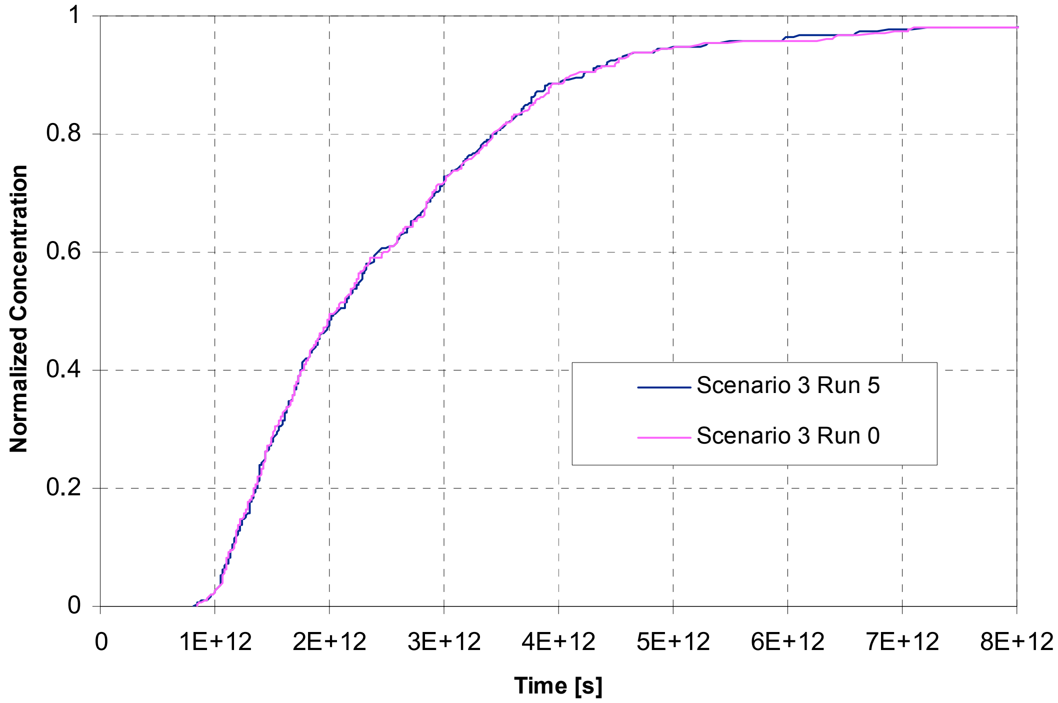

Figure 30.- Scenario 3 Run 5. BTC up to the main fracture (mass transfer rate heterogeneous, i.e water diffusion heterogeneous)

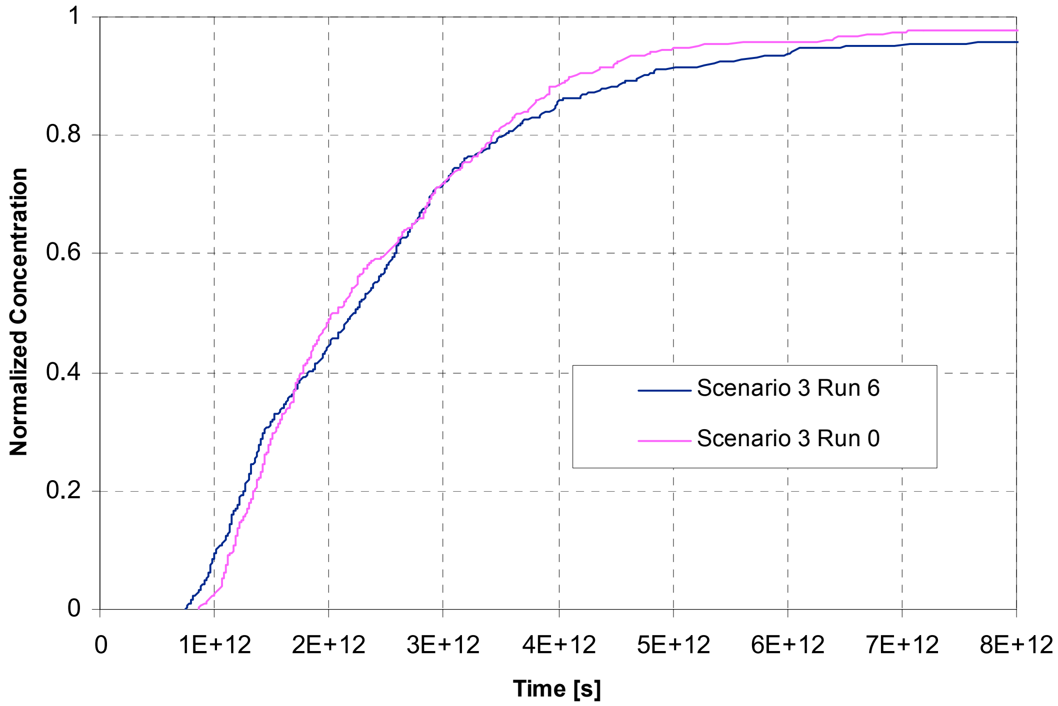

Figure 31.- Scenario 3 Run 6. BTC up to the main fracture (all parameters heterogeneous)

Table 6 shows the initial and final X and Y coordinates of the 10 first particles released. Results for 400 particles have been obtained and reported to ENRESA.

particle No.	x_inital	y_initial	x_final	y_final
1	3130,79705	2153,45817	3204	5800
2	3214,804063	2107,803285	3204	5800
3	2967,12449	2005,561107	3204	5800
4	3045,270093	2029,239309	3204	5800
5	2997,447048	1874,205115	3204	5800
6	3150,879252	1997,846934	3204	5800
7	3076,813021	2049,639999	3204	5800
8	2977,286546	1929,38777	3204	5800
9	2975,499763	1878,617919	3204	5800
10	3065,085491	1992,880023	3204	5800

Table 6.- Initial and final X-Y coordinates of the first 10 release particles

Table 7 shows the distance traveled in the matrix and in the fracture as well as the corresponding travel times for the 10 first particles released for 3 different scenarios. Results for 400 particles have been obtained and reported to ENRESA.

Distances in meters and times in seconds

Scenario 1 run 1				
particle No.	Distance in Matrix	Distance in Fracture	Matrix Time	Fracture Time
1	1729	2883	1,0962E+12	14315000000
2	1650	2989	2,77982E+12	14778500000
3	1625	2857	5,18391E+11	14547700000
4	1807	2715	1,1729E+12	14573600000
5	1768	2989	9,94107E+11	14972300000
6	1888	2907	2,74926E+12	1,38653E+11
7	1656	3038	3,8548E+12	75811900000
8	1735	2901	7,62428E+11	14601100000
9	1768	2889	6,61312E+11	15136600000
10	1755	2835	1,06805E+12	14322800000

Scenario 2 run 3				
particle No.	Distance in Matrix	Distance in Fracture	Matrix Time	Fracture Time
1	1729	2883	1,37025E+12	17893700000
2	1650	2989	3,47477E+12	18473100000
3	1625	2857	6,47989E+11	18184700000
4	1807	2715	1,46613E+12	18216900000
5	1768	2989	1,24263E+12	18715400000
6	1888	2907	3,43657E+12	1,73316E+11
7	1656	3038	4,81851E+12	94764800000
8	1735	2901	9,53035E+11	18251400000
9	1768	2889	8,2664E+11	18920700000
10	1755	2835	1,33506E+12	17903500000

Scenario 3 run 6				
particle No.	Distance in Matrix	Distance in Fracture	Matrix Time	Fracture Time
1	1729	2883	1,73808E+12	20764800000
2	1650	2989	4,27827E+12	20591000000
3	1625	2857	7,50129E+11	22015100000
4	1807	2715	1,62352E+12	30702600000
5	1768	2989	1,37092E+12	24997700000
6	1888	2907	3,96929E+12	2,56773E+11
7	1656	3038	5,22705E+12	98739200000
8	1735	2901	1,35515E+12	20431500000
9	1768	2889	9,70428E+11	28539500000
10	1755	2835	1,69117E+12	20384600000
1	1729	2883	1,73808E+12	20764800000
2	1650	2989	4,27827E+12	20591000000

Table 7.- Pathlines lengths and travel times. Scenario 1 Run 1- Scenario 2 Run 3 – Scenario 3 Run 6

4.- Flow and transport upscaling

In this chapter different alternatives for flow and transport upscaling in the granite reference case are used. Results show that acceptable results can be obtained when the appropriate upscaling techniques are applied

For the flow and transport simulations at the fine scale in this section, the same parameter definition used in the previous section are considered. More precisely when only advective transport is simulated, the parameters from scenario 2 run 3 are used but setting the local dispersion to zero; when advective and dispersive transport is simulated, the parameters from scenario 2 run 3 are used; and when advective and dispersive and matrix diffusion transport is simulated the parameters from scenario 3 run 6 are used. In all cases, we have considered the runs corresponding to heterogeneous flow and transport parameters over the entire aquifer.

4.1.- Upscaling geometry

The original field of 440 by 640 cells is upscaled into a coarser model of 44 by 64 blocks. The numerical model is thus reduced two orders of magnitude. Figure 50 shows the underlying fine scale hydraulic conductivity model and the overlaid upscaled model.

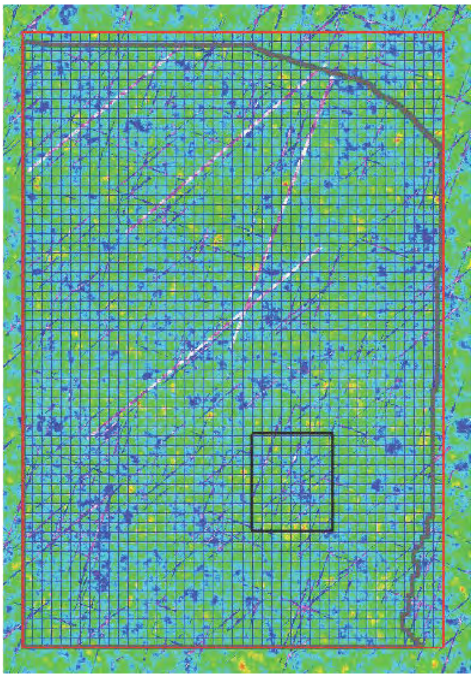

Figure 32.- Geometry of the upscaled model

4.2.- Flow upscaling

When upscaling flow, the objective is to preserve the total flow crossing the sides of the coarse scale model blocks.

We compared the results using very simple averaging of the conductivity values within the block, namely, arithmetic, geometric and harmonic averages of the cell values within the block were used as block conductivities.

Of all three averaging proposals, the geometric mean, which is know to be appropriate for mildly heterogeneous lognormal fields with isotropic heterogeneity, is the one that gives best results, yet, far from acceptable.

Figure 33 shows the comparison of the flows across all block faces in the upscaled model with respect to the flows computed through the same faces at the fine scale for the geometric average case.

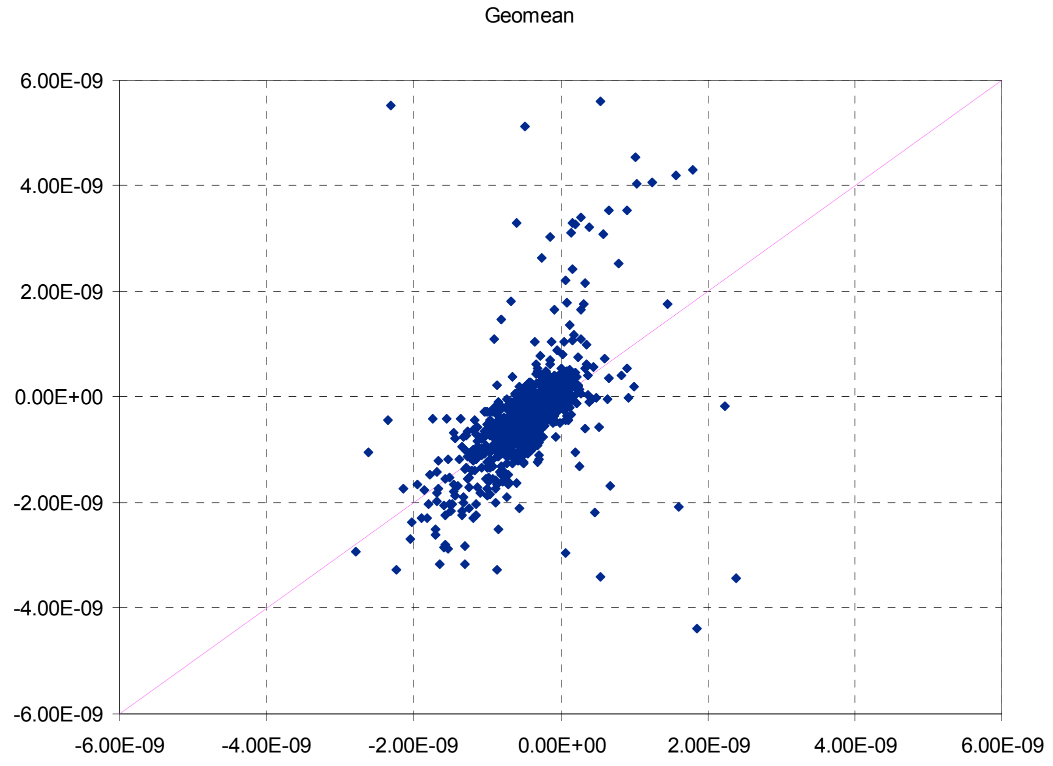

Figure 33.- Coarse scale (x-axis) vs. fine scale (y-axis) fluxes through block interfaces, when the geometric mean of cell values is used as the block conductivity.

Next, we use a more elaborate upscaling technique. The one formally know as Laplacian with skin, in which each block is isolated along a skin of cells surrounding it, and then the groundwater flow equation is solved for different piezometric head gradients.

In its simplest, and most common, implementation, only a diagonal tensor is sought, assuming that all blocks can be represented with a tensor, the principal directions of which are parallel to the Cartesian axes. Figure 34 shows the Kxx and Kyy components of the block conductivity tensor.

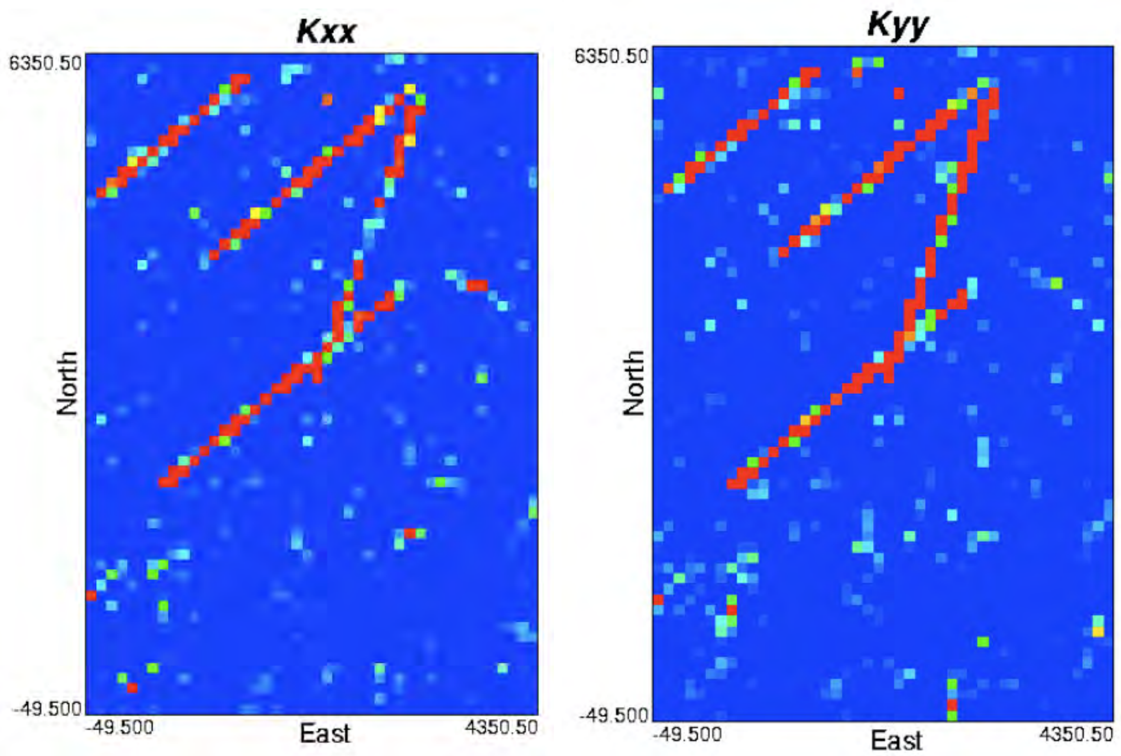

Figure 34.- Kxx and Kyy components of the block conductivity tensor

This approach, the results of which are shown in Figure 35, improves the results obtained with the geometric mean, but only slightly. It is clear that the cloud of points in the Figure 35 is tighter about the diagonal than in Figure 33, but still, the high flows observed at the fine scale are clearly underestimated.

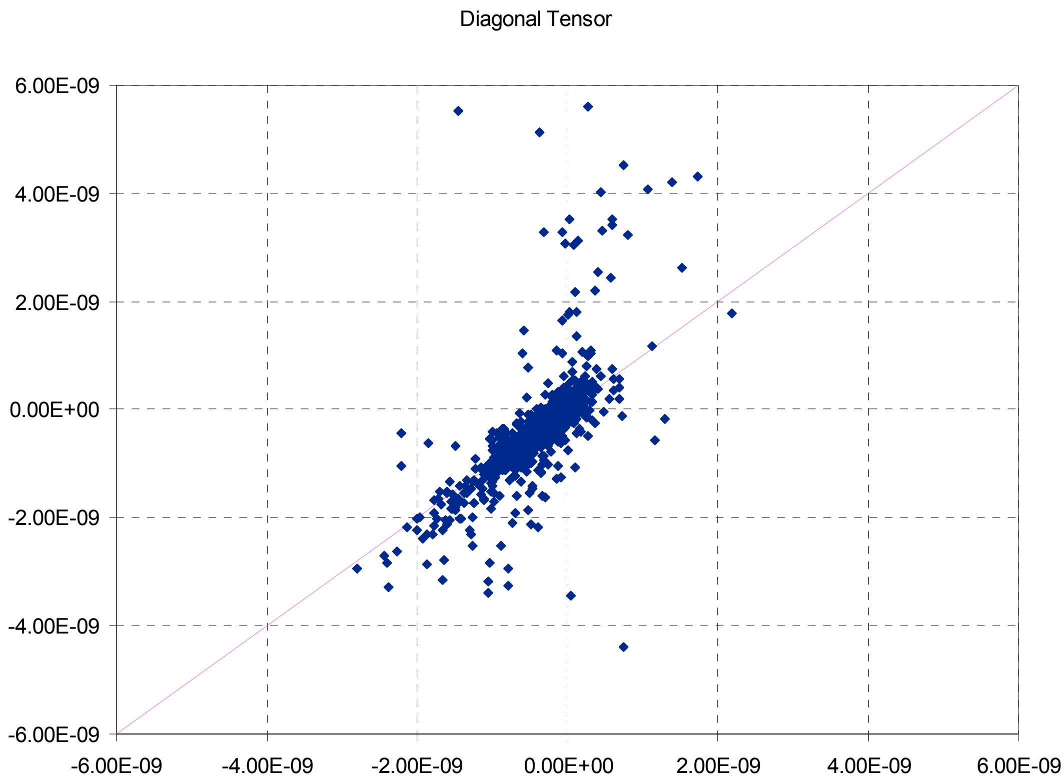

Figure 35.- Coarse scale (x-axis) vs. fine scale (y-axis) fluxes through block interfaces when a diagonal tensor is computed from the cell values

When we refine the computation and consider that the block has to be represented by a full tensor, then the results are dramatically improved, with the exception of a few block interfaces. These results can be seen in Figure 36. It is clear that in a fractured field, in which the fractures are not aligned with the Cartesian axes, the block conductivity must be modeled as a tensor to capture the influence of the fractures in the flow response.

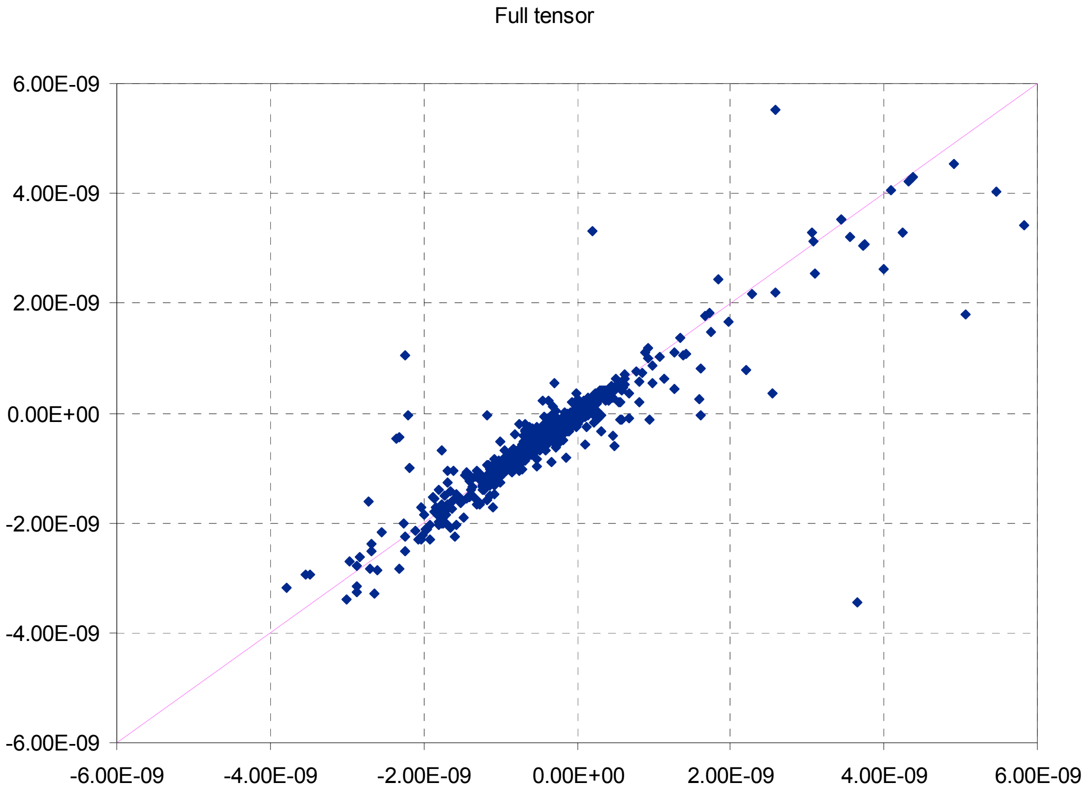

Figure 36.- Coarse scale (x-axis) vs. fine scale (y-axis) fluxes through block interfaces when a full tensor is computed from the cell values

In conclusion, when performing flow upscaling in a fractured media, it is essential to use a Laplacian approach aiming to compute full tensor conductivity values for each upscaled block.

4.3. Transport upscaling.

Two sets of transport simulations have been performed. The first set of simulations considers that particles are released uniformly through the entire repository, in this set three cases are modeled, the first case includes only advection, the second case includes advection and local dispersion, and the third case includes advection, local dispersion and matrix diffusion. The second set of simulations considers the repository divided onto nine equal-sized zones and particles are released uniformly from each of the zones.

For all sets and all cases the same tensor conductivities obtained in the flow upscaling section are retained, since the type of transport processes being modeled does not influence flow upscaling.

For all sets and all cases, the BTCs up to the fracture and up to the north boundary have been computed, the time taken in the main fracture is an order of magnitude or less than up to the fracture. Only the BTCs up to the fracture are displayed.

4.3.1. Release through the entire repository

4.3.1.1. Advective transport only

The first step is to simulate flow and transport at the fine scale. Figure 37 shows the paths followed by the particles released uniformly through the repository.

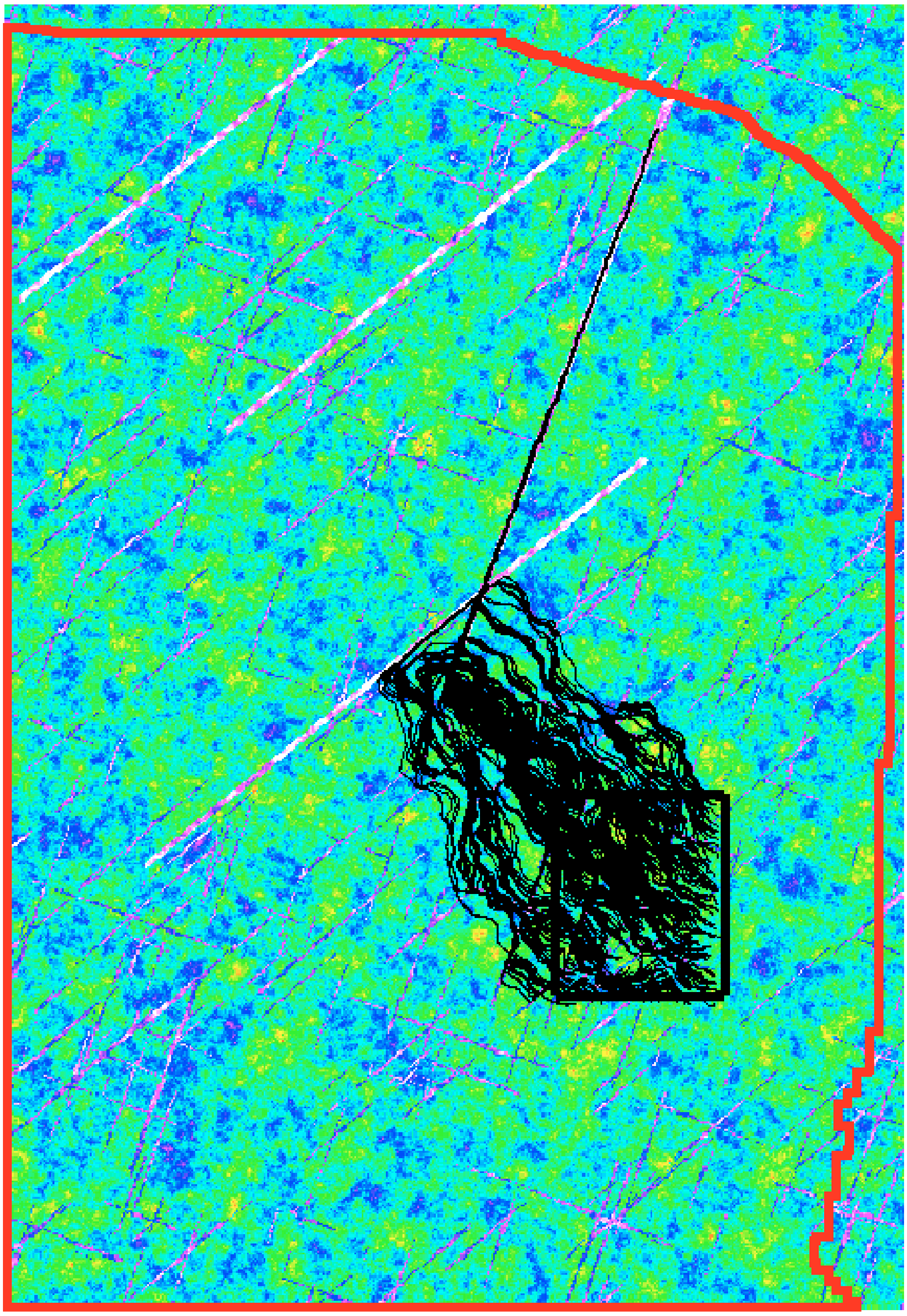

Figure 37.- Particle paths as released from all zones (Advection)

If purely advective transport is simulated with the coarse conductivities computed after flow upscaling the resulting particle paths are displayed in Figure 38. We can notice the step-wise approximation of the paths along the inclined main fracture that acts as a sink, induced by the coarse discretization.

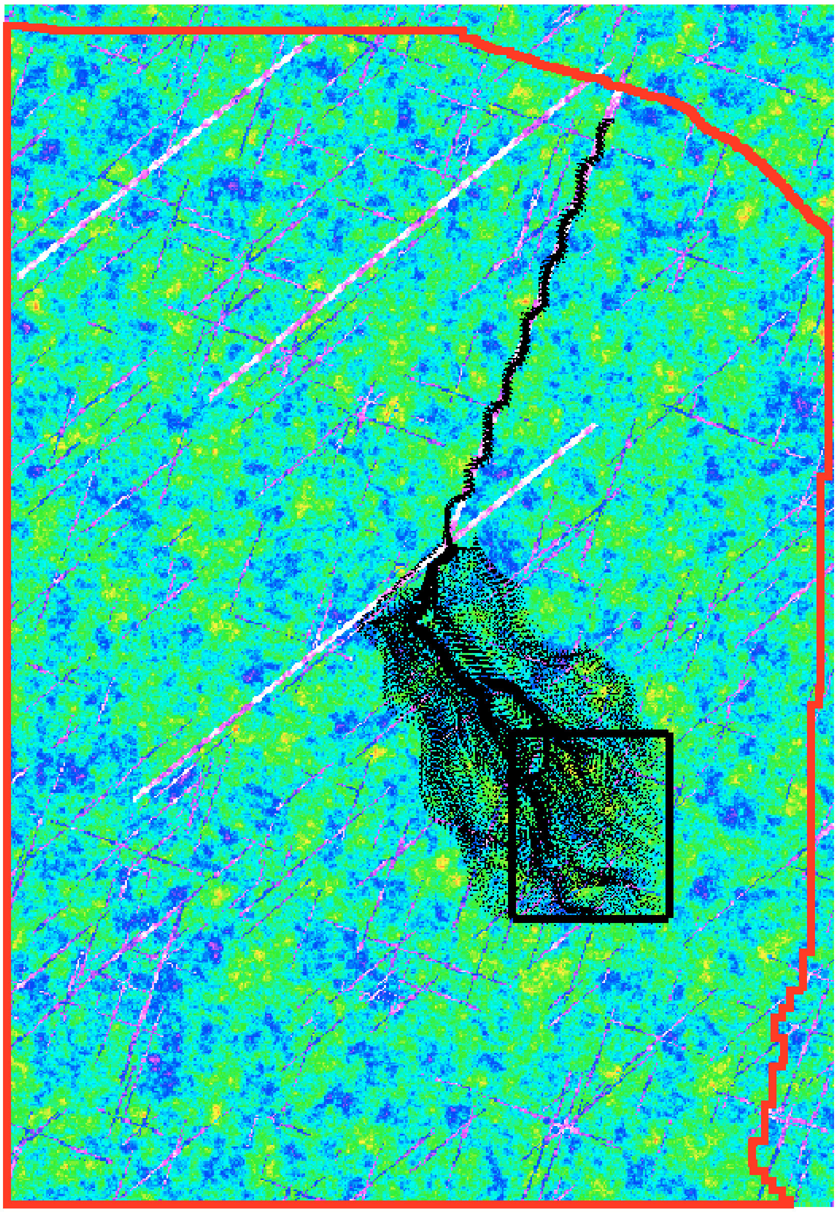

Figure 38.- Particle paths as released from all zones (upscaled the advection+dispersion model)

Figure 39 shows the breakthrough curves (up to the fracture) from the fine scale model and the coarse scale simulation with only flow upscaling. It can be noticed that just flow upscaling fails in capturing the long tailing of the BTC in the fine scale, with a small overestimation of the early arrival times.

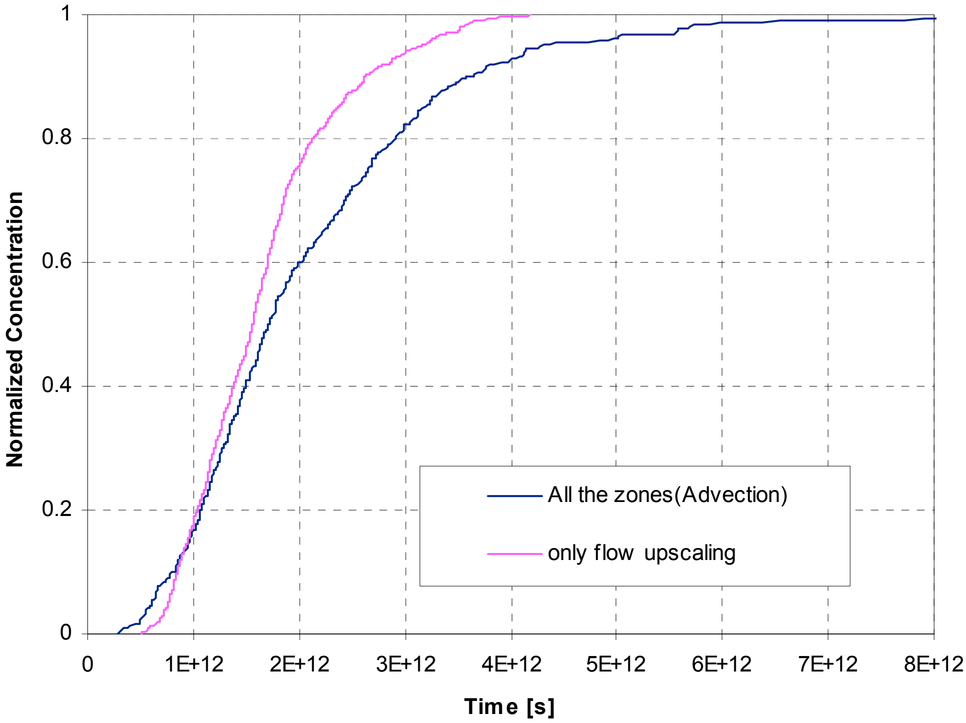

Figure 39.- BTCs from the fine scale model and the coarse scale simulation with only flow upscaling

In order to capture the enhanced tailing in the fine scale simulation there is a need to introduce some mechanism to induce some retardation in the particle travel ties that cannot be introduced just by considering a rigorous flow upscaling with generic full tensor conductivities.

This enhanced tailing can be introduced adopting the upscaling method proposed by Fernàndez-Garcia et. al [5]. In their approach, they propose to use the advection-dispersion equation with an additional sink-source term to account for mass transfer in and out of fictitious immobile zones at the coarse scale. The loss of resolution at the coarse scale is supplanted by these immobile zones, which try to mimic the variation in velocity of the particles as they traverse the coarse model blocks.

To determine the parameters defining these fictitious immobile zones, a local transport problem is solved for each of the coarse blocks. Each coarse block is isolated and transport is solved at the fine scale, the residence times of the particles as they cross the coarse block are recorded and then the best parameters for a mass transfer model with two immobile zones are determined. More precisely, values for the porosities, and the mass transfer rates of both immobile zones are determined (for this reason the approach is termed the “double-rate” model).

Figure 40 shows the BTCs for the fine scale simulation, flow upscaling only, and combined flow and transport upscaling. When transport upscaling is considered the tail is better reproduced although, conversely, some retardation for the earlier times produces a poor reproduction of the earlier times. The fictitious immobile zones included in the model help inducing a long tailing but at the same time introduce too much retardation.

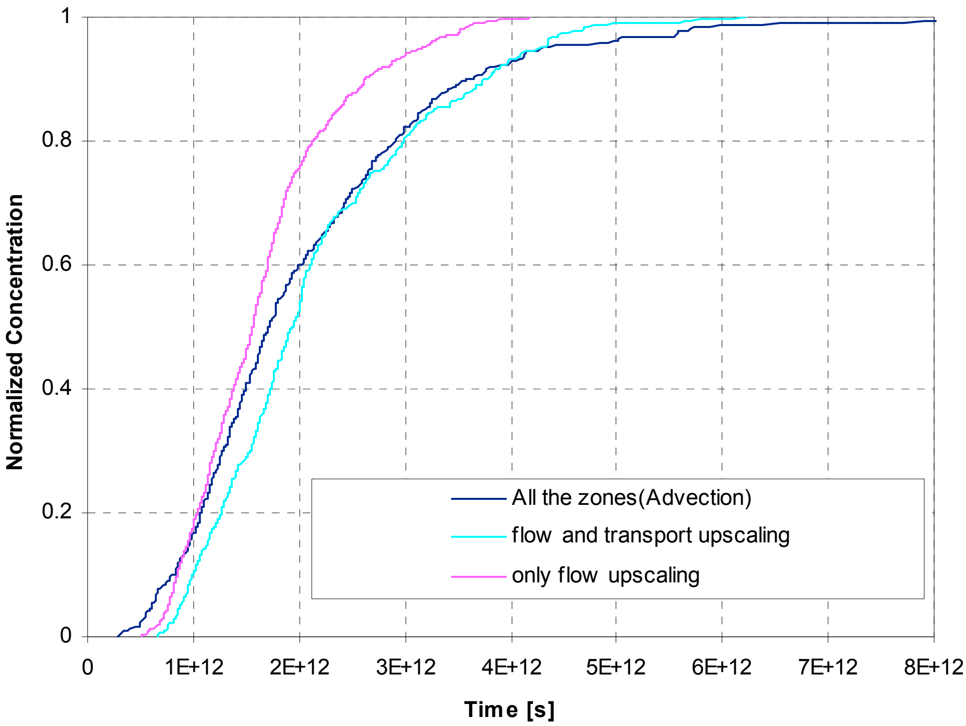

Figure 40.- BTCs for the fine scale simulation, flow upscaling only, and combined flow and transport upscaling

4.3.1.2 Advective and dispersive transport

The same exercise is repeated including local dispersion at the fine scale. More precisely, a constant longitudinal dispersivity of 0.2 m and a transversal dispersivity of 0.02 m is considered in all cells not corresponding to a fracture.

Figure 41 shows the BTCs for both simulations at the fine scale. As noticed the differences are minimal. Inclusion of local dispersion does not change the overall transport behavior of the study area.

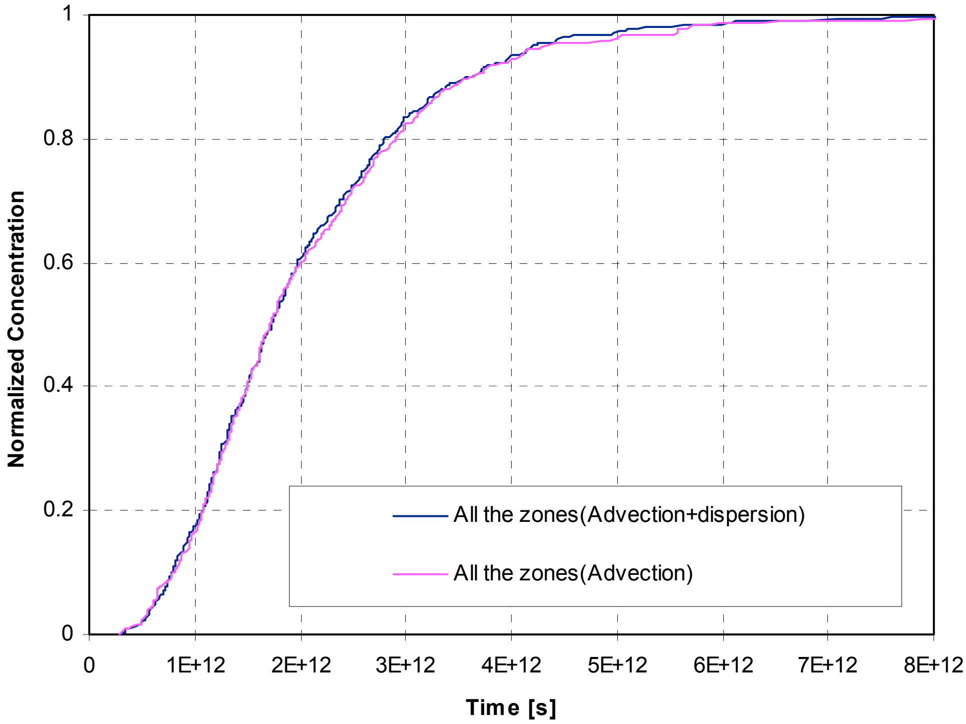

Figure 41.- BTCs considering advection and advection+dispersion at the fine scale

As in the previous case, simulation at the coarse scale is simulated considering only advection (i.e., only flow upscaling), the resulting BTC is shown in Figure 42. And then, transport upscaling using the double-rate mass transfer model is performed resulting in the BTC shown in Figure 43.

The same commentaries as before apply here: flow upscaling underestimates the tail, and flow and transport upscaling overestimates the early arrival times.

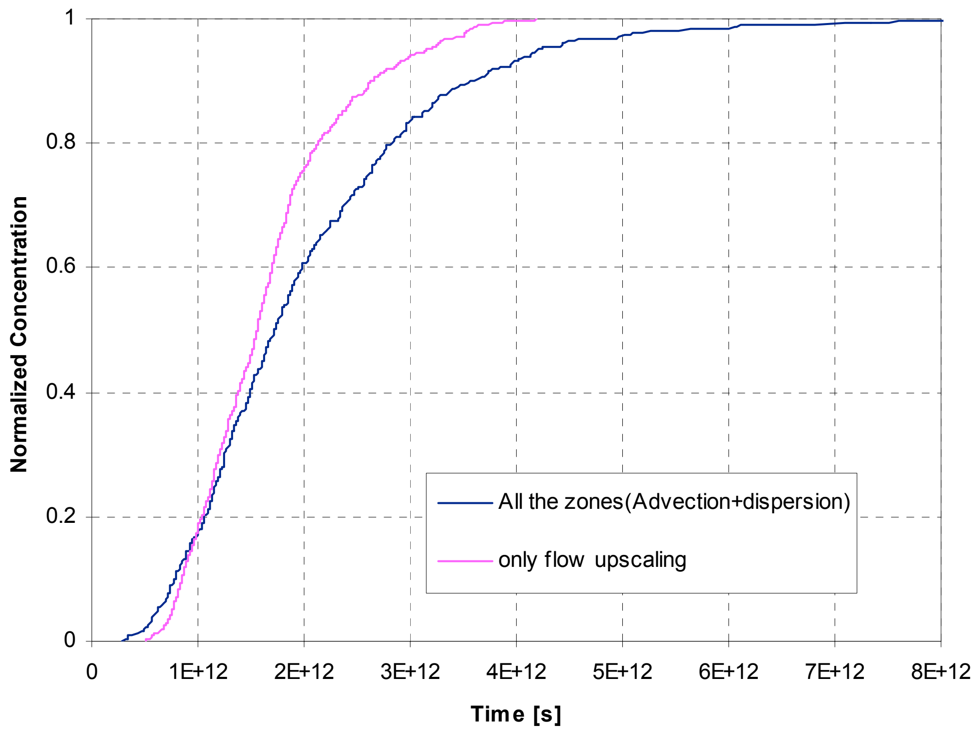

Figure 42.- BTCs at the coarse scale simulated considering only advection

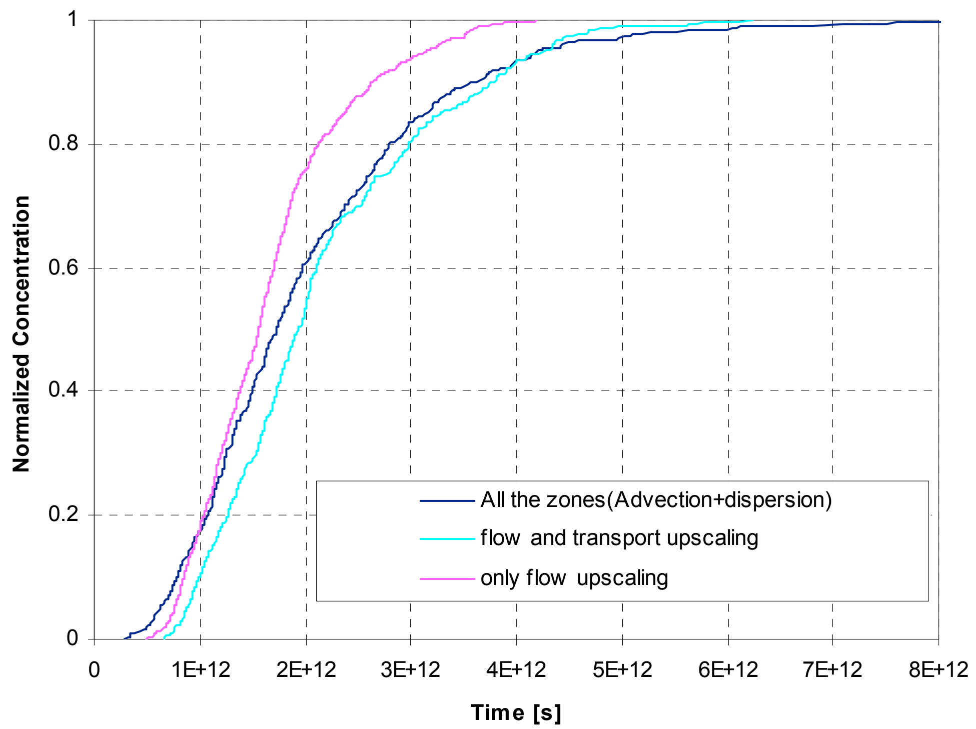

Figure 43.- BTCs for the transport upscaling method using the double-rate mass transfer model

4.3.1.3 Advective and dispersive transport with matrix diffusion

For this simulation all parameters listed in Scenario 3 run 6 in the previous section have been considered as heterogeneous at the fine scale. Local dispersion is also included in the non-fracture cells. The difference with the results in the previous section is that here particles are released over the entire repository whereas there only from the central zone out of nine equal-sized zones are released.

Figure 44 shows the BTCs from the advective-dispersive transport and the advective-dispersive transport with matrix diffusion. Matrix diffusion induces some retardation in the particle travel times as reflected in the graph.

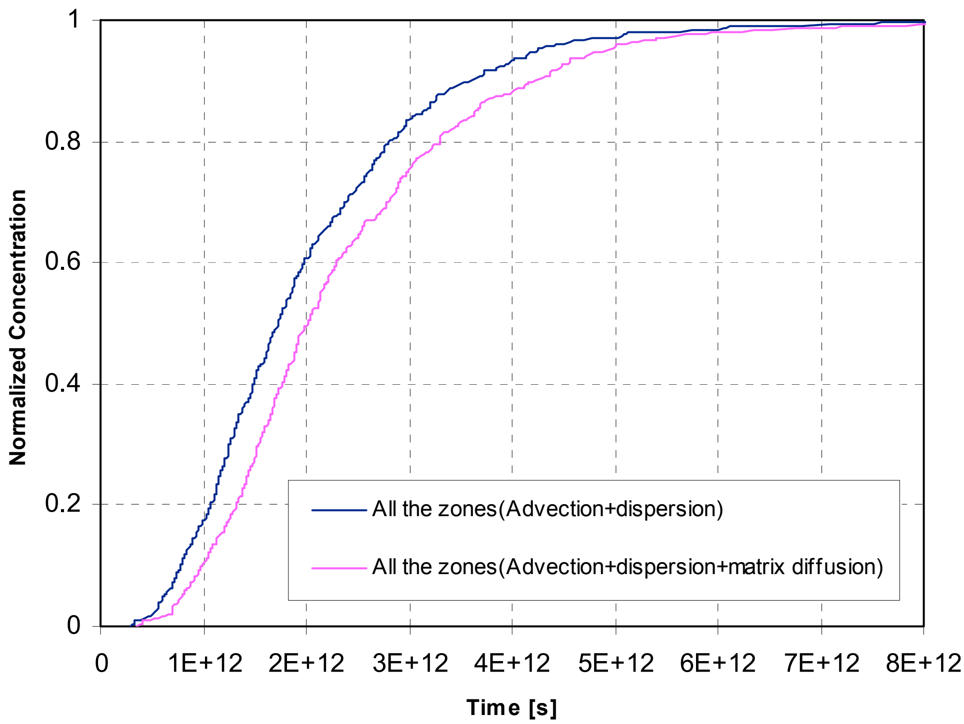

Figure 44.- BTCs computed from the dispersion and matrix diffusion

Figure 45 shows the comparison of the fine scale simulation and the coarse upscale simulation considering only flow upscaling. The coarse scale BTC when only flow upscaling is considered is the same as the one in the previous two cases, since flow upscaling cannot take into account the presence or not of a mass transport process such as matrix diffusion. The net result is that, now advective transport at the coarse scale underestimates clearly all travel times.

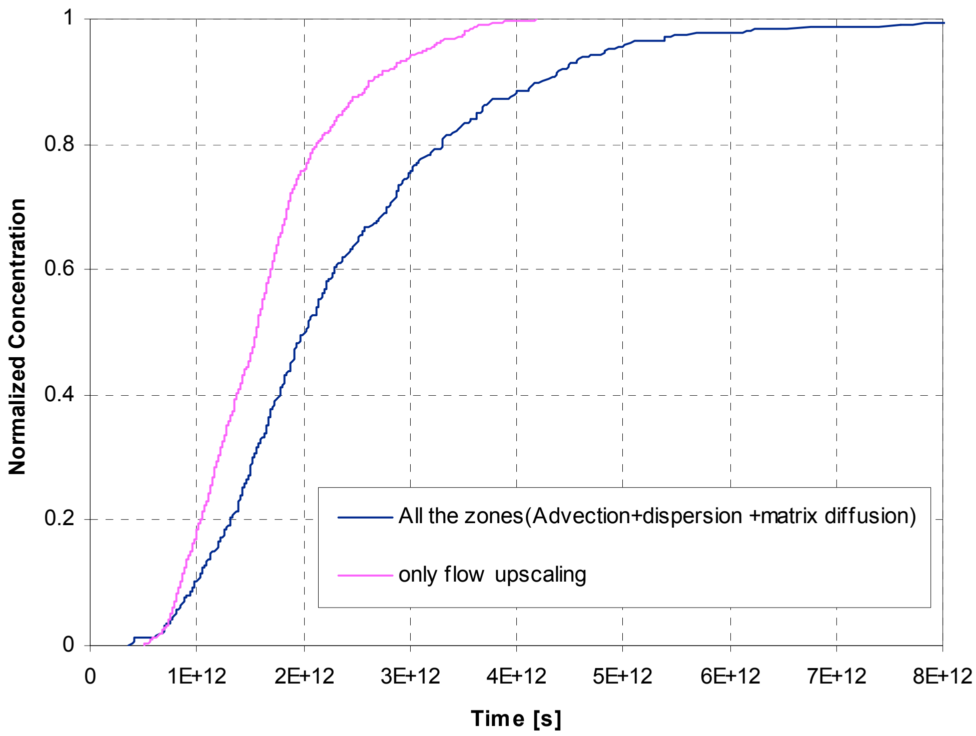

Figure 45.- BTCs computed at the fine scale and at the coarse scale considering flow upscaling (all the zones).

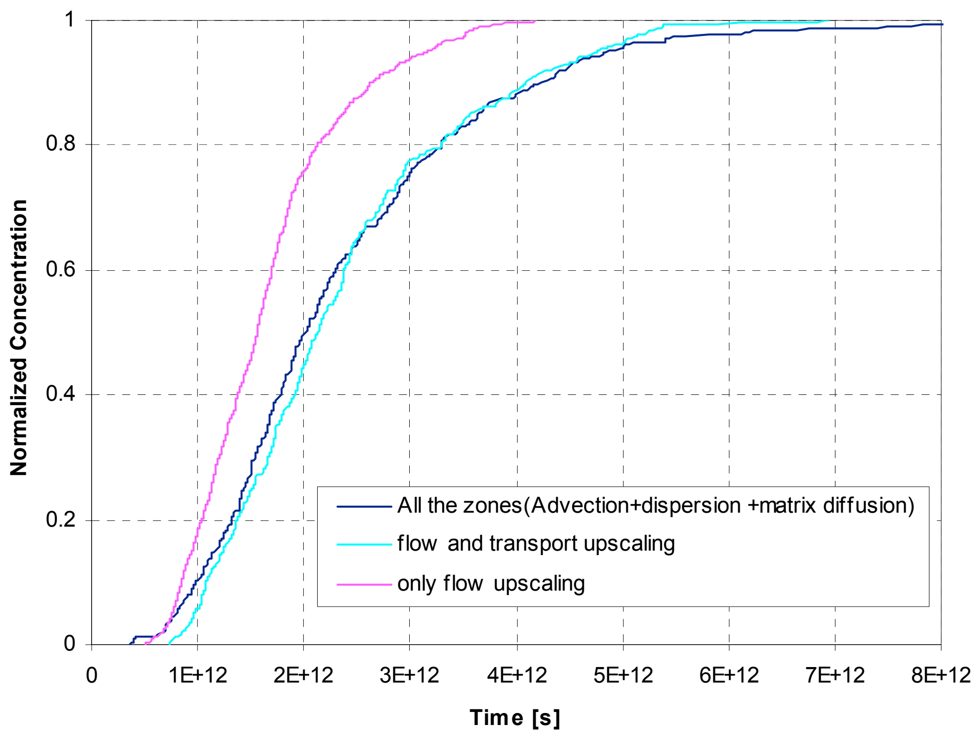

Figure 46.- Comparison of BTCs including the fine scale, the coarse scale with only flow upscaling, and the coarse scale with both flow and transport simulation models

Figure 46 shows a comparison of BTCs including the fine scale, the coarse scale with only flow upscaling, and the coarse scale with both flow and transport simulation models.
It can be seen the importance of accounting for transport upscaling in order to reproduce the fine scale results.

4.3.2 Zone releases

In this section, the upscaling parameters obtained in the previous case have been used to analyze how well they work in predicting more local transport predictions. Now, the breakthrough curves do not correspond to the particles released through the entire repository but through each of nine equal-sized zones in which the repository is compartmentalized. Two cases are analyzed, considering just advection, and considering advection and local dispersion.
For the purposes of analyzing upscaling, only the advective-dispersive results at the fine scale are considered, since, as it will be shown, local dispersion at the fine scale has very little impact in the BTCs.
Figures 47 *to* 55 show the particle paths for the releases from the nine zones when only advective transport is considered at the fine scale.
Figures 56 *to* 64 show the particle paths for the releases from the nine zones when advection and local dispersion are considered. The two sets of figures are very similar, the most noticeable difference being that some of the particles, when dispersion is considered, escape the highest conductivity flow channels at those locations where the channel has a slightly reduced conductivity or where the local gradient is not so pronounced along the channel. In any case, only one or two particles in a few cases display this behavior.

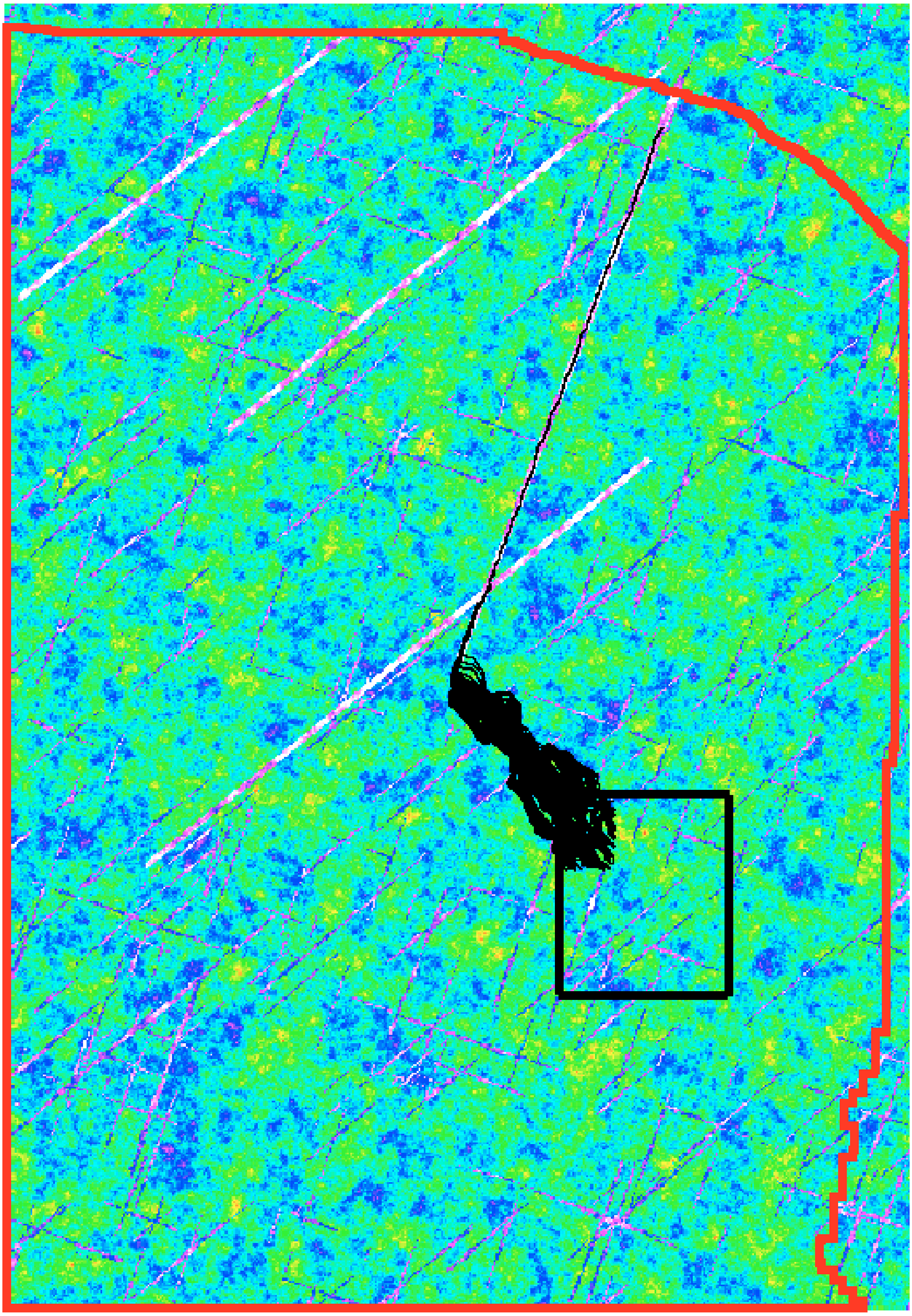

Figure 47.- Particle paths as released from zone 1 (only Advection)

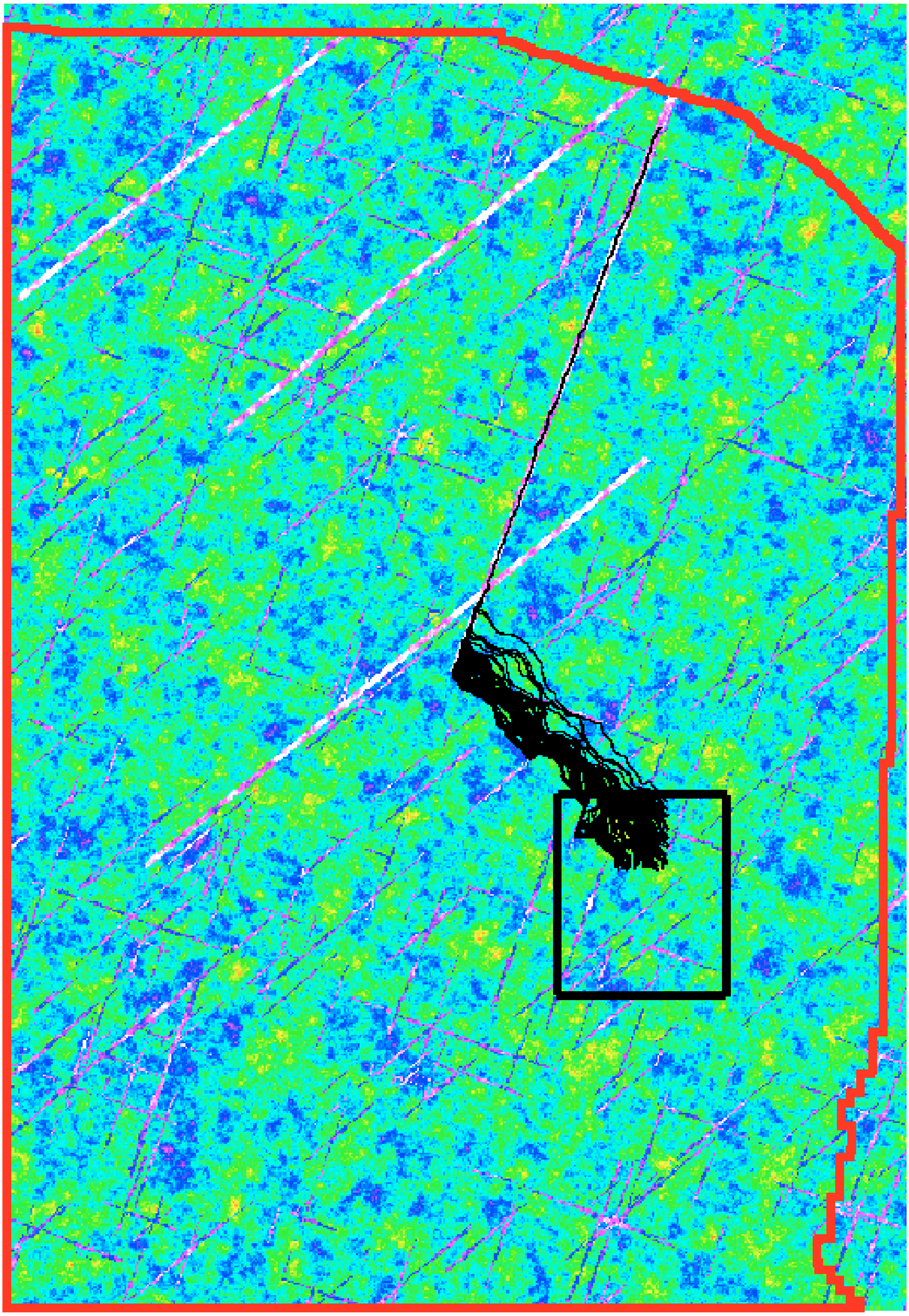

Figure 48.- Particle paths as released from zone 2 (only Advection)

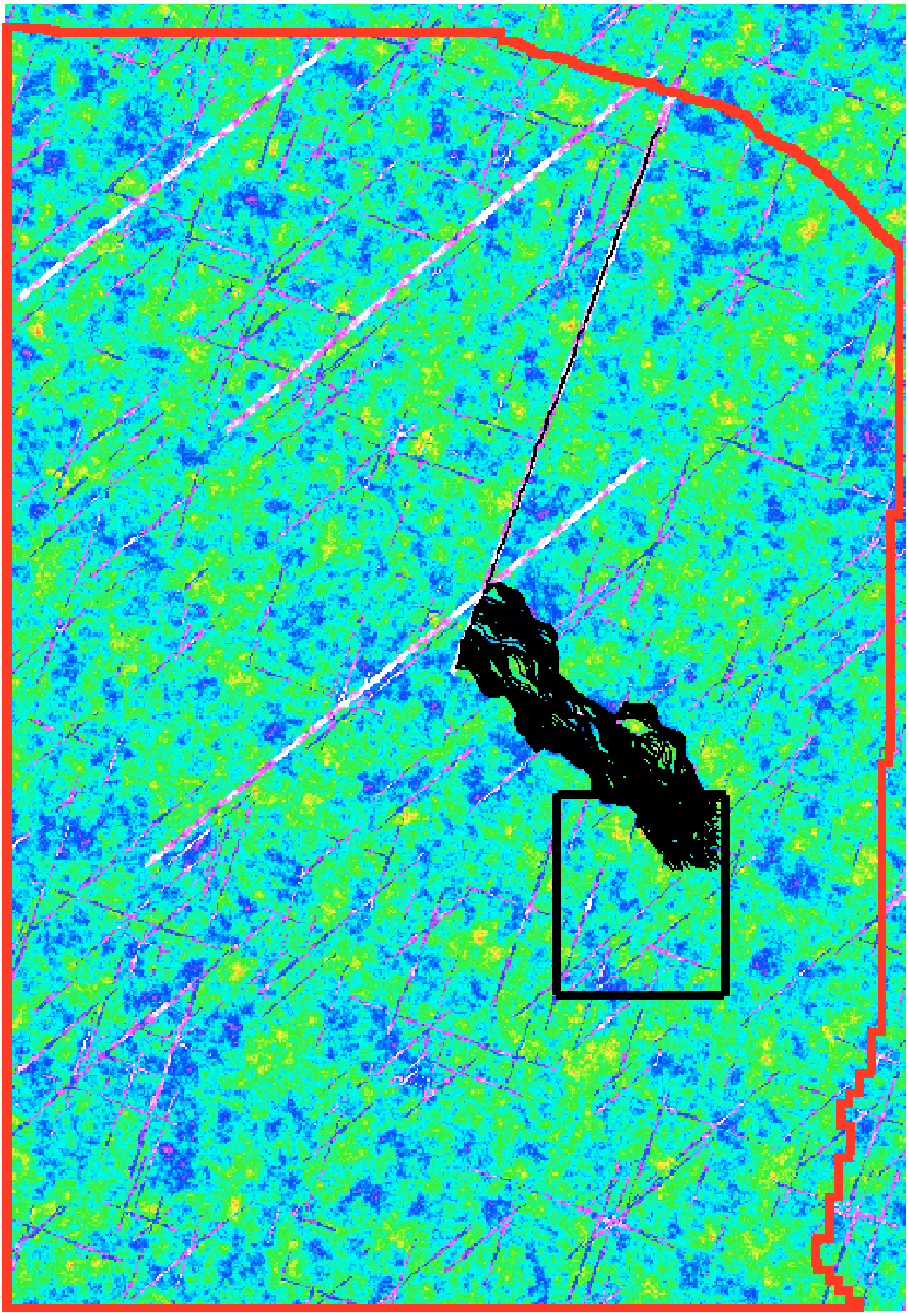

Figure 49.- Particle paths as released from zone 3 (only Advection)

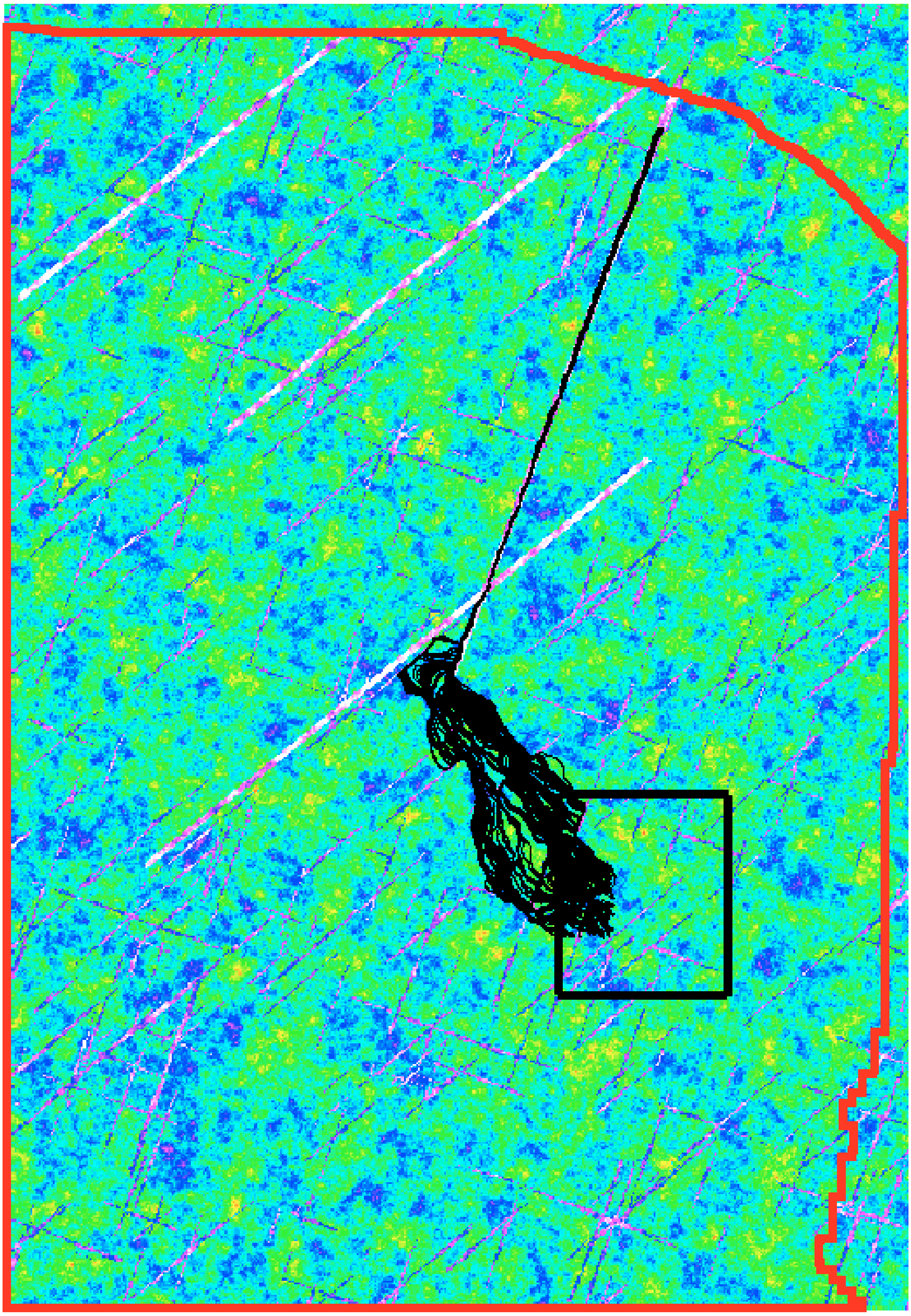

Figure 50.- Particle paths as released from zone 4 (only Advection)

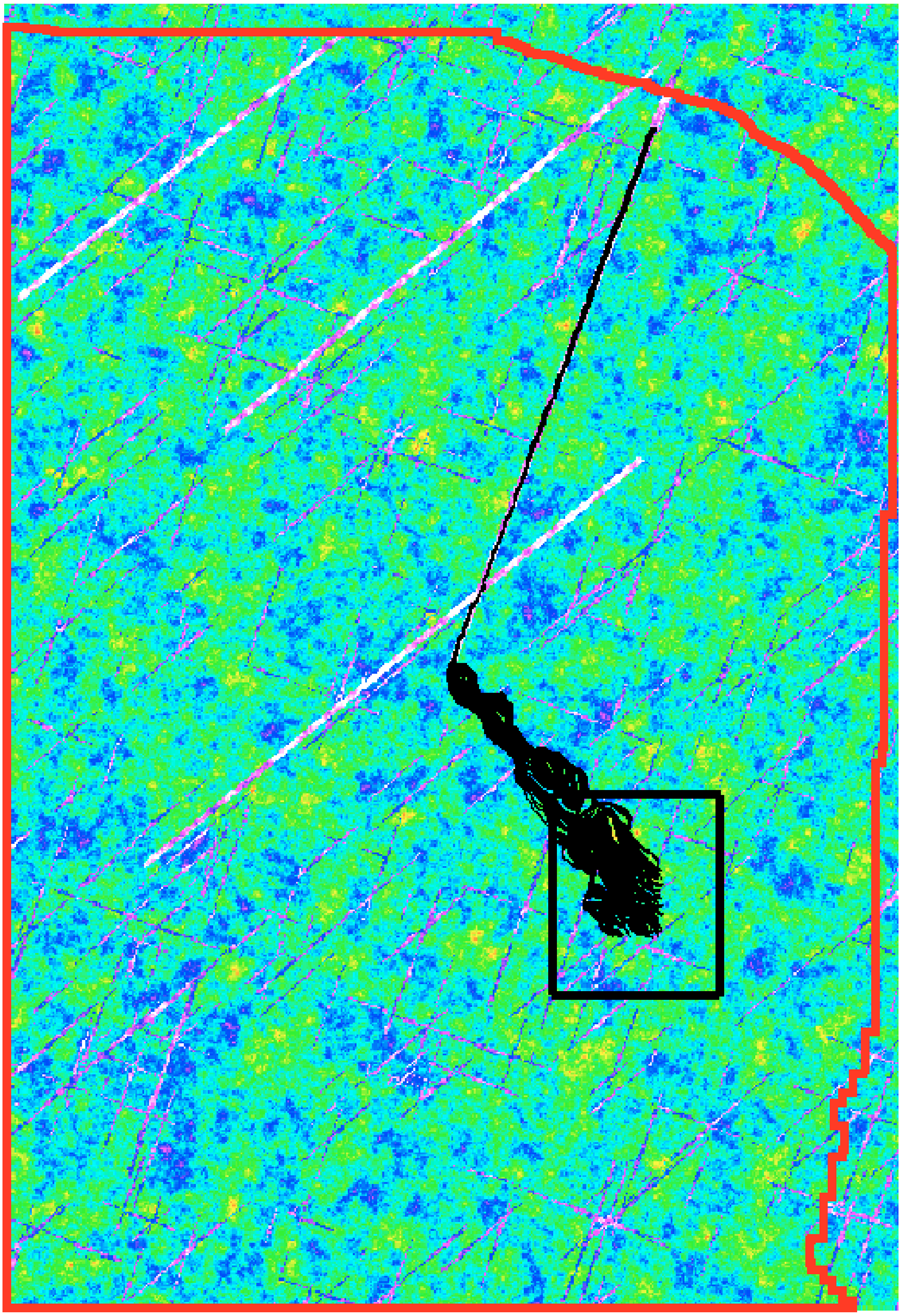

Figure 51.- Particle paths as released from zone 5 (only Advection)

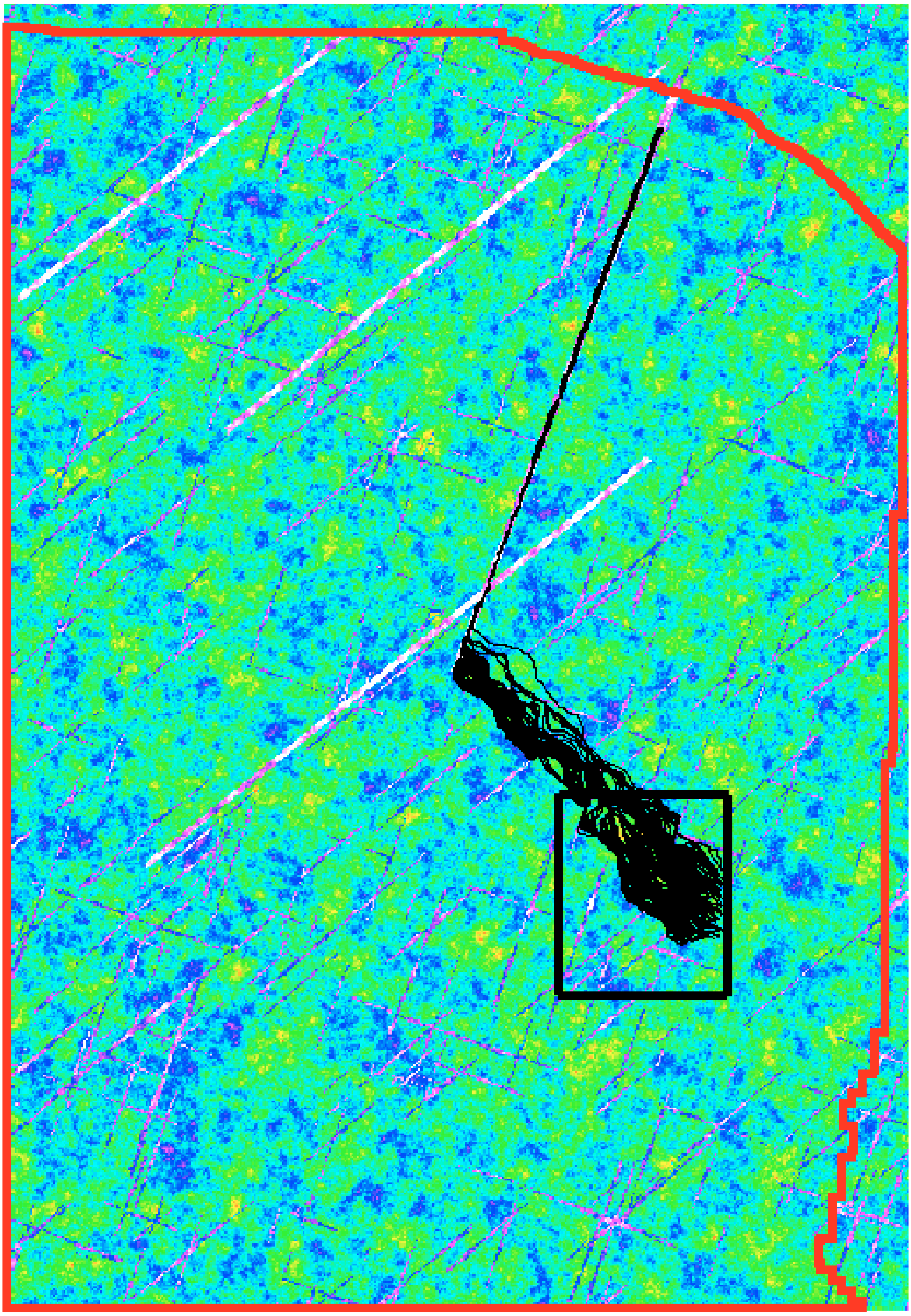

Figure 52.- Particle paths as released from zone 6 (only Advection)

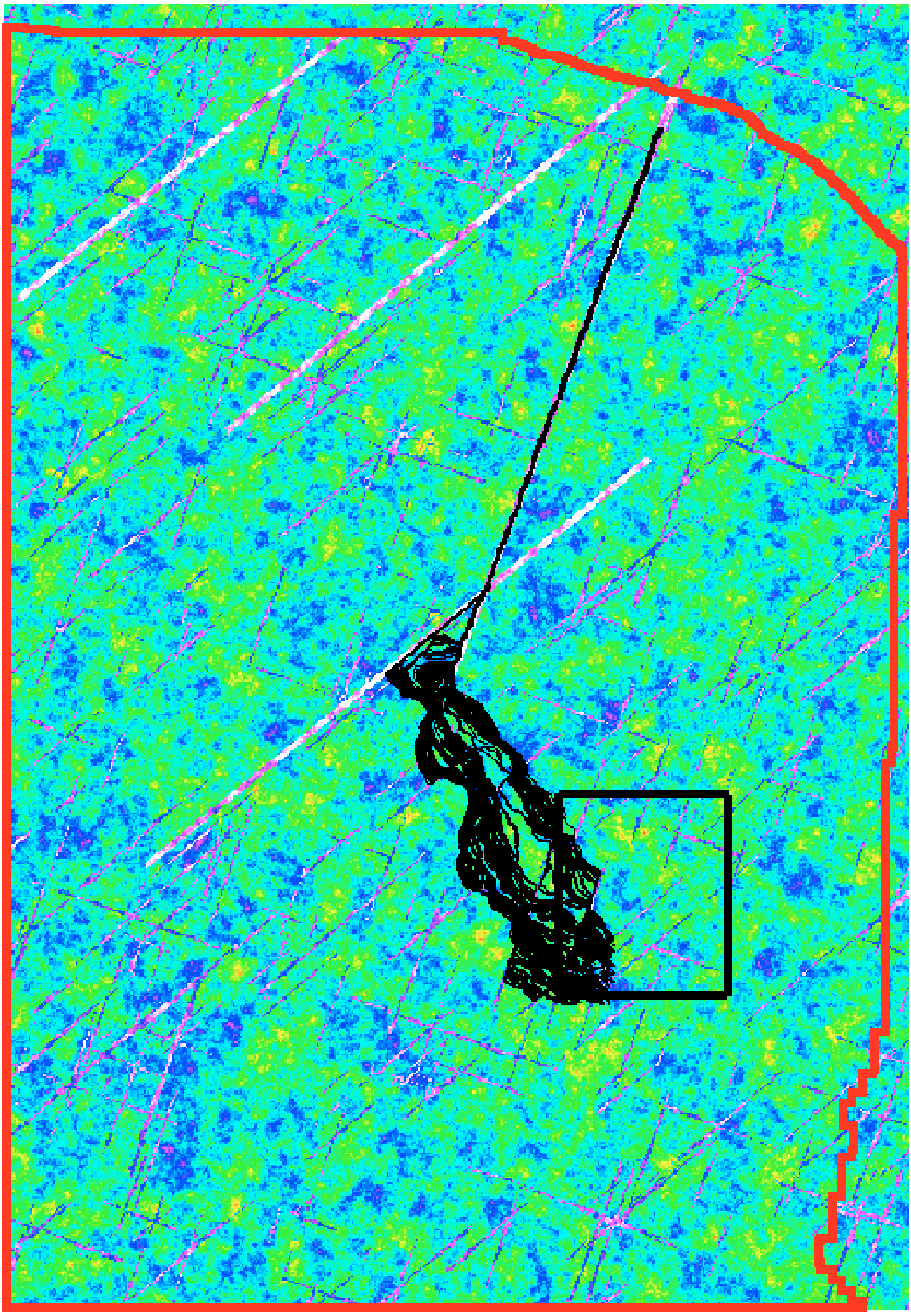

Figure 53.- Particle paths as released from zone 7 (only Advection)

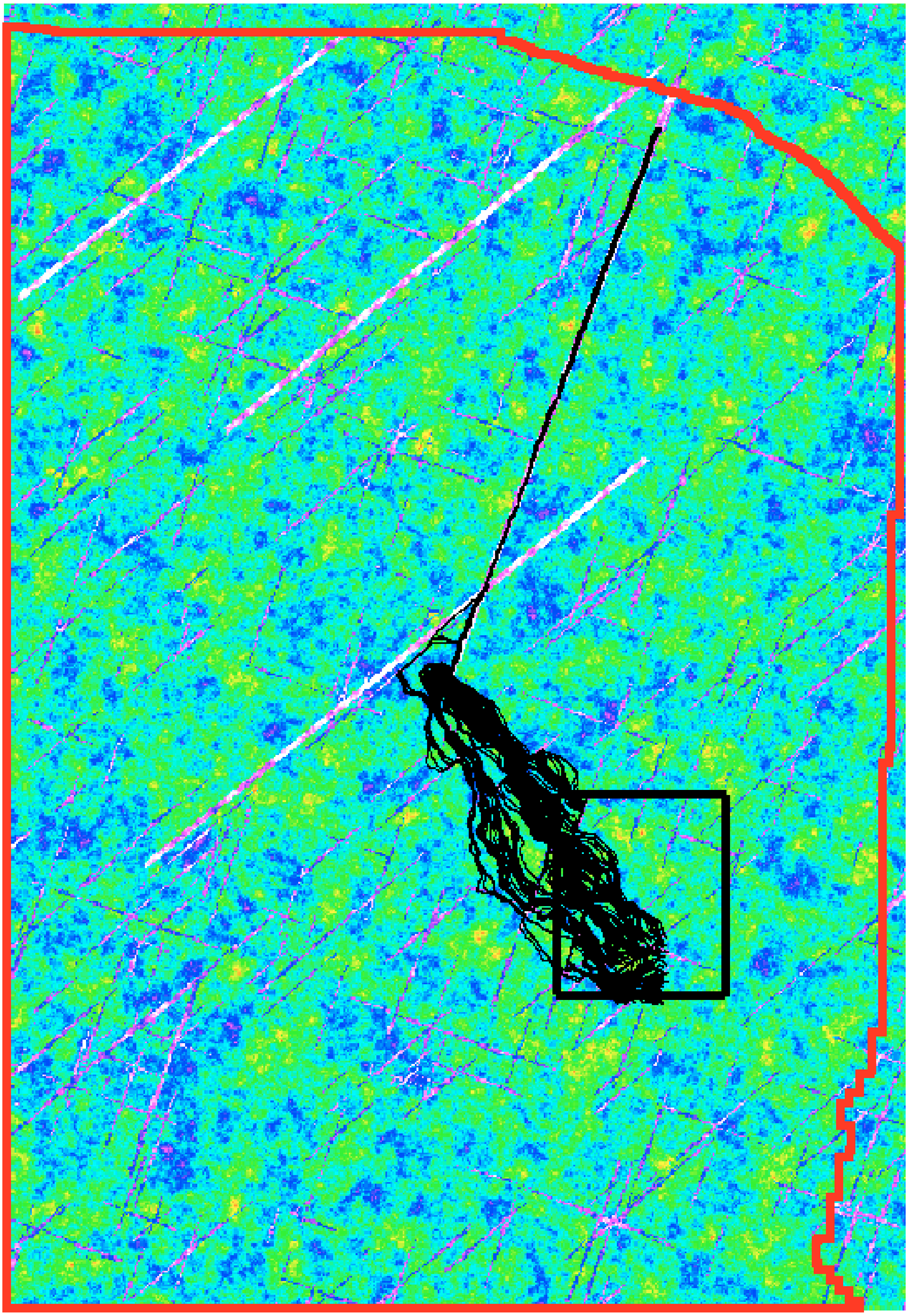

Figure 54.- Particle paths as released from zone 8 (only Advection)

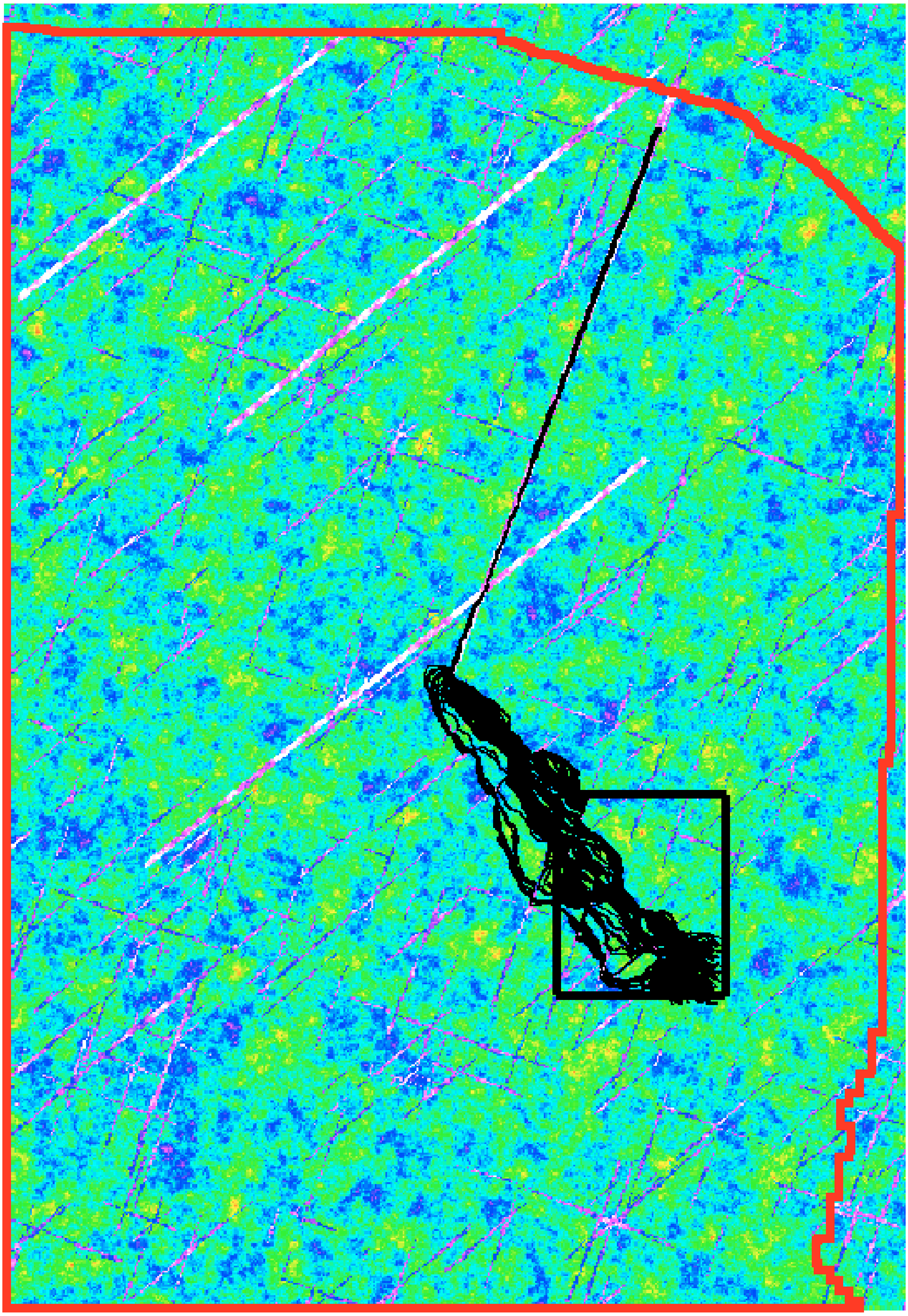

Figure 55.- Particle paths as released from zone 9 (only Advection)

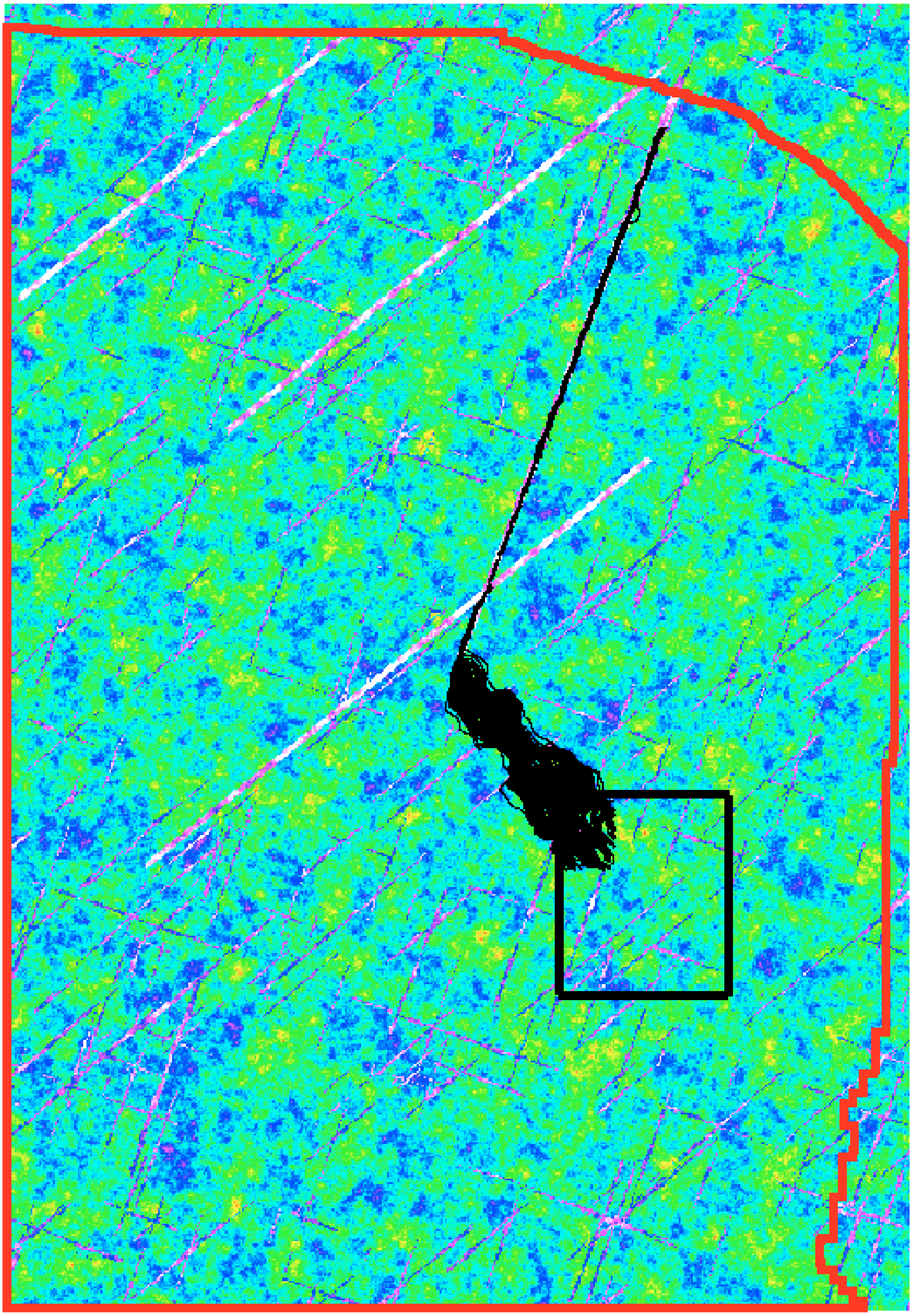

Figure 56.- Particle paths as released from zone 1 (Advection + Dispersion)

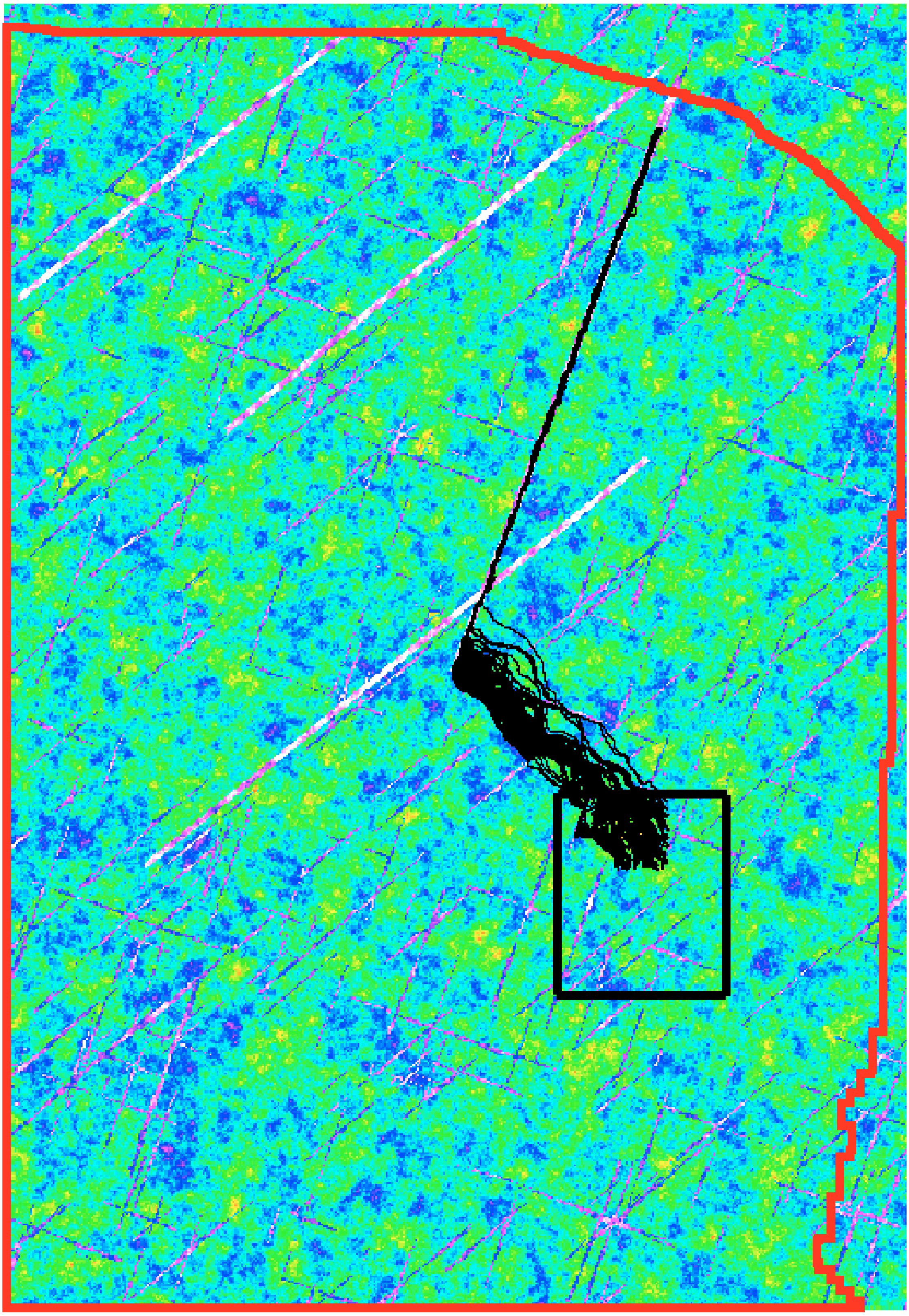

Figure 57.- Particle paths as released from zone 2 (Advection + Dispersion)

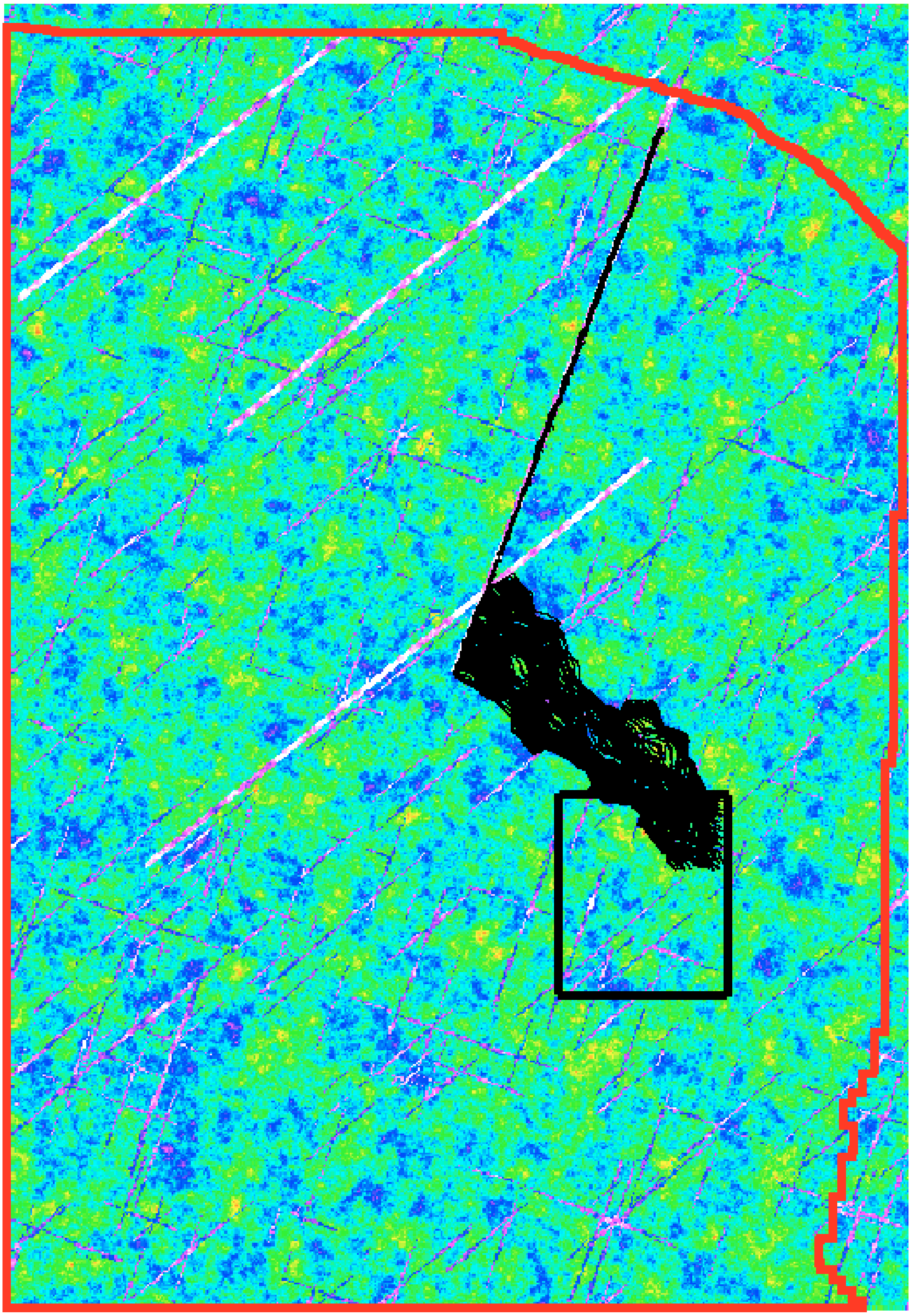

Figure 58.- Particle paths as released from zone 3 (Advection + Dispersion)

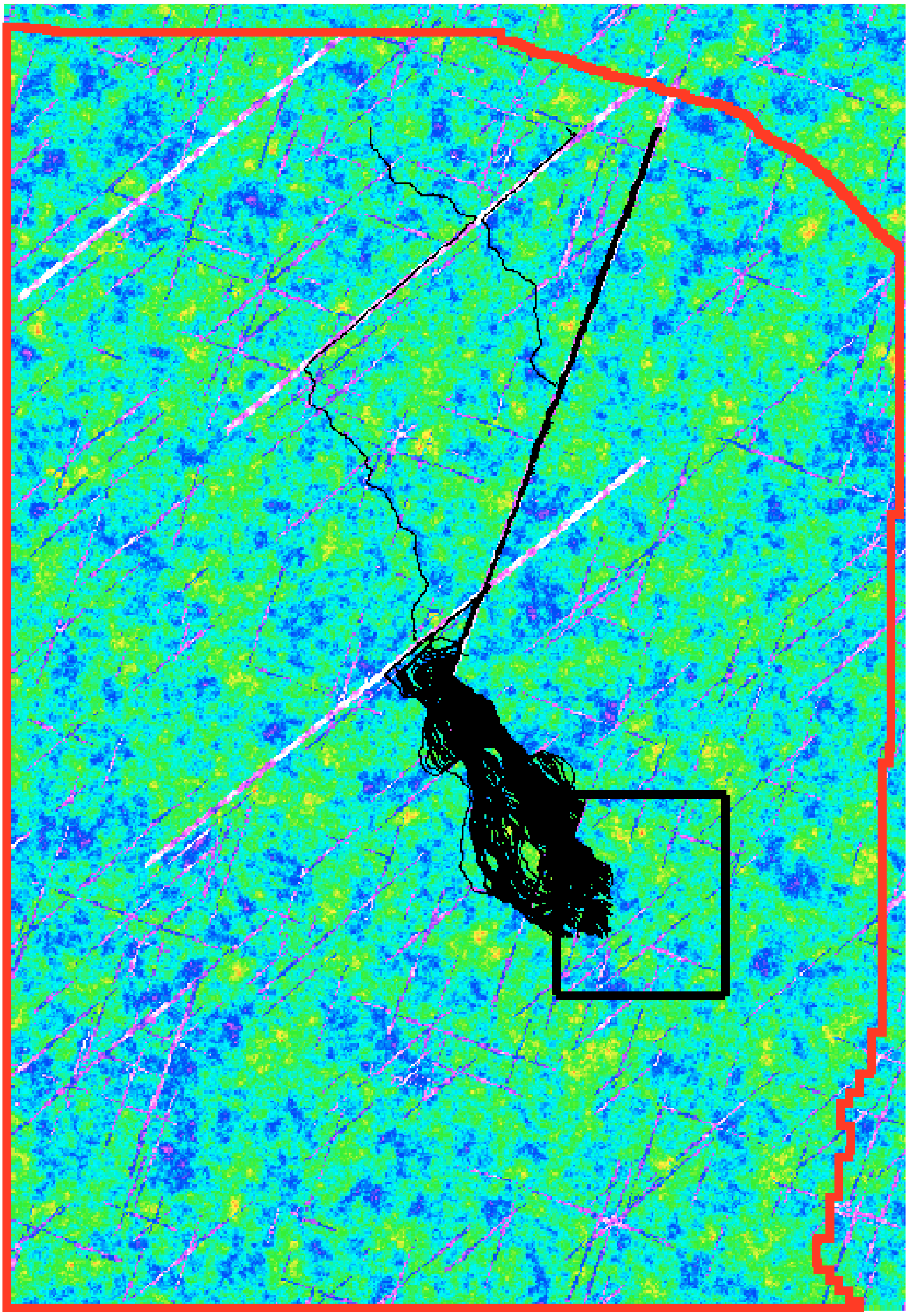

Figure 59.- Particle paths as released from zone 4 (Advection + Dispersion)

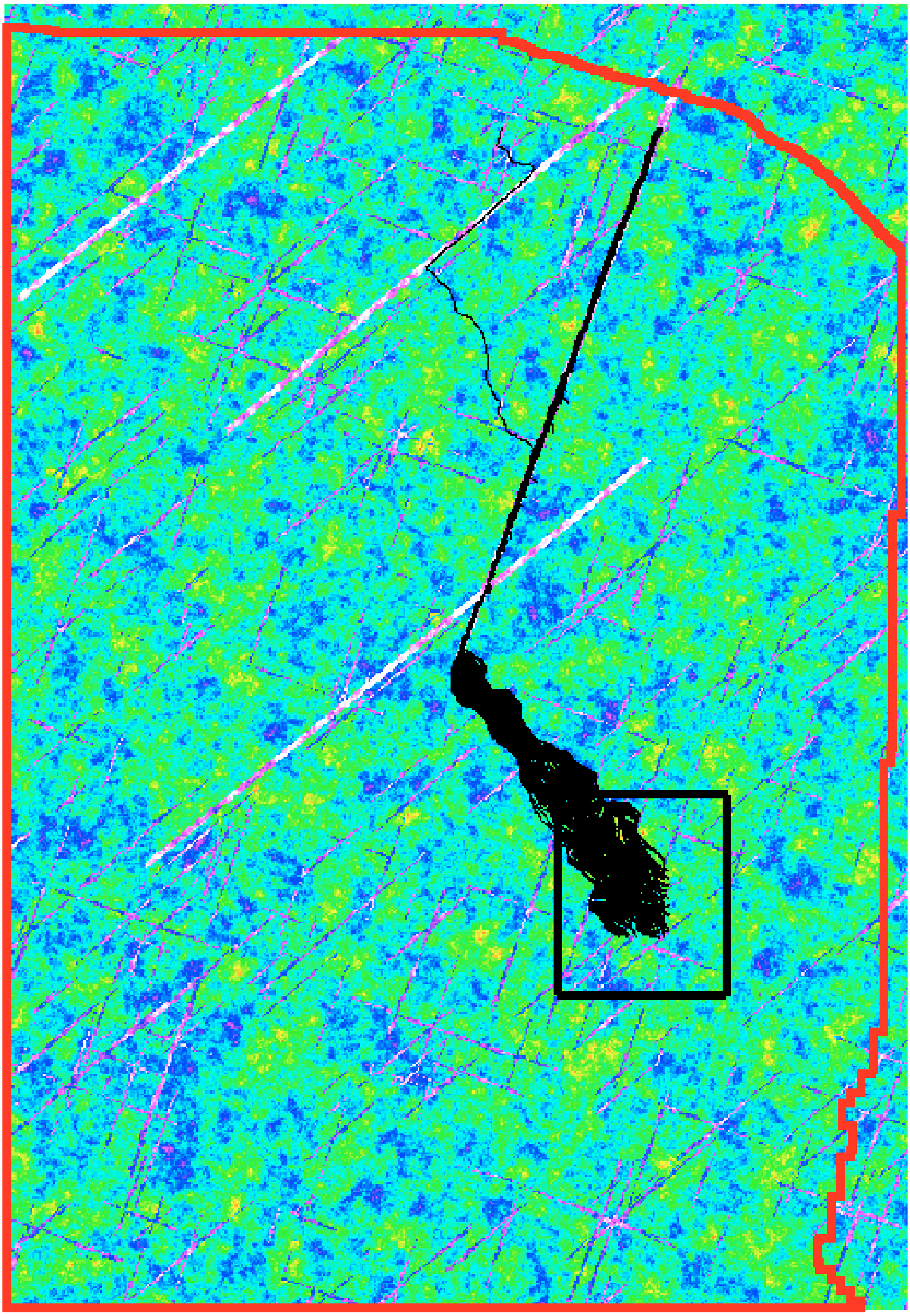

Figure 60.- Particle paths as released from zone 5 (Advection + Dispersion)

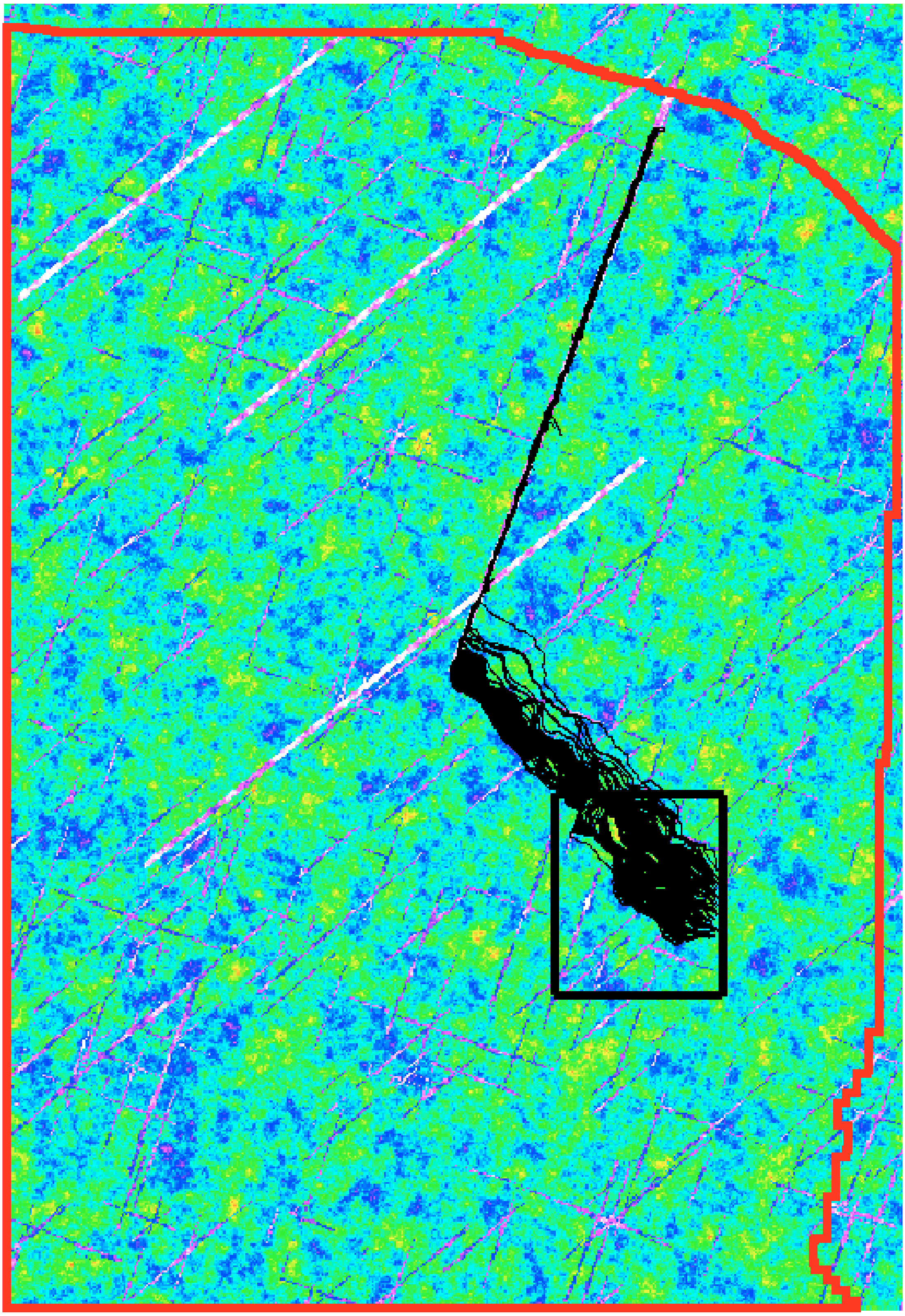

Figure 61.- Particle paths as released from zone 6 (Advection + Dispersion)

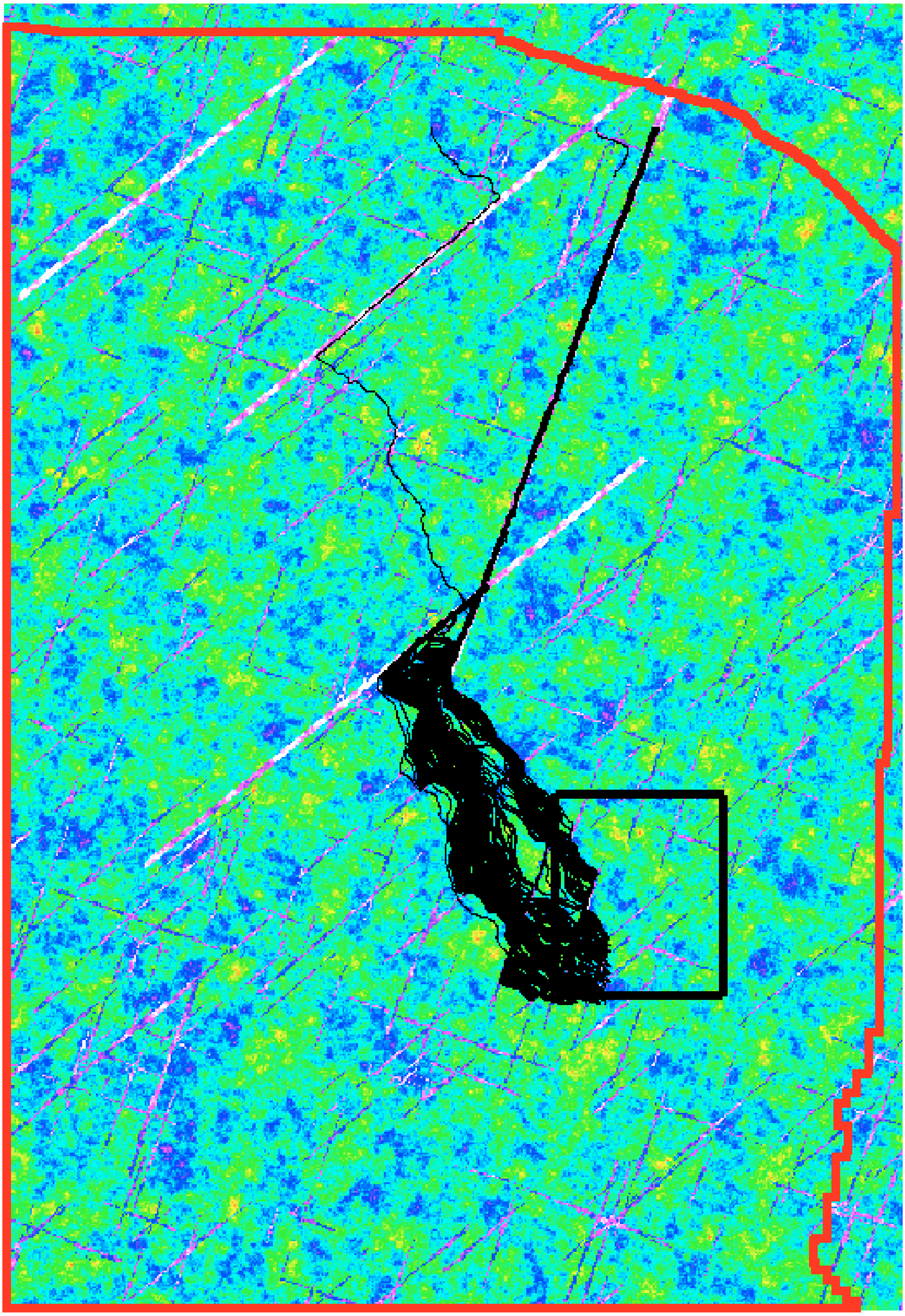

Figure 62.- Particle paths as released from zone 7 (Advection + Dispersion)

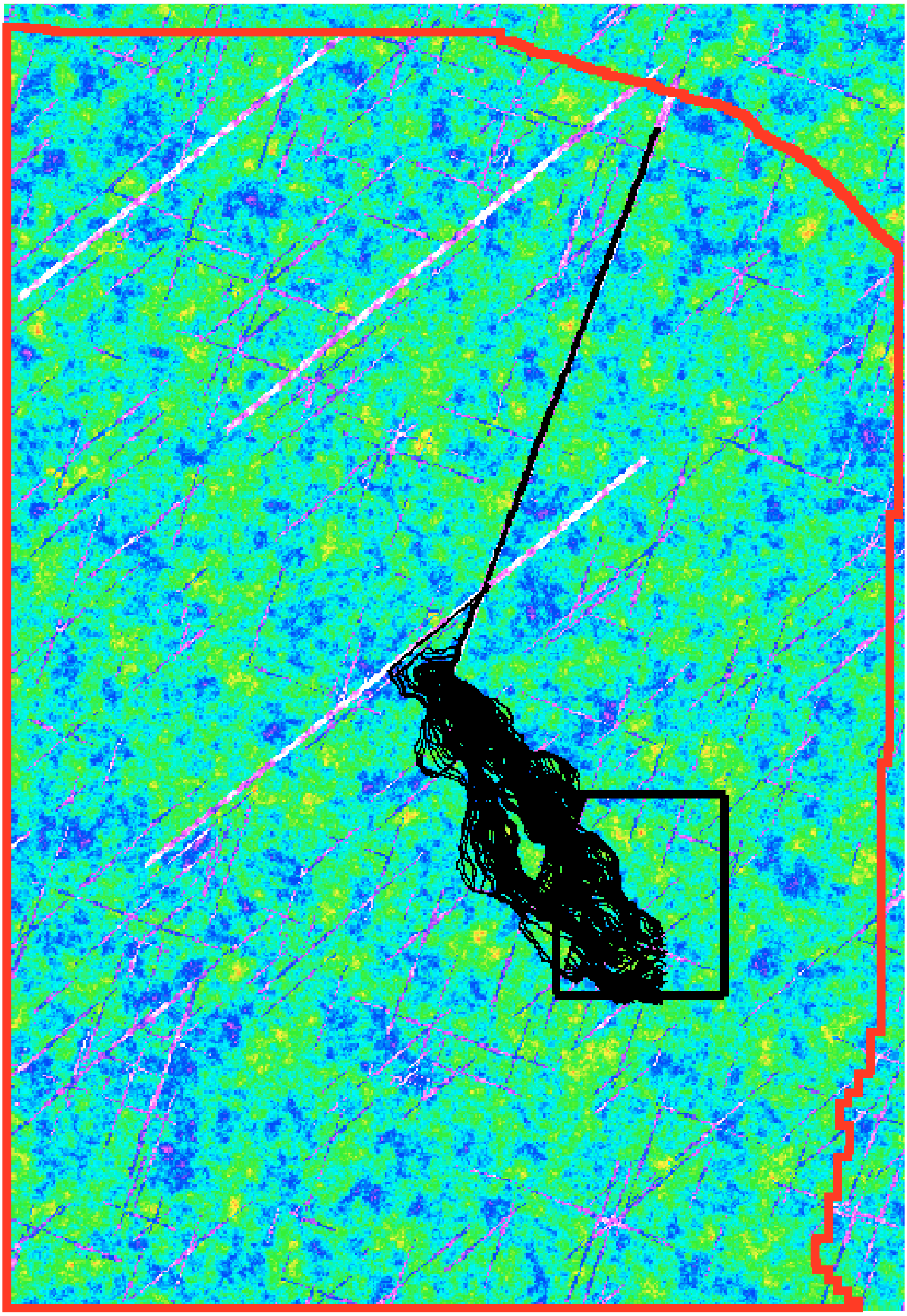

Figure 63.- Particle paths as released from zone 8 (Advection + Dispersion)

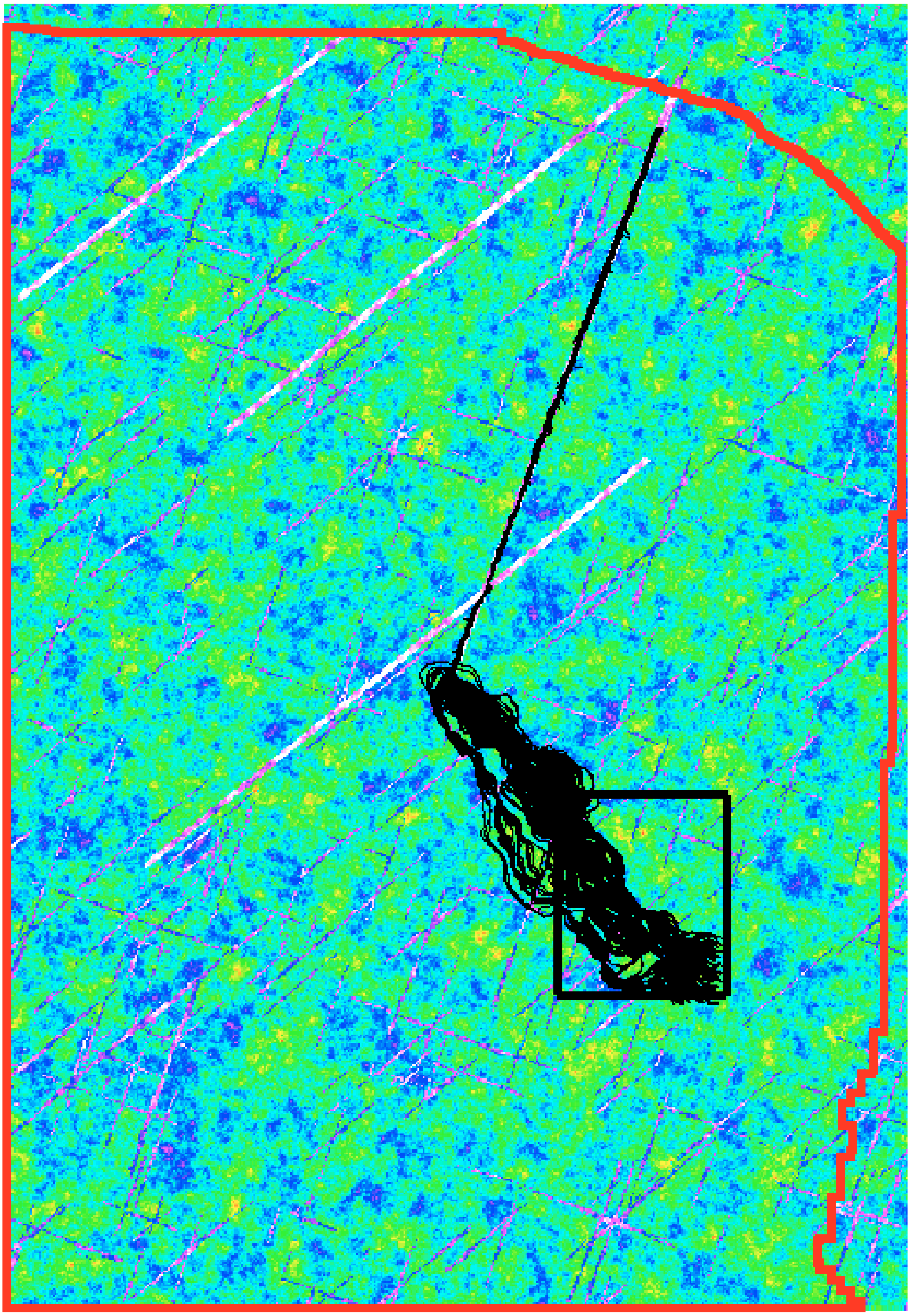

Figure 64.- Particle paths as released from zone 9 (Advection + Dispersion)

Figures 65 to 73 demonstrate the small effect that local dispersion has in the transport response of the model. In all cases, both BTCs are almost the same. It is for this reason that the upscaling analysis is performed only for the transport simulations with advection and dispersion.

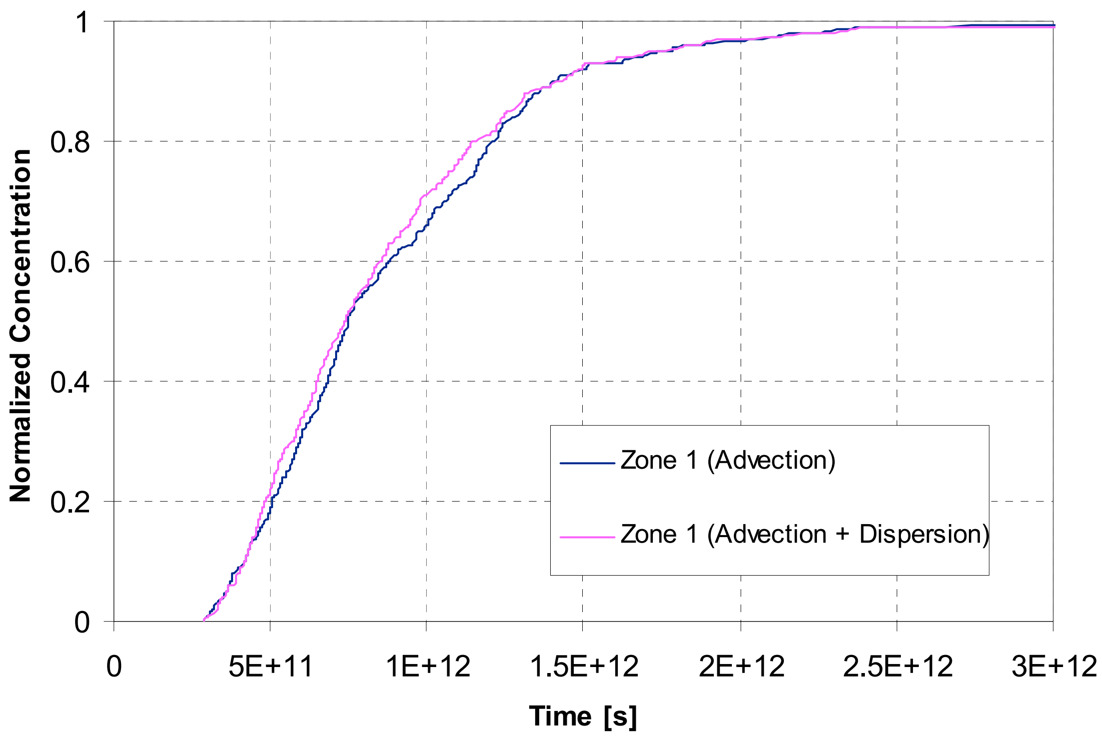

Figure 65.- BTCs computed from the advection and advection and dispersion at zone 1

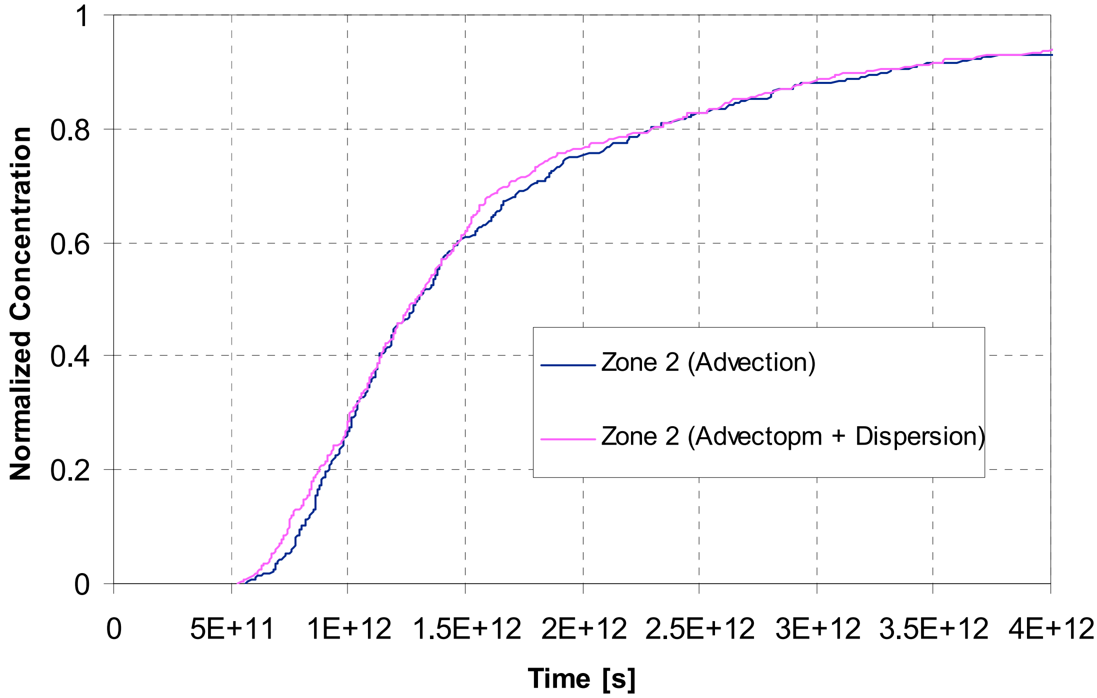

Figure 66.- BTCs computed from the advection and advection and dispersion at zone 2

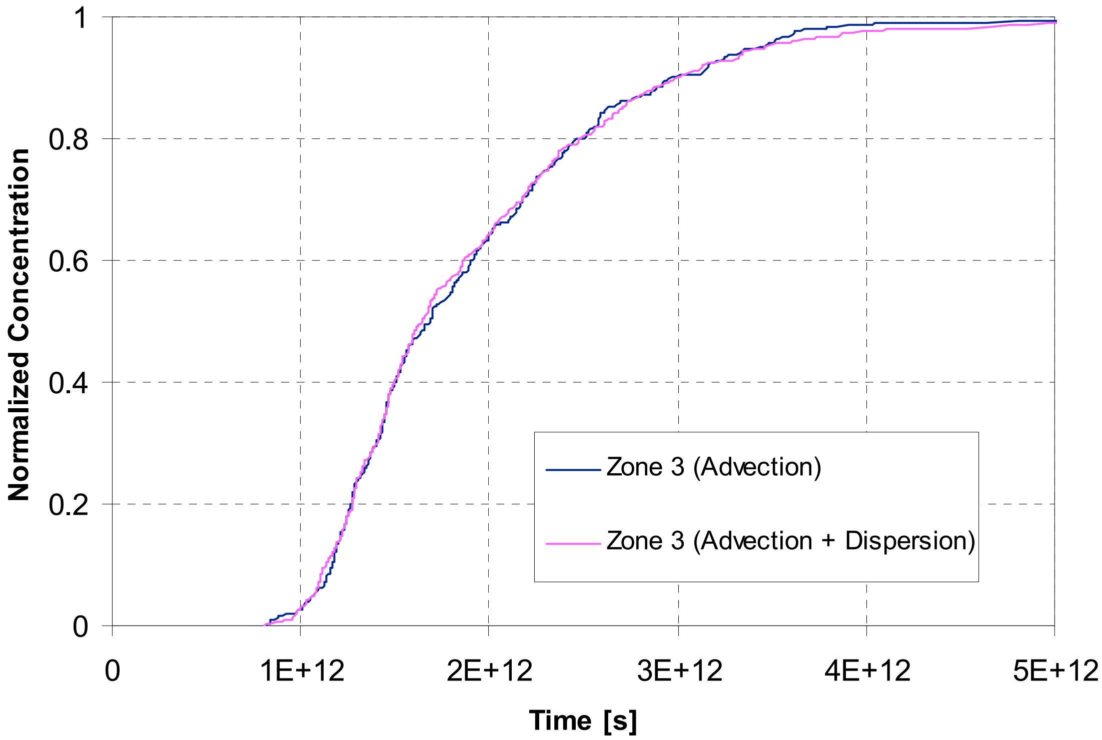

Figure 67.- BTCs computed from the advection and advection and dispersion at zone 3

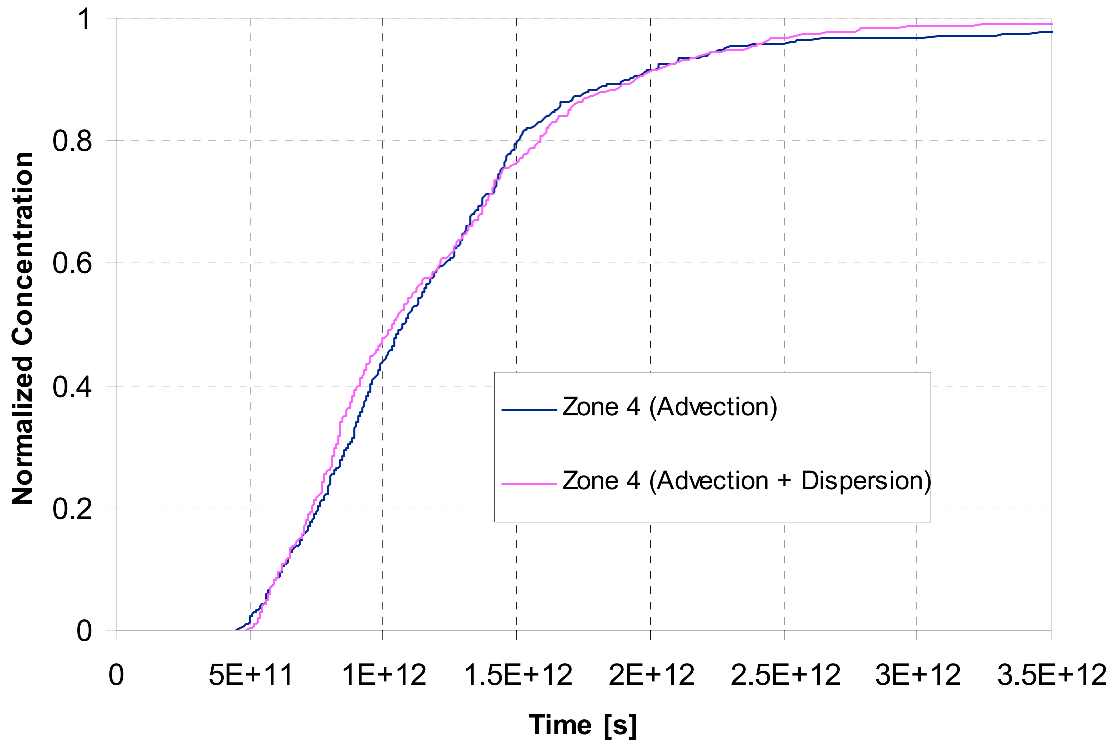

Figure 68.- BTCs computed from the advection and advection and dispersion at zone 4

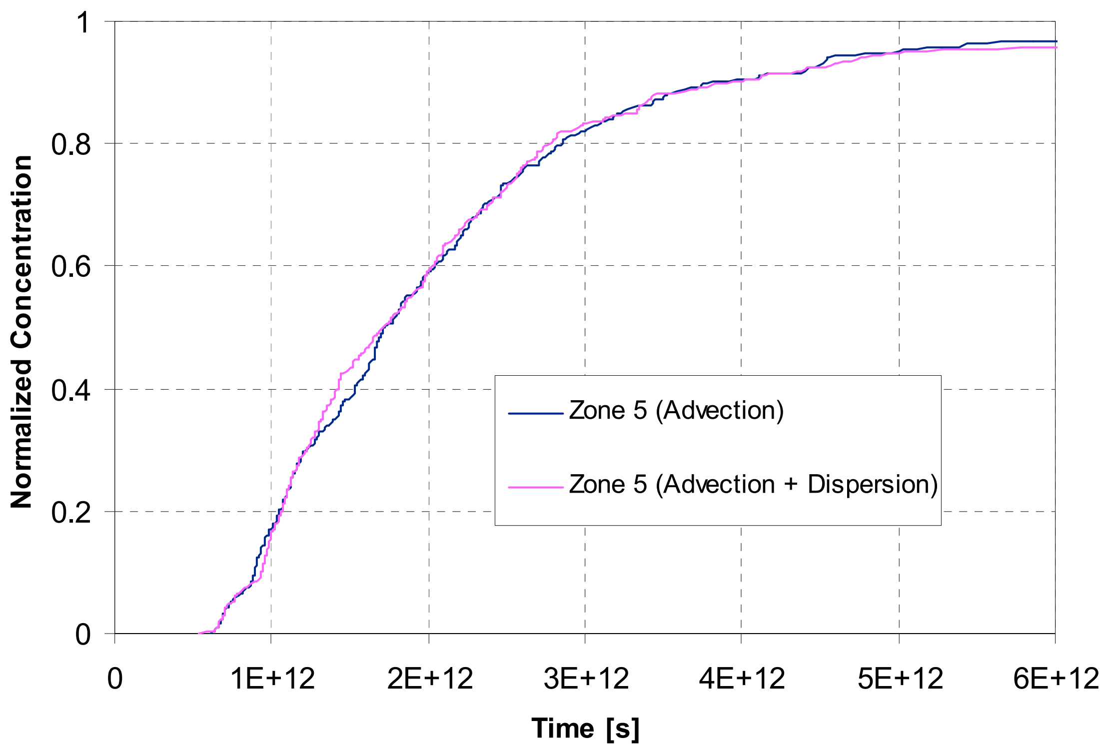

Figure 69.- BTCs computed from the advection and advection and dispersion at zone 5

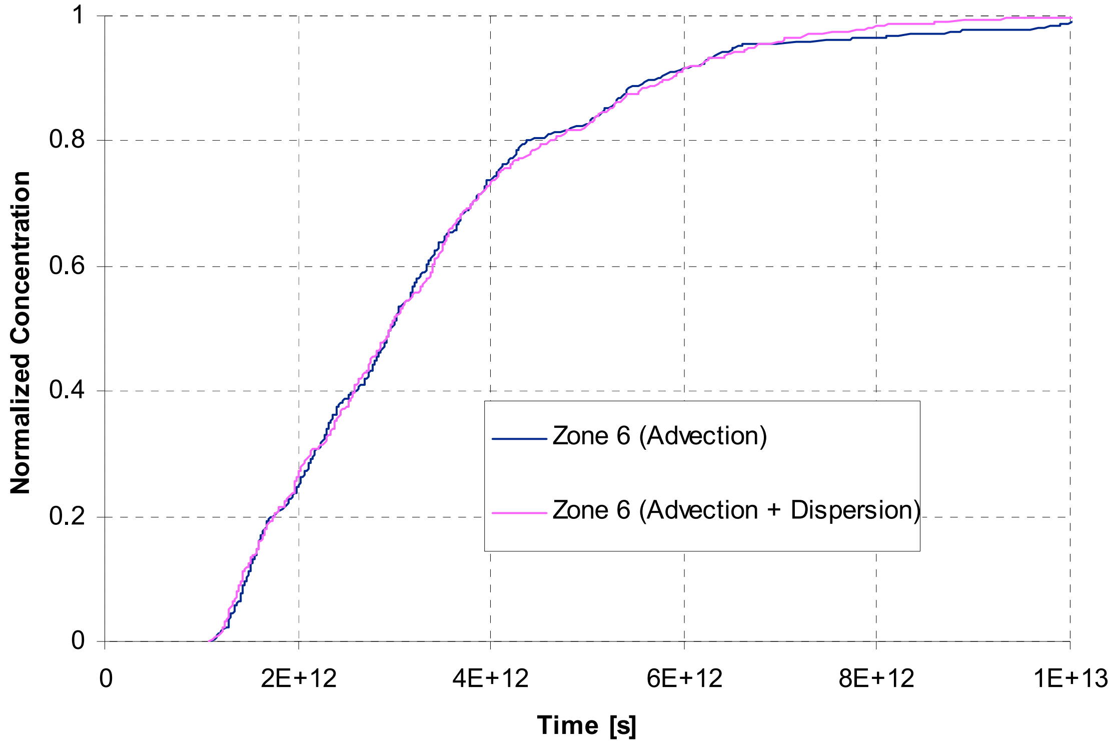

Figure 70.- BTCs computed from the advection and advection and dispersion at zone 6

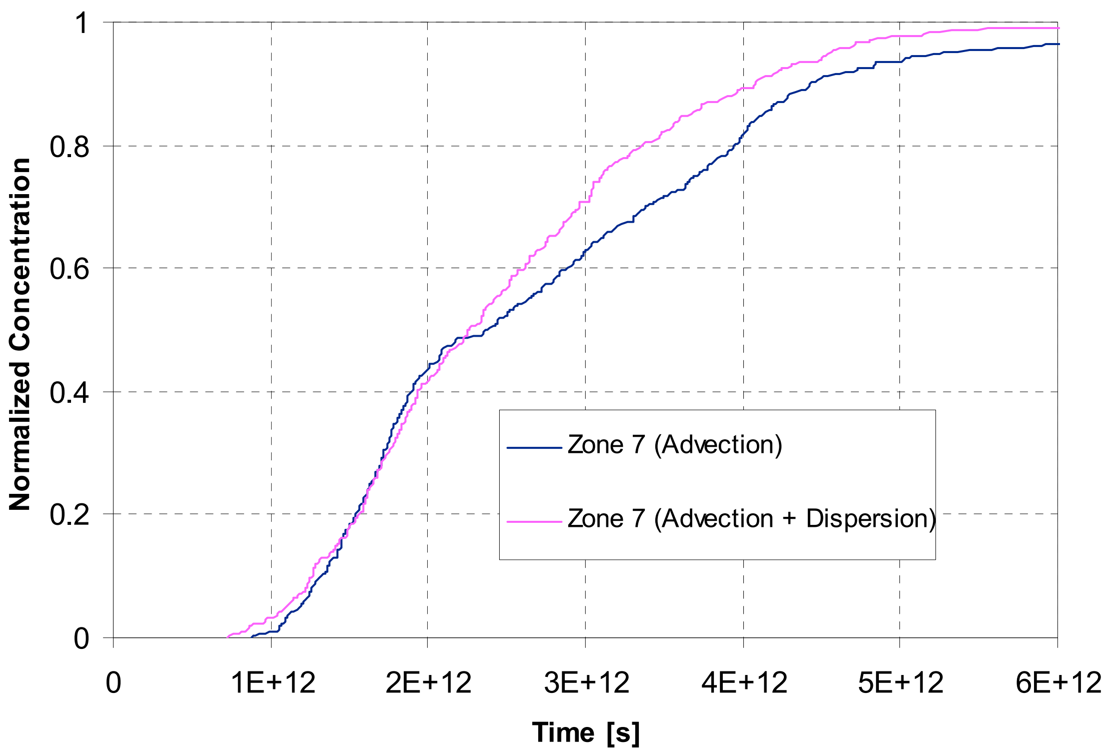

Figure 71.- BTCs computed from the advection and advection and dispersion at zone 7

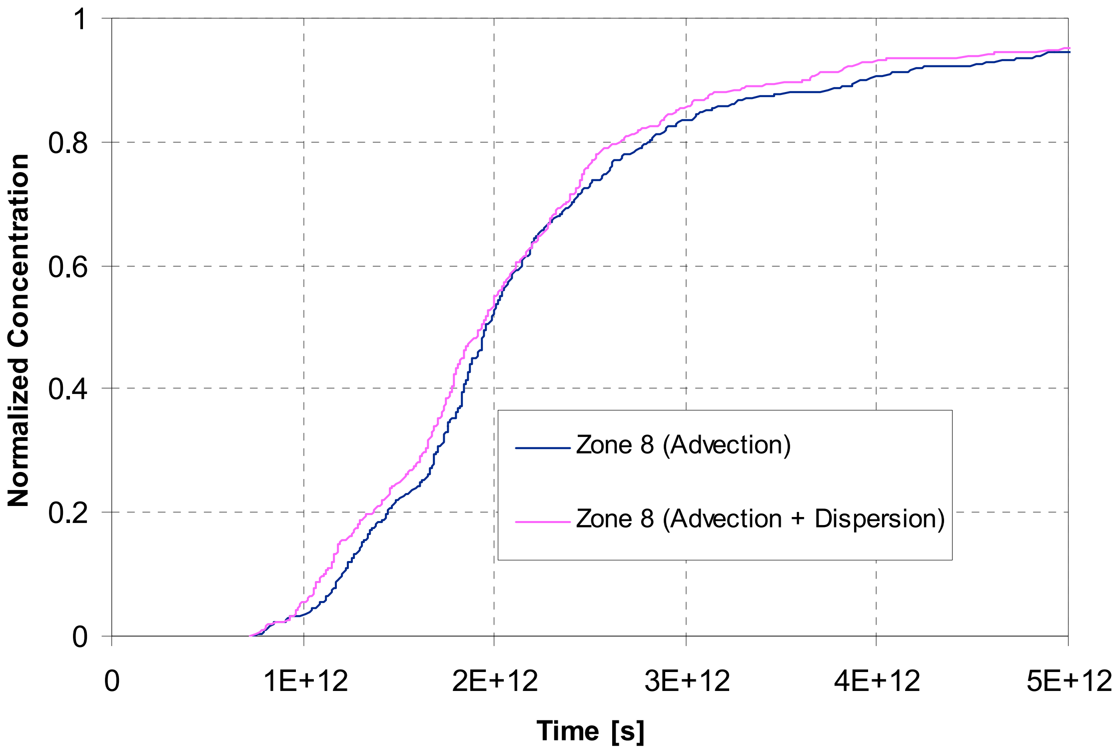

Figure 72.- BTCs computed from the advection and advection and dispersion at zone 8

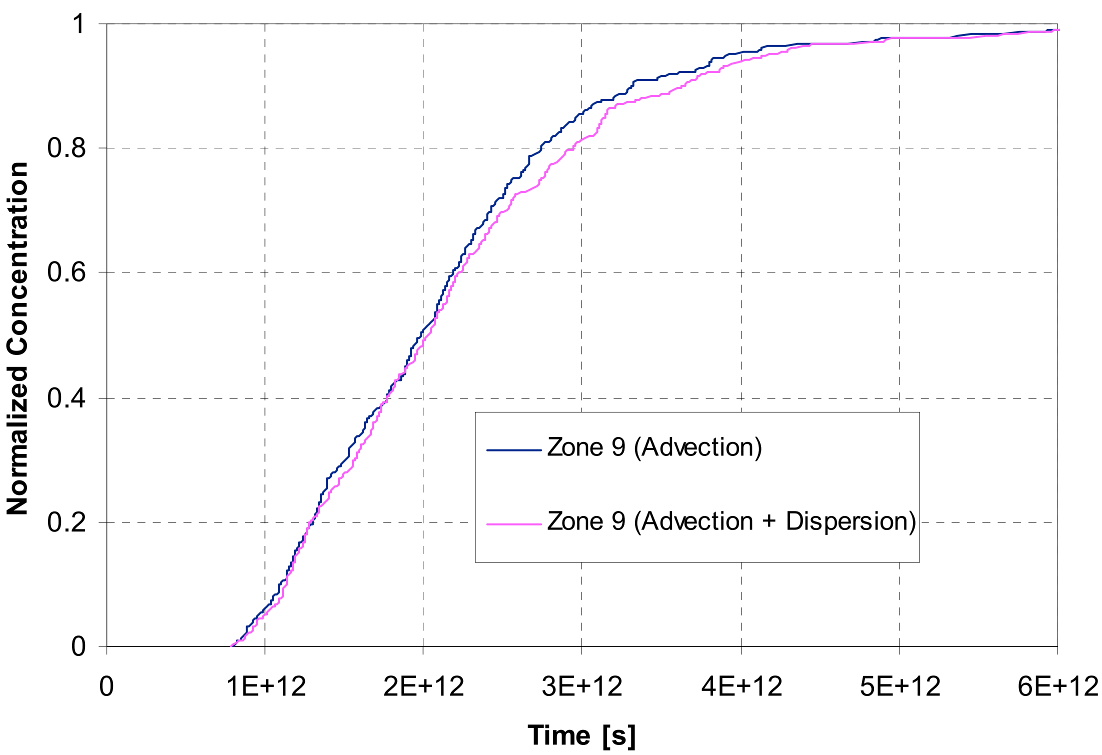

Figure 73.- BTCs computed from the advection and advection and dispersion at zone 9

Both advective simulation at the coarse scale, i.e., just flow upscaling, and simulation at the coarse scale using a mass transfer model with two (fictitious) immobile zones using transport upscaling were performed. Figures 74 to 82 show the comparison, for each zone, of the three BTCs: fine scale model with advection and dispersion, coarse scale model with flow upscaling only, coarse scale model with both coarse scale and transport scale.

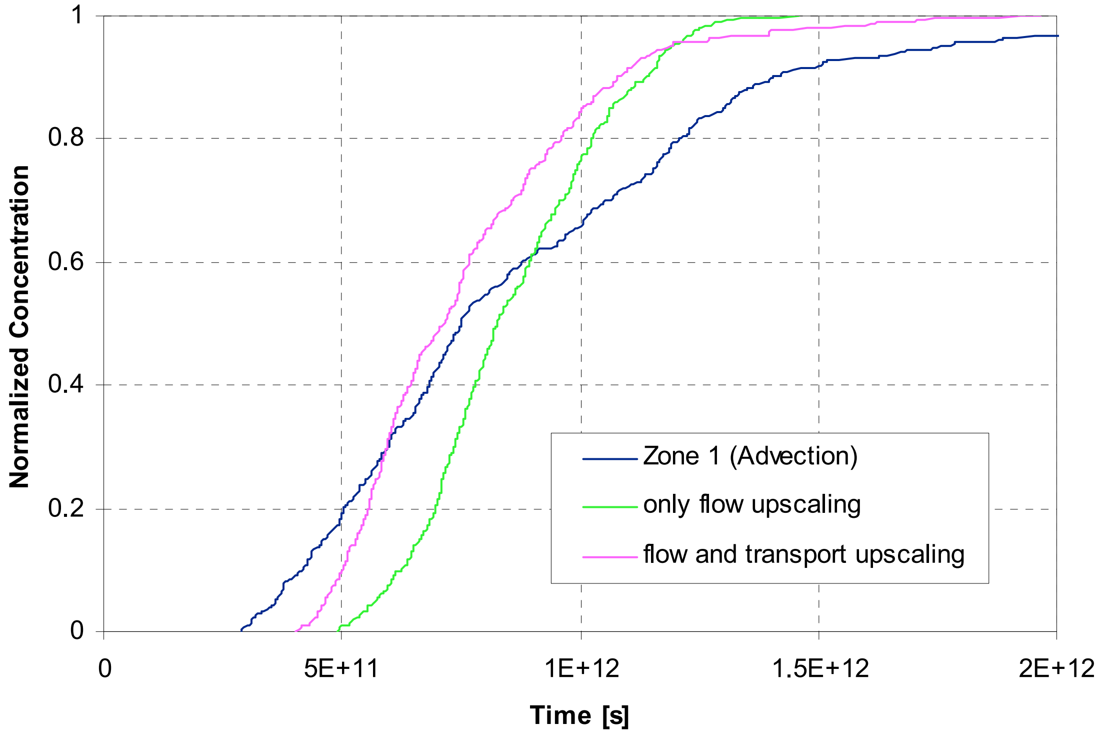

Figure 74.- BTCs computed at the fine scale, at the coarse scale with double-rate mass transfer upscaling and at the coarse scale without transport upscaling (zone 1).

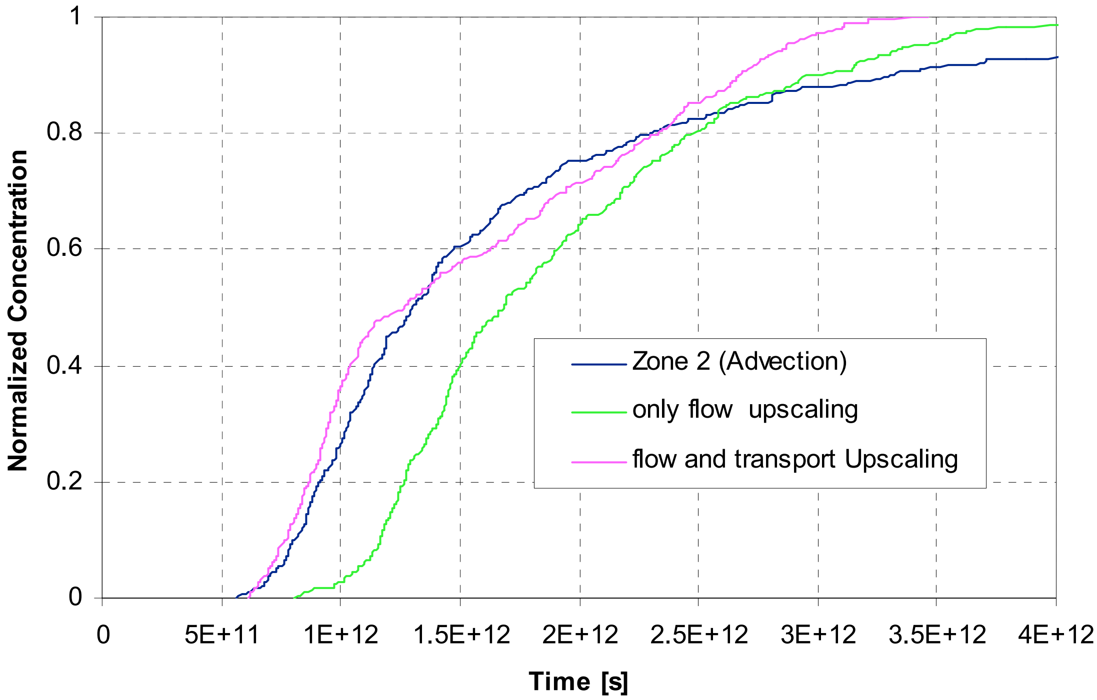

Figure 75.- BTCs computed at the fine scale, at the coarse scale with double-rate mass transfer upscaling and at the coarse scale without transport upscaling (zone 2).

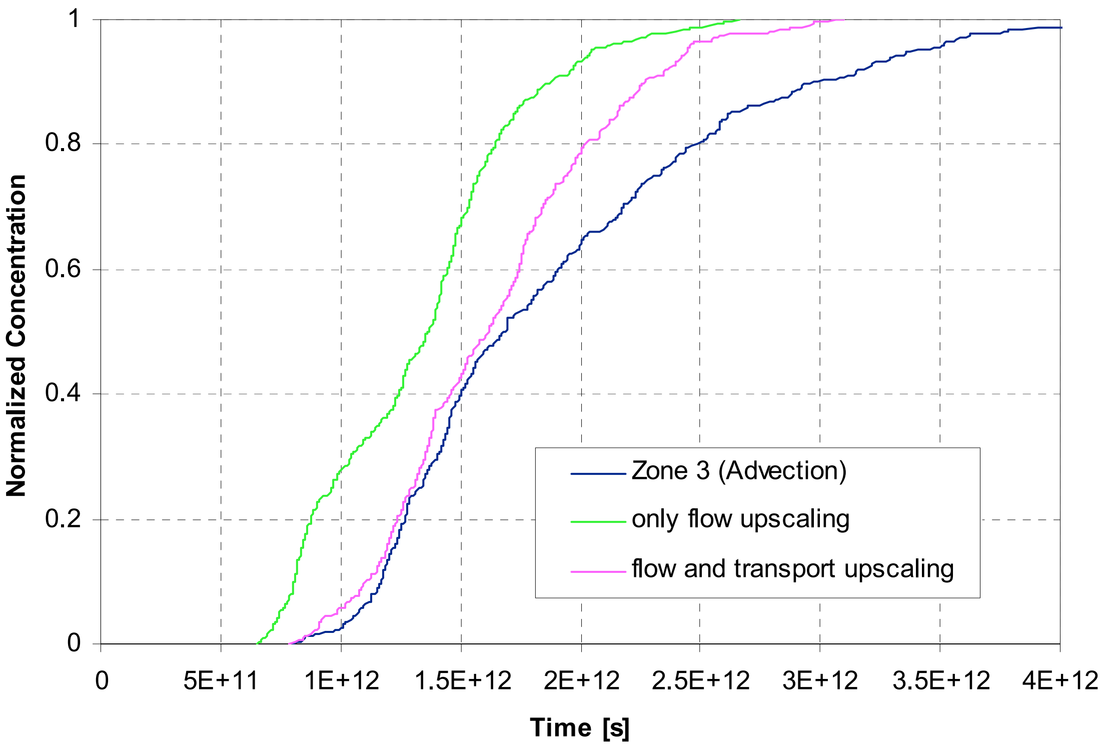

Figure 76- BTCs computed at the fine scale, at the coarse scale with double-rate mass transfer upscaling and at the coarse scale without transport upscaling (zone 3).

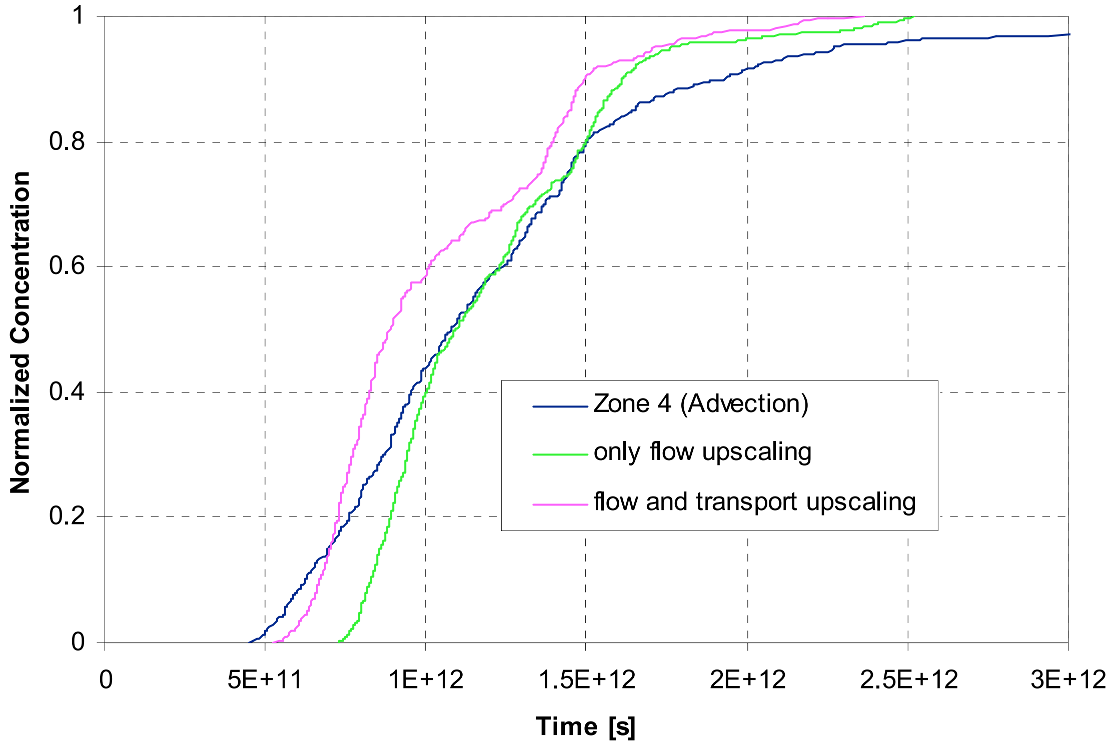

Figure 77.- BTCs computed at the fine scale, at the coarse scale with double-rate mass transfer upscaling and at the coarse scale without transport upscaling (zone 4).

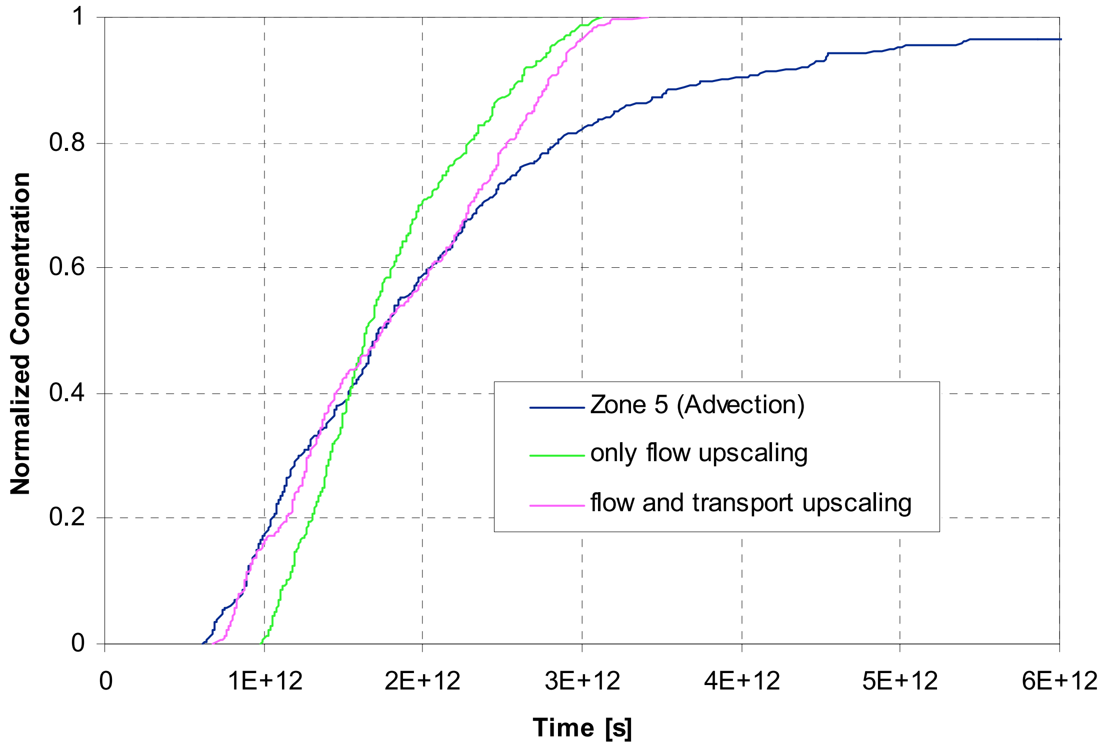

Figure 78.- BTCs computed at the fine scale, at the coarse scale with double-rate mass transfer upscaling and at the coarse scale without transport upscaling (zone 5).

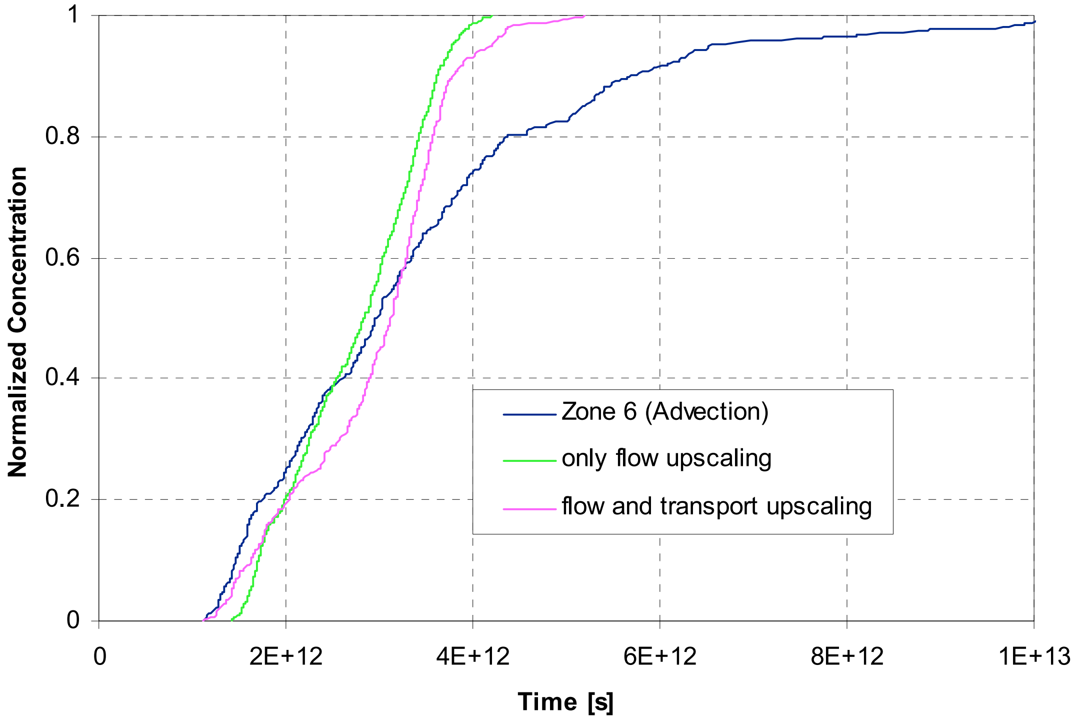

Figure 79.- BTCs computed at the fine scale, at the coarse scale with double-rate mass transfer upscaling and at the coarse scale without transport upscaling (zone 6).

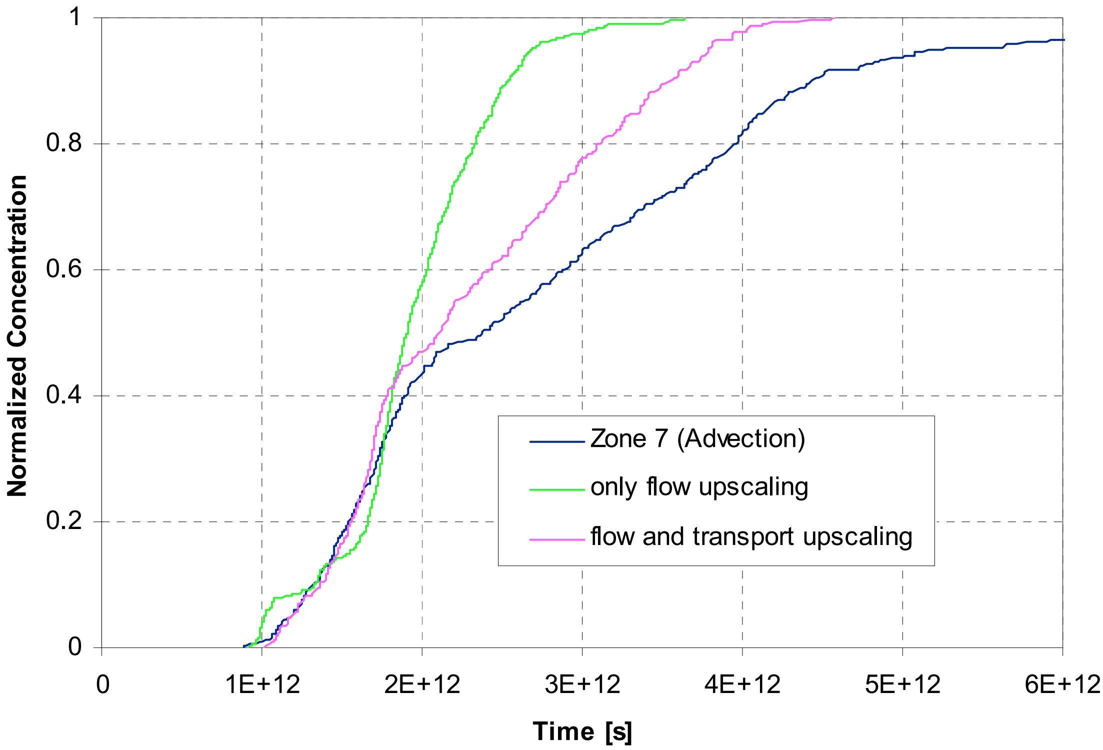

Figure 80.- BTCs computed at the fine scale, at the coarse scale with double-rate mass transfer upscaling and at the coarse scale without transport upscaling (zone 7).

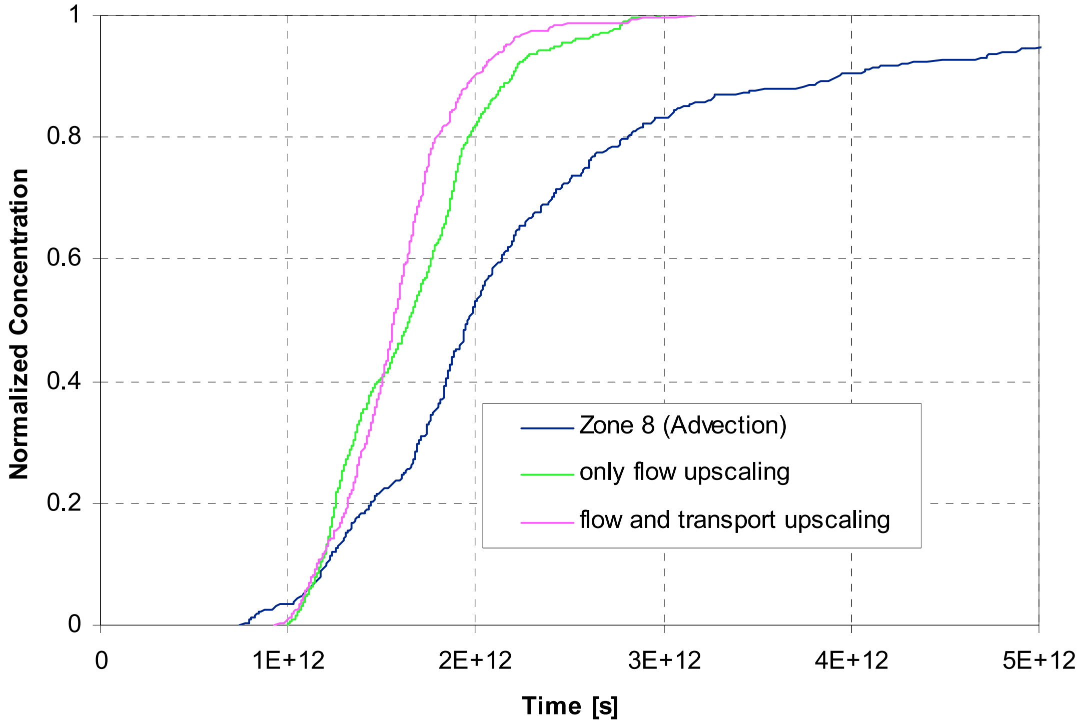

Figure 81.- BTCs computed at the fine scale, at the coarse scale with double-rate mass transfer upscaling and at the coarse scale without transport upscaling (zone 8).

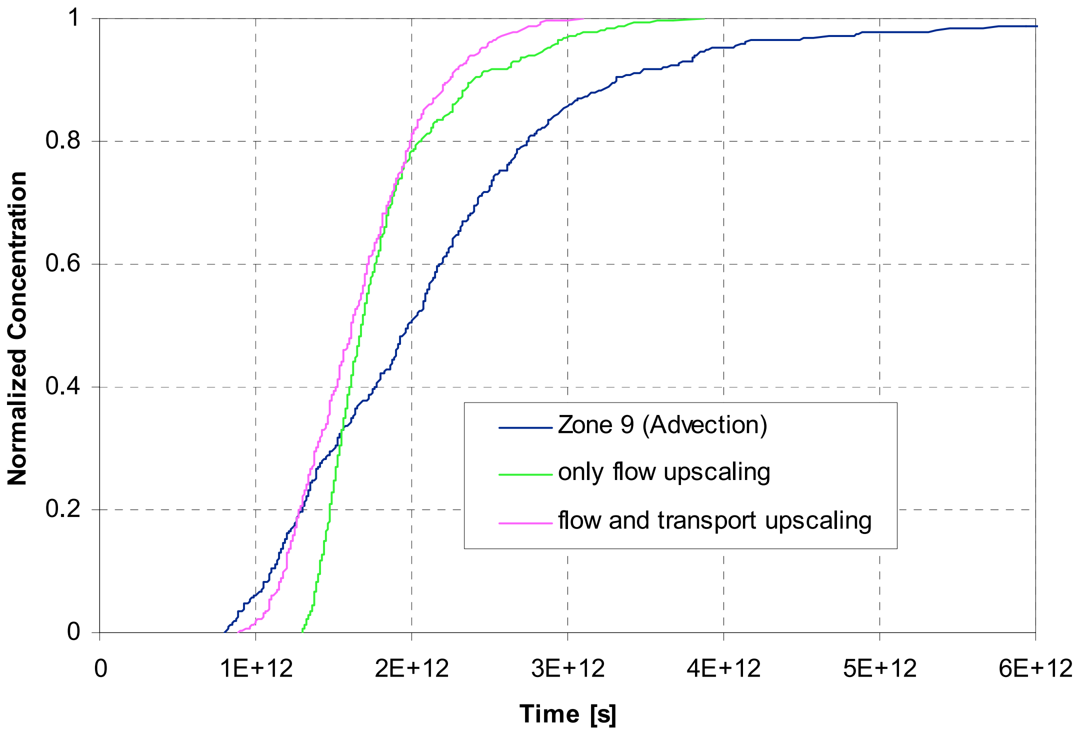

Figure 82.- BTCs computed at the fine scale, at the coarse scale with double-rate mass transfer upscaling and at the coarse scale without transport upscaling (zone 9).

In general, it can be seen that including transport upscaling improves the reproduction of the fine scale BTCs, but this improvement is quite irregular and, for some zones unnoticeable. For instance in zone 1, transport upscaling is able to correct the sever underestimation of the early travel times incurred when only flow upscaling is performed. But for zones 7 or 8 practically no difference is introduced by including transport upscaling. It has been attempted to improve these results increasing the number of particles or using different mass transfer models at the coarse scale but no significant change has been found. We are currently working to get consistently better results at the coarse scale with transport upscaling is included.

5.- Definition of the 1D advective pathway

5.1.- Input data

The starting point of ENRESA calculations for the definition of the 1D advective pathway is the breakthrough curves (BTC´s) obtained by UPV using the fine scale model in 2 cases: "advection+dispersion" and "advection+ dispersion+matrix diffusion" assuming releases from the whole repository area. These BTC´s are represented in Figure 83 and some numerical values are included in Table 8.

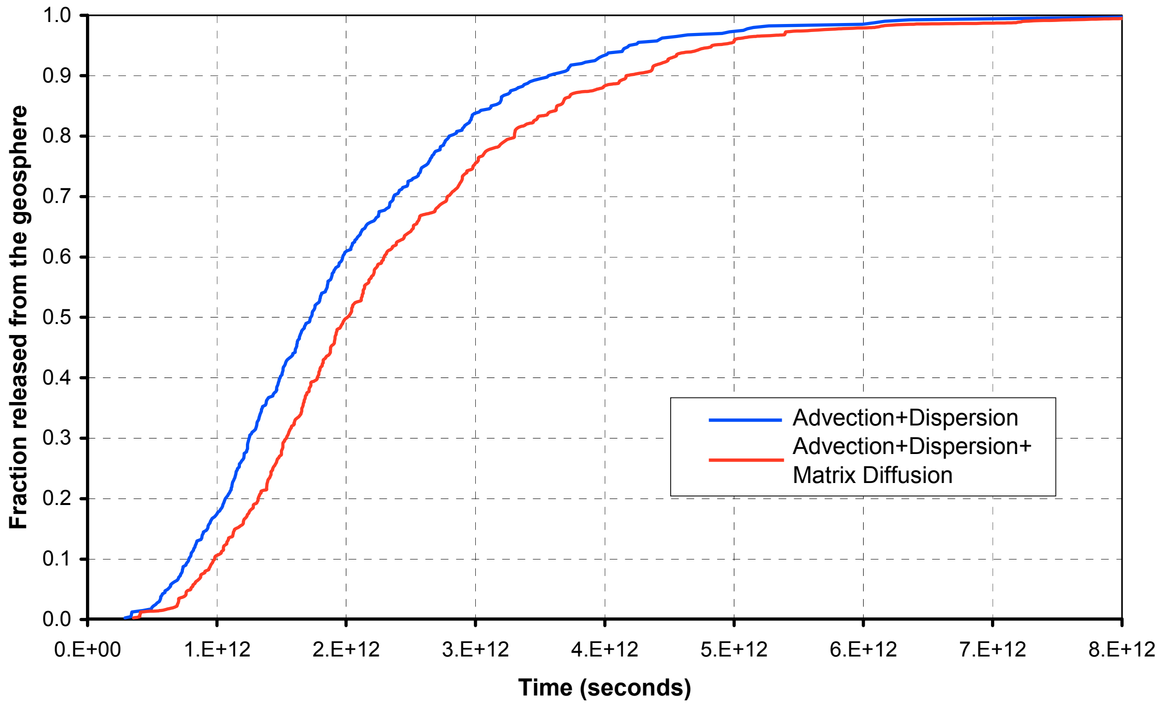

Figure 83.- BTC´s with the fine scale model assuming homogeneous releases from the whole repository area.

Time instant (i)	Time (s)	Advection Dispersion	Advection Dispersion Matrix diffusion
1	5.0E+11	2.028E-02	1.394E-02
2	8.0E+11	1.073E-01	5.212E-02
3	1.1E+12	2.102E-01	1.358E-01
4	1.4E+12	3.676E-01	2.328E-01
5	1.7E+12	4.910E-01	3.757E-01
6	2.0E+12	6.091E-01	4.987E-01
7	2.3E+12	6.781E-01	6.029E-01
8	2.6E+12	7.496E-01	6.702E-01
9	2.9E+12	8.128E-01	7.329E-01

10	3.2E+12	8.629E-01	7.877E-01
11	3.5E+12	8.949E-01	8.330E-01
12	4.0E+12	9.338E-01	8.829E-01
13	4.5E+12	9.638E-01	9.283E-01
14	5.0E+12	9.733E-01	9.571E-01
15	6.0E+12	9.852E-01	9.792E-01

Table8.- Numerical values of the breakthrough curves presented in Figure 83.

5.2.- ENRESA calculations

ENRESA has used GoldSim (previously called RIP) computer code in the three performance assessment exercises for repositories in granite done up to now. GoldSim includes an element called "pipe", that is a 1D streamtube used to model the transport of solutes through fractured media taking into account:

- advection
- longitudinal dispersion
- radioactive decay/ingrowth
- matrix diffusion
- sorption on fracture infill, fracture surface and granite matrix

In ENRESA calculations a pulse of stable conservative (unretarded) solute is injected into the "pipe" at t=0, and the flux leaving the pipe is calculated. The breakthrough curve is obtained with the cumulated flux that has left the pipe up to a given time.

The breakthrough curves obtained by UPV are constructed with the travel times up to an important fracture of 400 particles released homogeneously from the whole repository surface.

ENRESA has used the data in section 5.1 to define the parameters of the "pipe" that best reproduces the BTC´s obtained by UPV with the fine scale model:

- first, the results obtained by UPV considering advection and dispersion were used to estimate the parameters of the stream tube related to the transport in the fracture (case 1), and
- then the parameters of the stream tube related to matrix diffusion were estimated using the results of the fine scale model with advection, dispersion and matrix diffusion (case 2).

In case 1 and case 2 the parameters of the "pipe" are represented by probability distributions. GoldSim is used to perform a Monte Carlo calculation with 1,000 realizations sampling uncertain parameters from the previous distributions. In each realization a BTC is calculated and the differences between the BTC´s calculated with GoldSim and the results obtained by UPV with the fine scale model are quantified by magnitude Error, defined as:

$$\text{Error} = \sum_{i=1}^{15} (\text{BTC}(t_i)\big|_{\text{FINE SCALE}} - \text{BTC}(t_i)\big|_{\text{GOLDSIM}})^2$$

where i=1,2,…, 15 are the time instants included in Table 8.

5.3.- Case 1: Advection + Dispersion

From the analytical solution of the 1D advection-dispersion equation (without matrix diffusion) it is known that, if the dispersion coefficient is considered proportional to the water velocity and the length of the stream tube ($D=\alpha \cdot v \cdot L$), the flux leaving the pipe depends only on three parameters: the retardation factor (R), the water travel time (t_w) and the Alpha factor (α). Since in the calculations we are considering a conservative tracer, R is equal to 1, and the flux leaving the pipe depends only on t_w and the Alpha factor (α).

A model of GoldSim is created assigning probability distributions to both parameters:

- t_W is a uniform distribution $[1.5 \cdot 10^{12}$ - $2.5 \cdot 10^{12}]$ s
- α is a uniform distribution [0.1 , 0.3]

With GoldSim 1000 realisations are done and Error is calculated in each one. Graphics have been created to represent Error vs. Alpha factor (Figures 84 and 85) and t_w (Figures 86 and 87) in the 1000 realisations.

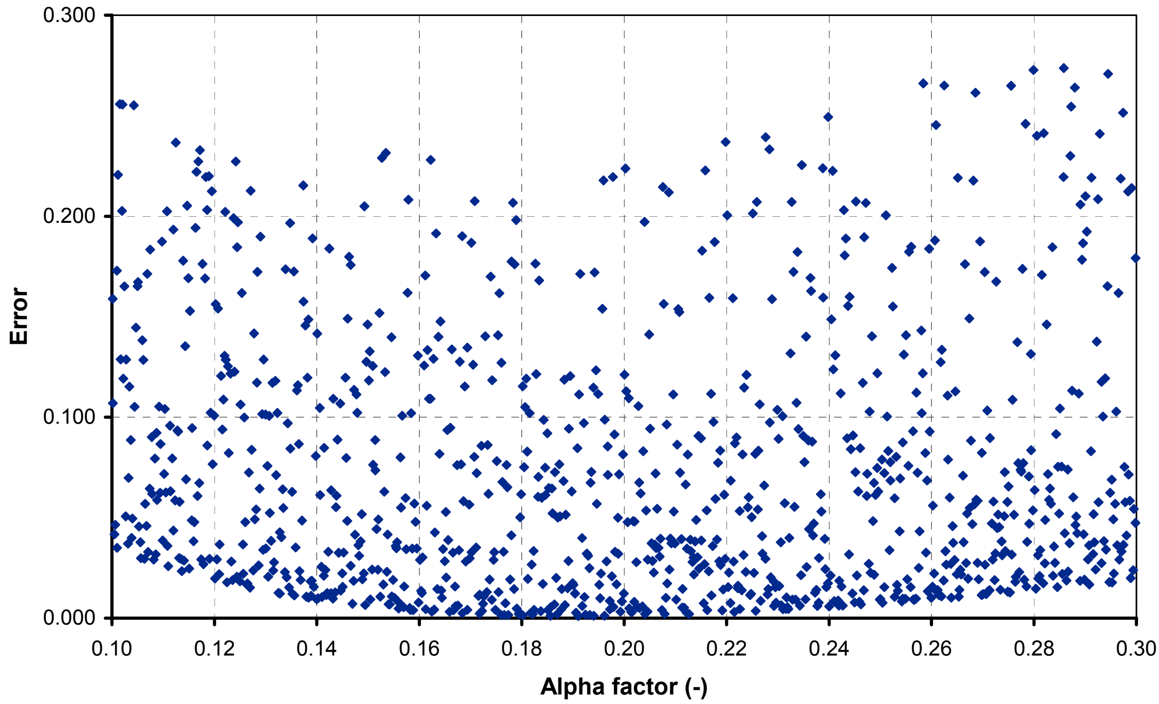

Figure 84.– Scatter plot of Alpha factor vs. Error in the 1000 realisations of the GoldSim calculation.

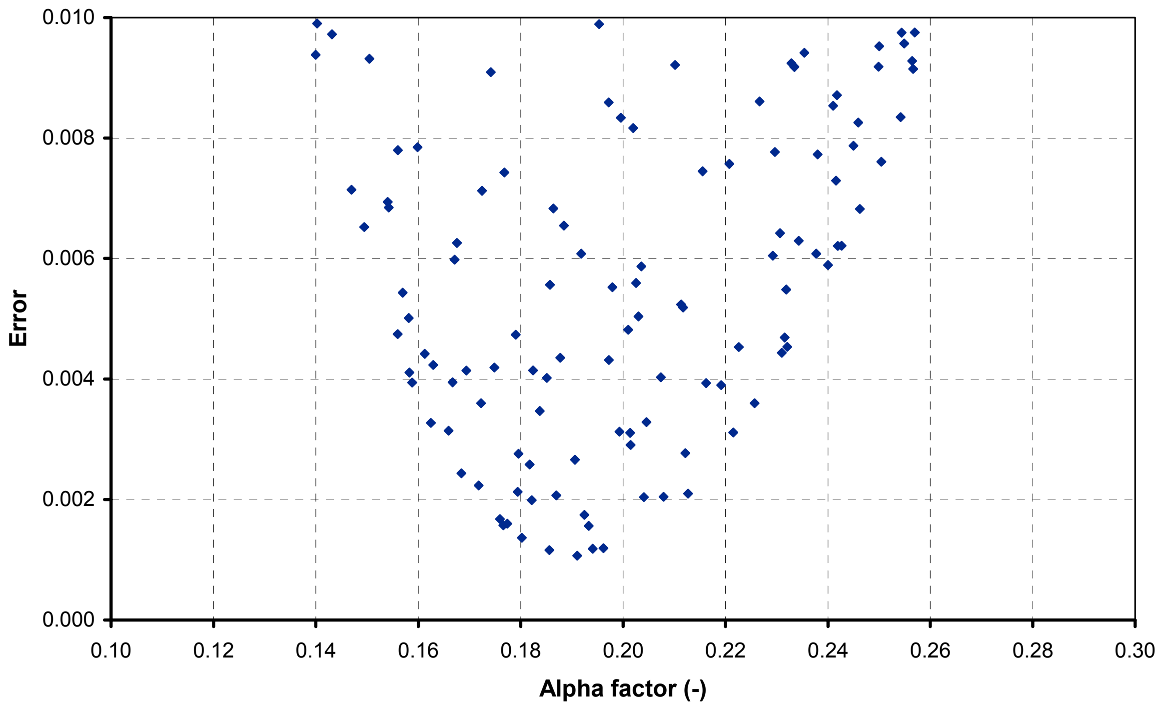

Figure 85.– Scatter plot of Alpha factor vs. Error in the 1000 realisations of the GoldSim calculation (detail of Figure 84).

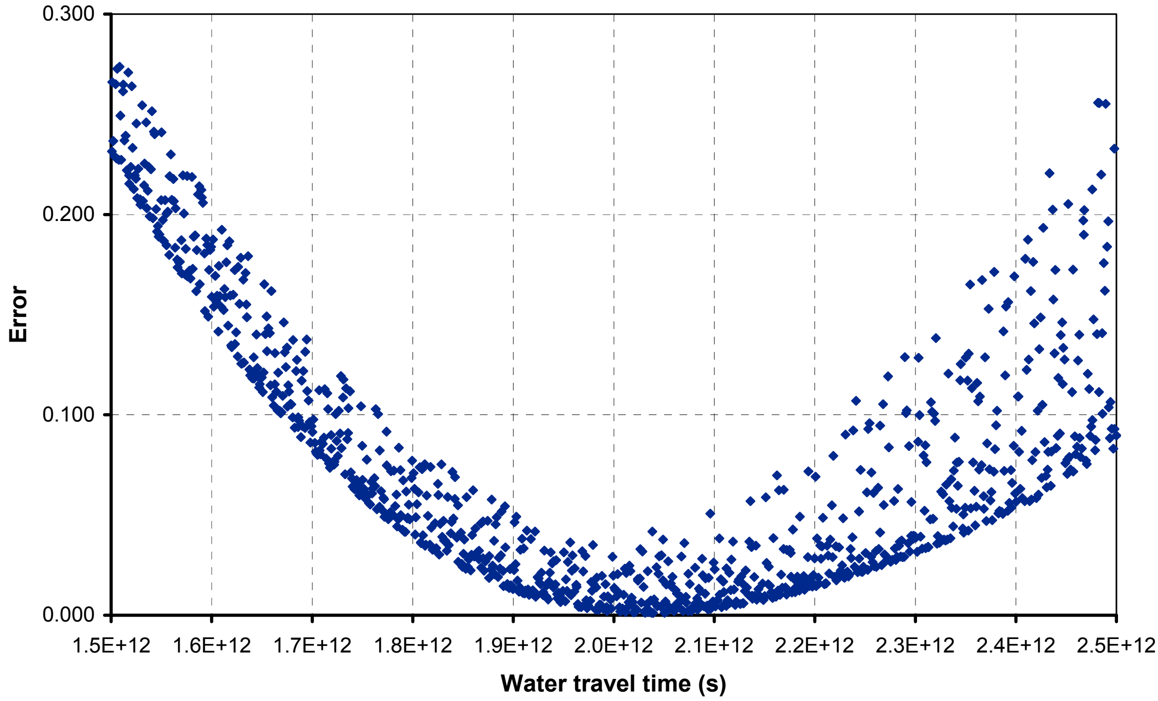

Figure 86.– Scatter plot of Water travel time vs. Error in the 1000 realisations of the GoldSim calculation.

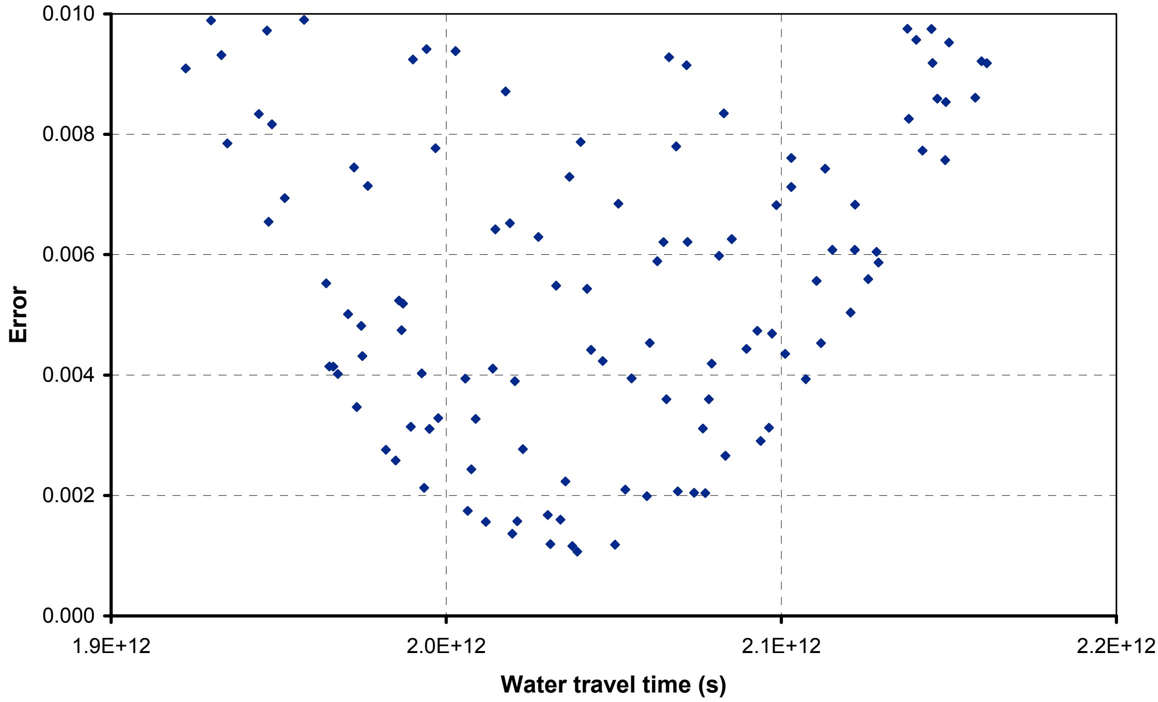

Figure 87.– Scatter plot of Water travel time vs. Error in the 1000 realisations of the GoldSim calculation (detail of Figure 86).

Figures 84 to 87 show a clear correlation of Error with the Alpha factor and t_w. The minimum value of Error is obtained in realisation #578 that corresponds to $t_w = 2.0391 \cdot 10^{12}$ s and α=0.191. From the previous figures it can be seen that the value of Error is smaller than 2 times the minimum value of error for narrow ranges of values of $t_w(2.0 \cdot 10^{12}$ to $2.1 \cdot 10^{12}$ s) and α (0.17 to 0.21).

Figure 88 shows the BTCs obtained with the fine scale model with homogeneous releases from the repository area and GoldSim run #578 ($t_w = 2.0391 \cdot 10^{12}$ s and α=0.191). A very good agreement is observed and, as a consequence, these values of t_w and α are selected for the GoldSim "pipe".

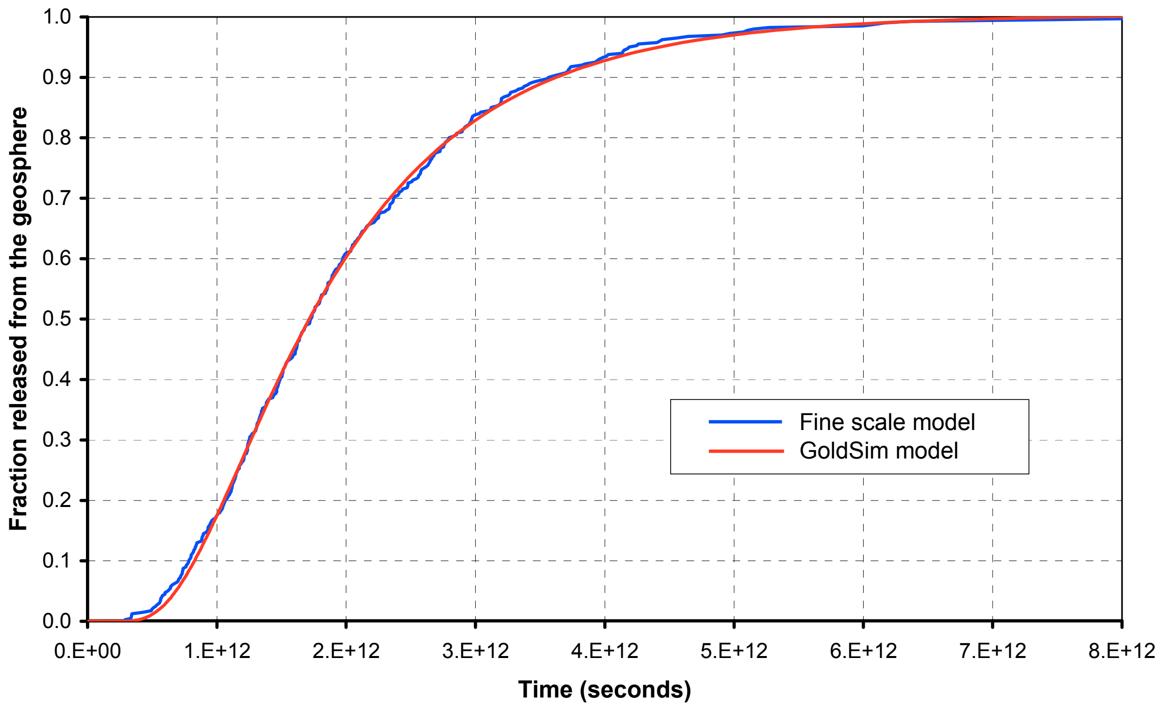

Figure 88.– BTC´s with the fine scale model and GoldSim realisation #578 (advection+dispersion case)

5.4.- Case 2: Advection + Dispersion + Matrix Diffusion

In the next calculation constant values are used for the fracture parameters: $t_w = 2.0391 \cdot 10^{12}$ s and α=0.191. The parameters that can affect the matrix diffusion are represented by broad pdf´s:

- fracture aperture (2b) is a log-uniform distribution $[3 \cdot 10^{-4}, 3 \cdot 10^{-3}]$ m
- porosity (θ) is log-uniform distribution [0.002 , 0.02]

- thickness of matrix (TM) is a log-uniform [0.5 , 10] cm
- diffusion coefficient in matrix porewater (D_p) is a log-uniform distribution [10^{-12},10^{-10}] m^2/s

If diffusion into the matrix is fast compared with the advection in the fracture, the water in the fracture has roughly the same concentration that the water in the whole thickness of adjacent matrix. In this case a retardation factor can be defined as:

$$R = \frac{\text{Total mass of solute}}{\text{Mobile mass of solute (fracture)}} = 1 + \frac{\theta \cdot TM}{b}$$

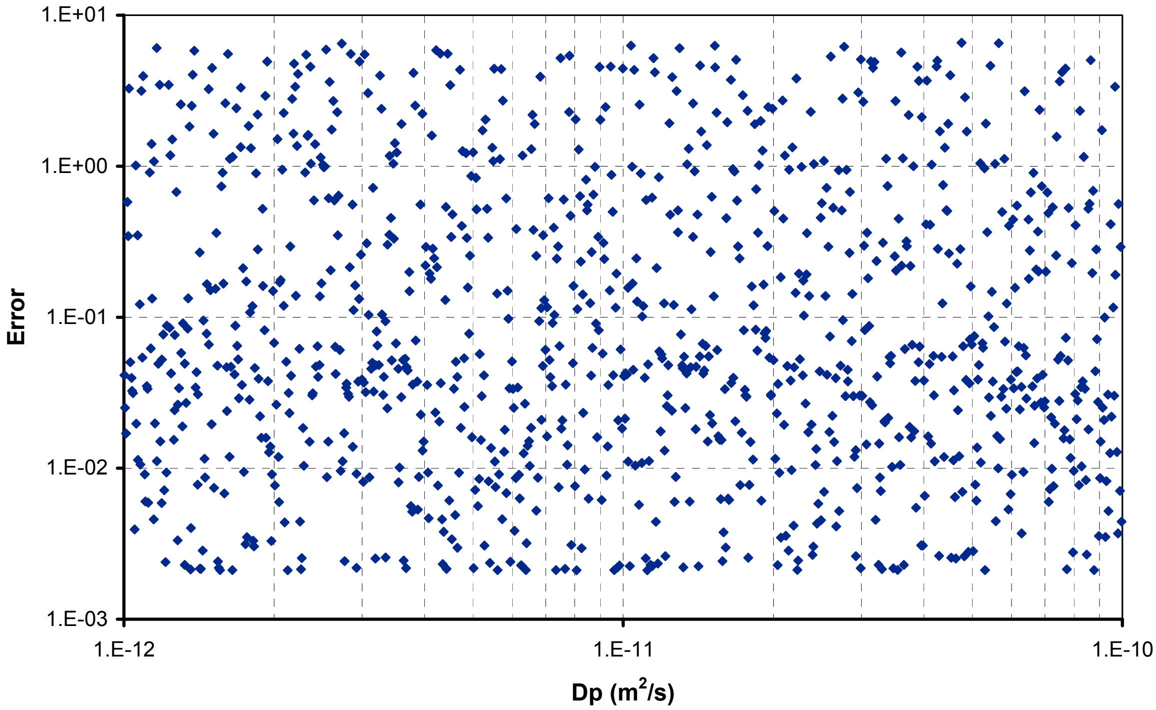

Figure 89.– Scatter plot of the diffusion coefficient in matrix porewater (D_p) vs. Error in the 1000 realisations of the GoldSim calculation.

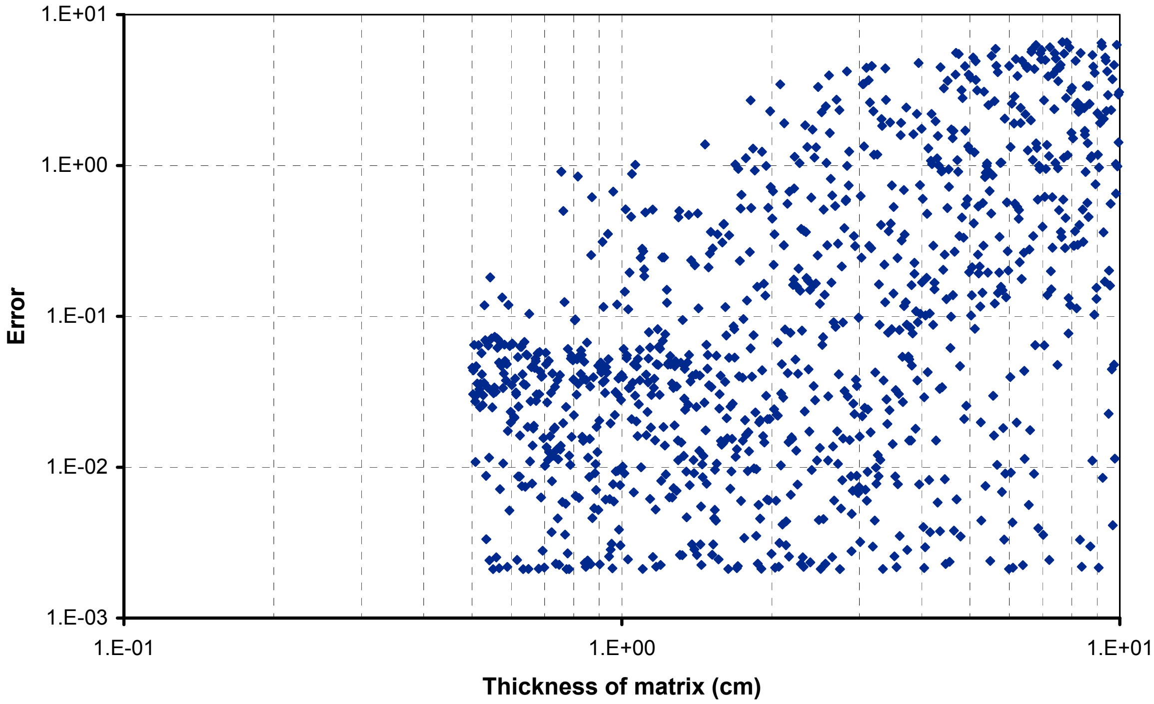

Figure 90.– Scatter plot of the thickness of matrix vs. Error in the 1000 realisations of the GoldSim calculation.

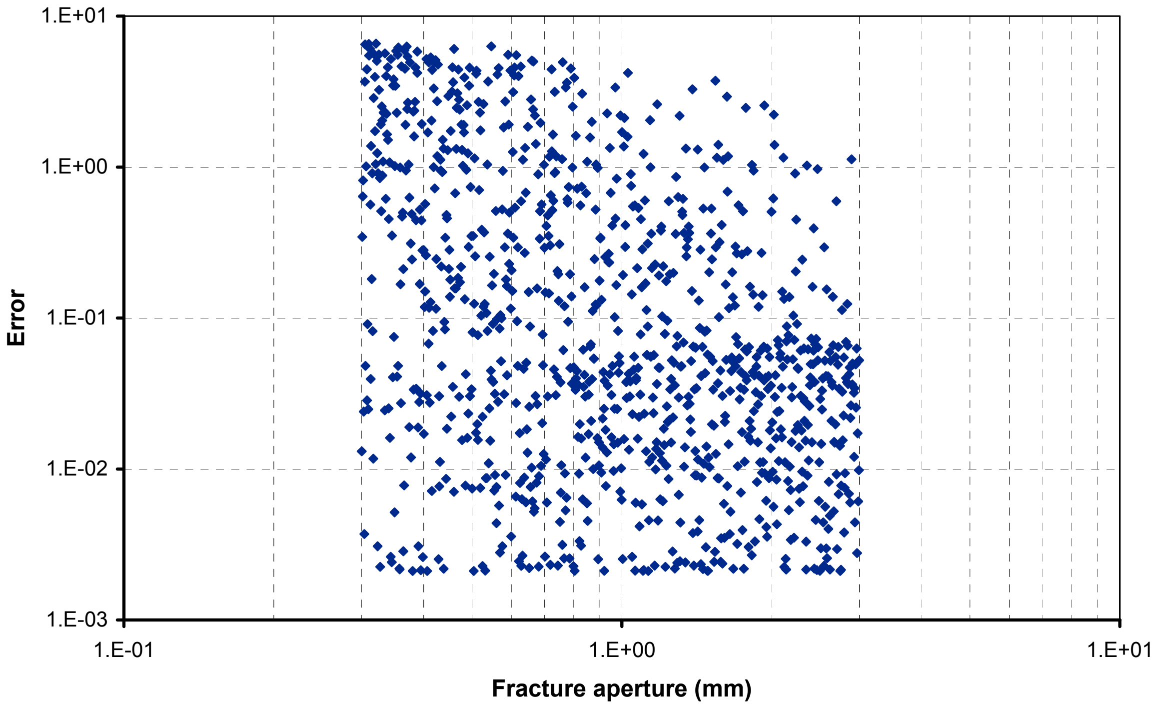

Figure 91.– Scatter plot of the fracture aperture vs. Error in the 1000 realisations of the GoldSim calculation.

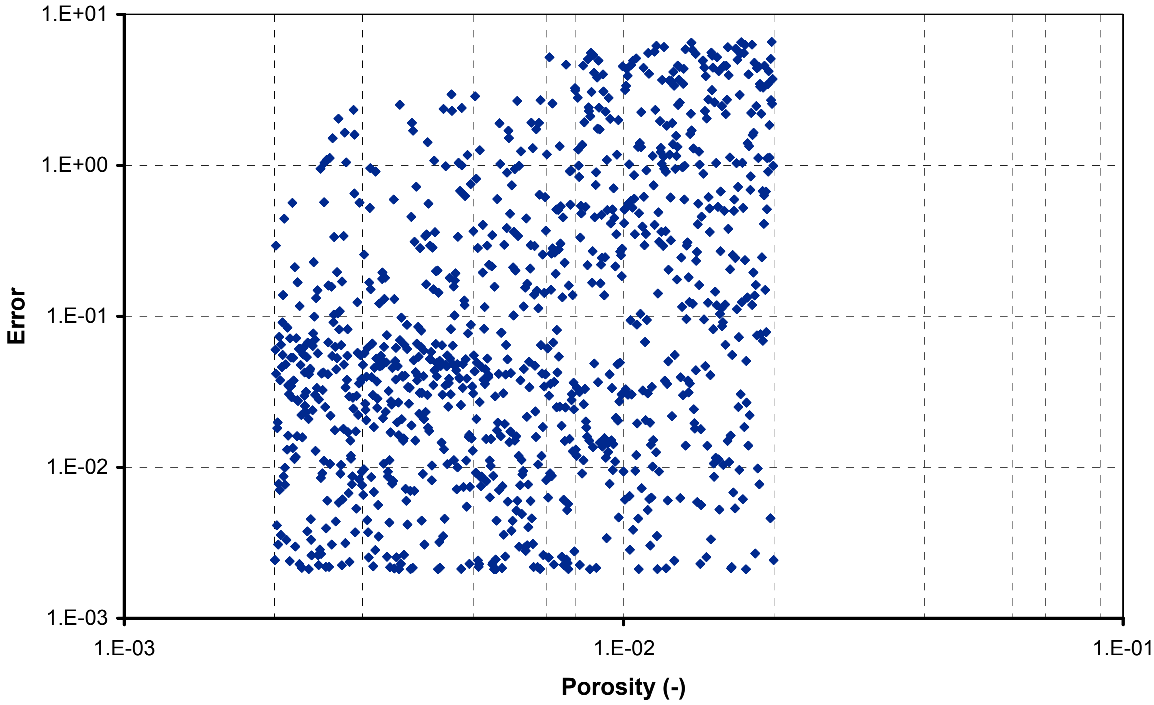

Figure 92.– Scatter plot of the matrix porosity vs. Error in the 1000 realisations of the GoldSim calculation.

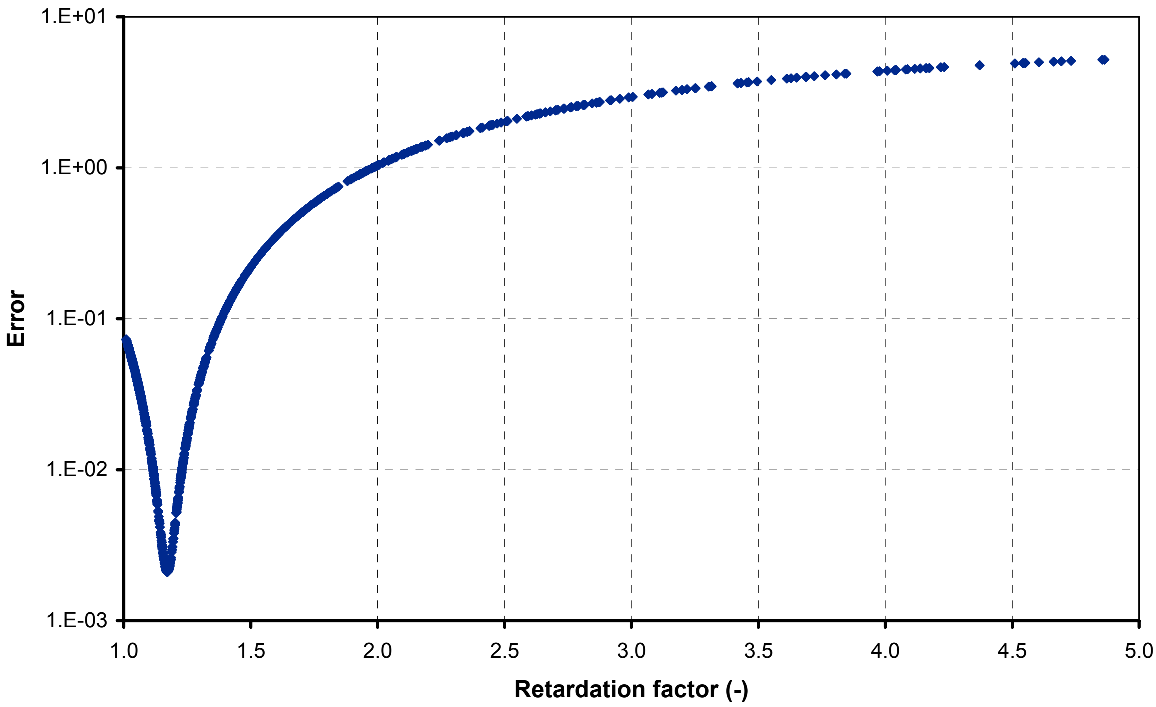

Figure 93.– Scatter plot of the retardation factor vs. Error in the 1000 realisations of the GoldSim calculation.

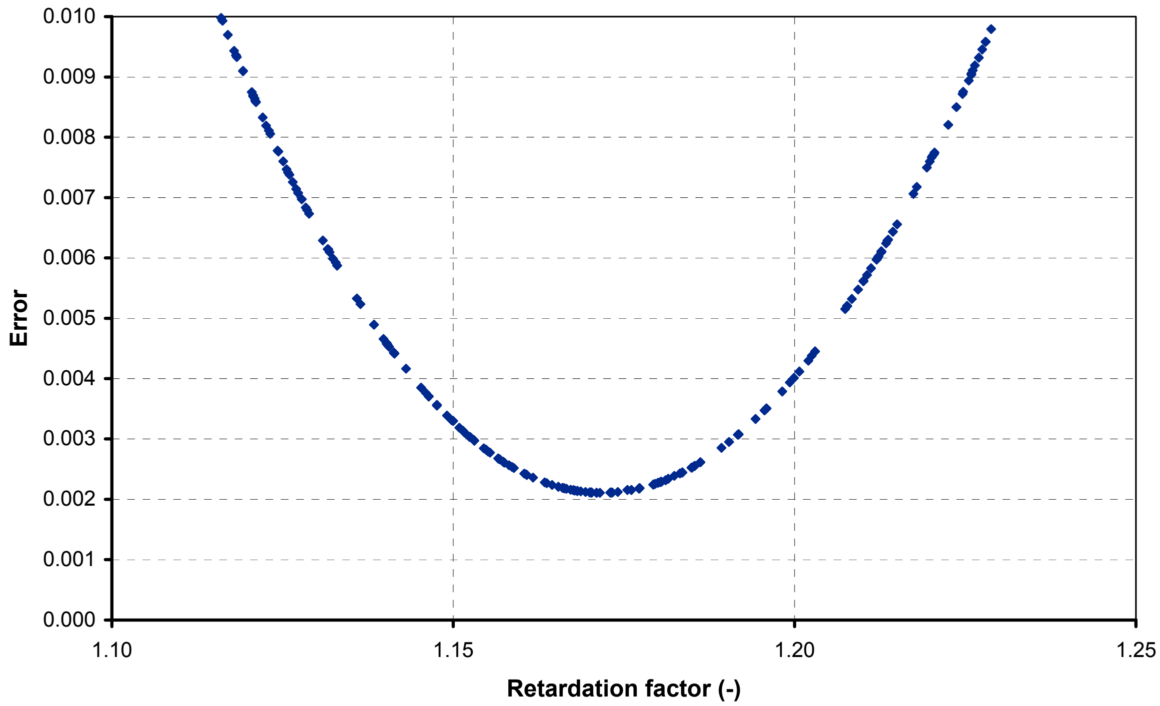

Figure 94.– Scatter plot of the retardation factor vs. Error in the 1000 realisations of the GoldSim calculation (detail of Figure 93).

Figures 89 to 92 clearly show that none of the random input parameters (θ, TM, D_p and 2b) are correlated with Error. By the contrary, a total correlation is observed between the retardation factor and Error (Figures 93 and 94).

The minimum value of Error (2.107E-3) is obtained in realisation #405, that corresponds to R= 1.17146. Error is smaller than 2 times its minimum value for a narrow range of values of R between 1.14 and 1.20.

Figure 95 shows the BTCs obtained with the fine scale model with homogeneous releases from the repository area and GoldSim run #405 (R=1.17146). A good agreement is observed, and it can be concluded that:

- the results of the fine scale model can be reproduced with a simple "pipe",
- no explicit modelling of the kinetics of matrix diffusion is necessary (no dependence on D_p), and
- using a retardation factor (based on geometric data) to take into account matrix diffusion is appropriate.

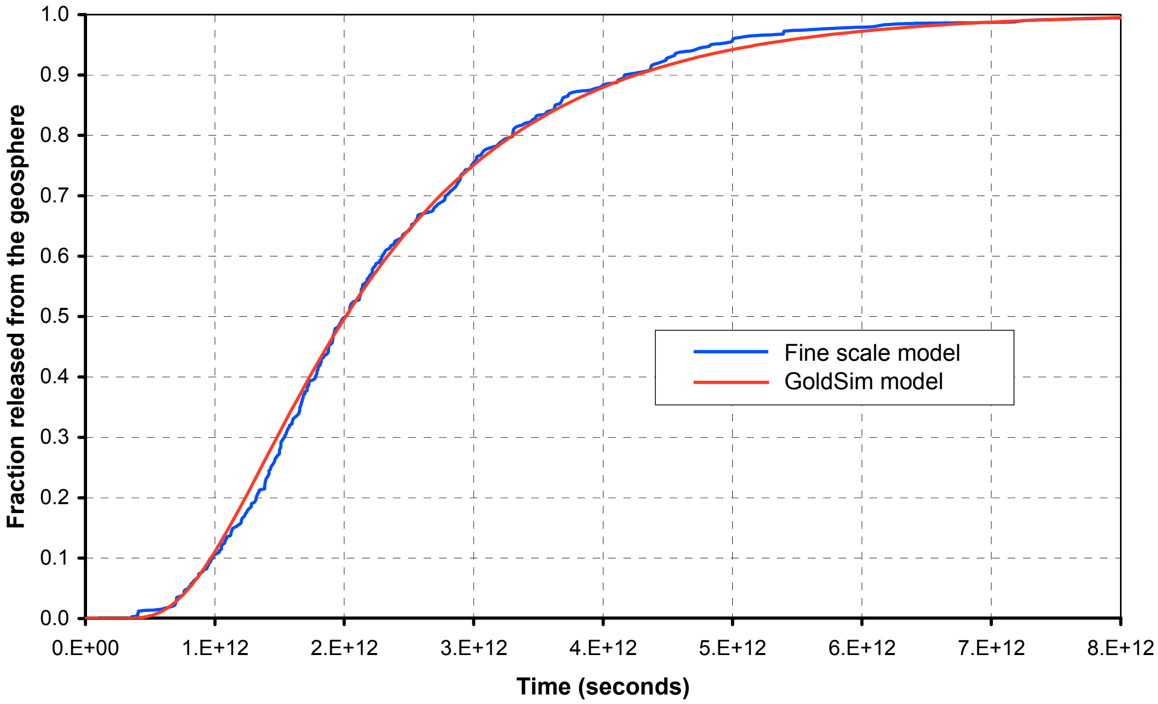

Figure 95.– BTC´s with the fine scale model and GoldSim realisation #405 (advection+dispersion+matrix diffusion case)

6. Conclusions

"Fine scale" and "coarse" models

The impact of heterogeneity in transport simulations in a granite block with different degrees of fracturing has been analyzed using an equivalent porous media model with a small discretization. Also an upscaling exercise has been performed aimed at reproducing the transport simulations observed at the fine scale with a coarser model with two order of magnitude less numerical cells than the fine scale model.

From the analysis of the heterogeneity of the parameters we conclude that, within the ranges of variability of the different parameters considered, it is important to account for the heterogeneity in fracture porosity (both mobile and immobile), the flow wetted area and the matrix thickness, but it is not sensitive to heterogeneity in matrix porosity or diffusion coefficient in the matrix porewater.

From the analysis of the upscaling results we conclude that it is particularly important to perform flow upscaling considering full tensors at the coarse scale with principal directions not necessarily aligned with the Cartesian axes, in order to reproduce properly the interblock fluxes at the coarse scale. Regarding transport upscaling, it has been found that the best results are obtained when the release zone is the largest; it seems that the upscaling approach used it is more suited to reproduce transport breakthrough curves when the particles sample a larger fraction of the model area, the more local the release is, the more difficult for the transport upscaling to produce good results. However, we could conclude with certain generality, that the transport predictions at the coarse scale approximate better the fine scale results when both flow and transport upscaling is performed.

1D advective pathway

Results obtained in section 5 have shown that the BTC´s obtained with the fine scale model can be reproduced with good precision using a 1D advective-dispersive pathway (or "pipe") of GoldSim with the following parameter values:

- water travel time (t_W) of $2.0391 \cdot 10^{12}$ s
- alpha factor (α) equal to 0.191
- retardation factor equal to 1.17146

With the ranges of transport parameters values considered in the fine scale model, diffusion into the granite matrix is fast compared with advection in the fracture. As a consequence, it is appropriate to use a retardation factor (based on geometric data) to take into account matrix diffusion, without modelling explicitly the process.

Taking into account the important uncertainties involved in Performance Assessment calculations, the precision of the results obtained with the 1D advective pathway used by GoldSim to represent the geosphere model is satisfactory.

7.References

[1] Enresa 2000. Evaluación del Comportamiento y de la Seguridad de un Almacenamiento de Combustible Gastado en una Formación Granítica. 49-1PP-M-15-01 Rev.0. December 2001. (In Spanish)

[2] Gomez-Hernandez, J.J., 1991. A stochastic approach to the simulation of block conductivity fields conditioned upon data measured at a smaller scale. Ph.D. thesis, Stanford University, CA.

[3] D. Fernàndez-Garcia, T.H. Illangasekare and H. Rajaram, Differences in the scale dependence of dispersivity and retardation factors estimated from forced-gradient and uniform flow tracer tests in three-dimensional physically and chemically heterogeneous porous media, Water Resources Research 41 (2005)

[4] ENRESA, Task 2.1.D Sensitivity/Uncertainty Analyses Definition of the calculation case for a repository in granite, PAMINA, FP6-036404, (2008)

[5] D. Fernàndez-Garcia and J. J. Gómez-Hernández, "Impact of upscaling on solute transport: Travel times, scale dependence of dispersivity, and propagation of uncertainty," Water Resources Research 43, no. 2 (2007).

[6] Integrated Project PAMINA "Performance Assessment Methodologies in Application to Guide the Development of the Safety Case". Annex I – "Description of Work". 23 April 2009.